Tandem Mass Spectrometry

9

Learning Objectives

- Tandem MS – concepts and terminology
- Modes of operation
- Different instrumental platforms
- Methods of ion activation to induce dissociation
- Applications to analytical problems
- Versatile tool for gas phase ion chemistry

Electron ionization mass spectra show a wealth of fragment ion peaks allowing to retrieve structural information, often though at the expense of abundance of the molecular ion. For decades, EI has served as the one and only ionization method of organic mass spectrometry. With the advent of soft ionization methods such as CI or FD we just dealt with, spectra exhibiting minor or even no fragment ion signals could be generated. While highly advantageous at first sight, in the long run, the lack of structural information presents a severe drawback for analytical applications. The development of numerous new techniques to store, manipulate, activate, fragment, and re-analyze ions in the gas phase by means of mass spectrometry have been driven both by the desire to understand the energetics, reactivity, and detailed fragmentation pathways of ions and the strong need for techniques to derive structural information from soft ionization mass spectra.

9.1 Concepts of Tandem Mass Spectrometry

The term *tandem mass spectrometry*, or briefly *tandem MS*, encompasses the numerous techniques where mass-selected ions are subjected to a second mass spectrometric analysis [1, 2]. Tandem mass spectrometry comprises the acquisition

J.H. Gross, *Mass Spectrometry*, DOI 10.1007/978-3-319-54398-7_9

and study of the spectra of ionic products or precursors of *m*/*z*-selected ions, or of precursor ions of a selected neutral mass loss. Tandem MS is also denoted as *mass spectrometry*/*mass spectrometry* from which the common acronym MS/MS is derived.

A mass spectrometer designed for MS/MS, also termed *tandem mass spectrometer*, requires to incorporate at least two stages of *m*/*z* analysis, often referred to as MS1 and MS2, respectively. Thus, many aspects of tandem MS are closely related to instrumentation [3]. In retrospect, we recognize that tandem MS has already been anticipated in some sections of the instrumentation chapter (Sects. 4.4.4, 4.5, 4.7.12, 4.8.4 and 4.9). Here, more principal considerations of the topic will follow.

9.1.1 Tandem-in-Space and Tandem-in-Time

There are two basic instrumental concepts for MS/MS. The first is *tandem mass spectrometry in space* (or *tandem-in-space* MS) [4]. In order to perform two consecutive mass-analyzing steps, two mass analyzers may be mounted in tandem. Thus, tandem-in-space refers to MS/MS instrumentation where product ion spectra are recorded using spatially separated *m*/*z* analyzers. Specific *m*/*z* separation is performed so that in one section of the instrument ions are selected, then dissociated in an intermediate region, and the products thereof are finally transmitted to a second analyzer for mass analysis (Fig. 9.1). All beam transmitting devices, e.g., multiple sector, ReTOF, TOF/TOF, QqQ, and QqTOF instruments follow this route to tandem MS (Fig. 9.2) [5]. The second approach, *tandem mass spectrometry in time* (or *tandem-in-time* MS), employs a single *m*/*z* analyzer (QIT, LIT, FT-ICR) that may be operated by executing the discrete steps of ion selection, activation, and product ion analysis in the very same place but sequentially in time [5].

In principle, both instrumental concepts can be expanded to allow for multiple-stage mass spectrometry, i.e., multiple stages of precursor ion selection followed by product ion detection for successive *n*th generation product ions [7]. While it is convenient to talk about MS/MS, acronyms like MS/MS/MS are clearly out of place. Therefore, it is common practice to use MS^2, MS^3, and generally MS^n to denote the number of stages of a tandem mass spectrometric experiment. Accordingly, in the sequential fragmentation scheme

$$m_1^+ \rightarrow m_2^+ \rightarrow m_3^+ \rightarrow m_4^+ \rightarrow m_5^+ \tag{9.1}$$

m_4^+ is the precursor ion of m_5^+, m_4^+ is a 1st generation product ion of m_3^+, a 2nd generation product ion of m_2^+, and also a 3rd generation product ion of m_1^+ [8, 9]. The corresponding spectra are analogously termed *n*th generation product ion spectra.

Clearly, the vast majority of tandem MS experiments is designed to deliver fragment ion data. Nonetheless, selected ions may also be allowed to react with neutrals in ion–molecule reactions to form products with a gain in mass (Sect. 2.13):

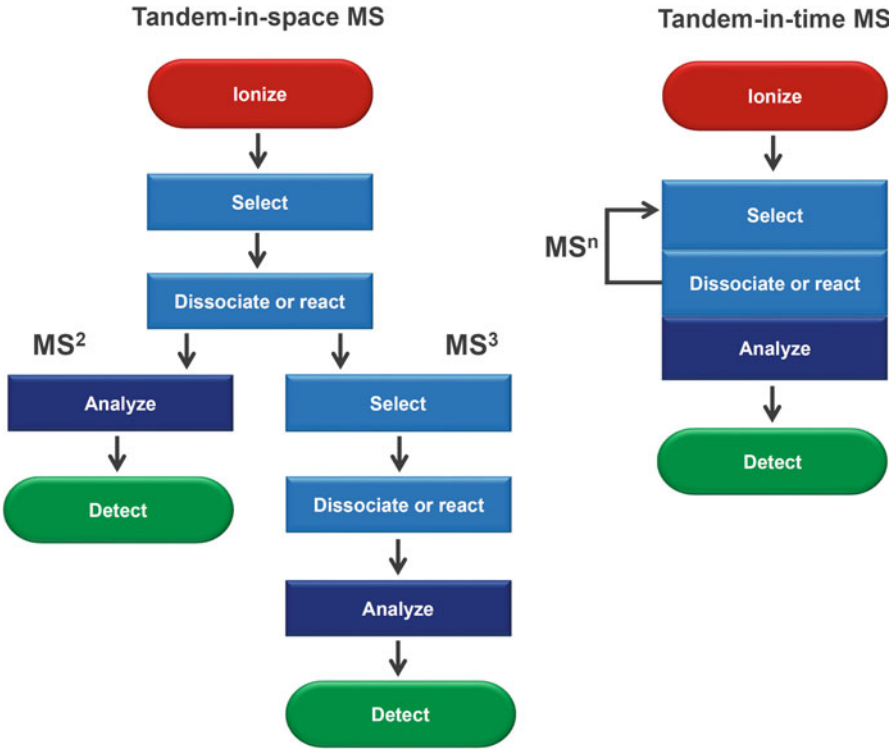

Fig. 9.1 Comparison of tandem-in-space and tandem-in-time MS. Obviously, higher order MS^n can be better realized by tandem-in-time setups, whereas tandem-in-space instrumentation is usually designed for MS^2 with MS^3 representing already the rare exception

$$m_1^+ + n \rightarrow m_2^+ \tag{9.2}$$

Ion–molecule reactions can thus be conducted under carefully controlled conditions. This sort of tandem MS is frequently employed in fundamental studies of ion reactivity.

Tandem MS is highly variable

Obviously, tandem MS experiments can be adapted according to need. They can set up as ion fragmentations, typically by energetic collisions of fast ions with an inert gas (Sect. 9.3) or as addition reactions with an according increase in precursor ion mass by addition of a reactive gaseous neutral upon very low-energy collisions (Sect. 9.18). However, ion–neutral collisions can even be soft and still nonreactive as exploited for thermalizing ions by multiple low-energy collisions with a buffer gas (Sect. 4.4.4).

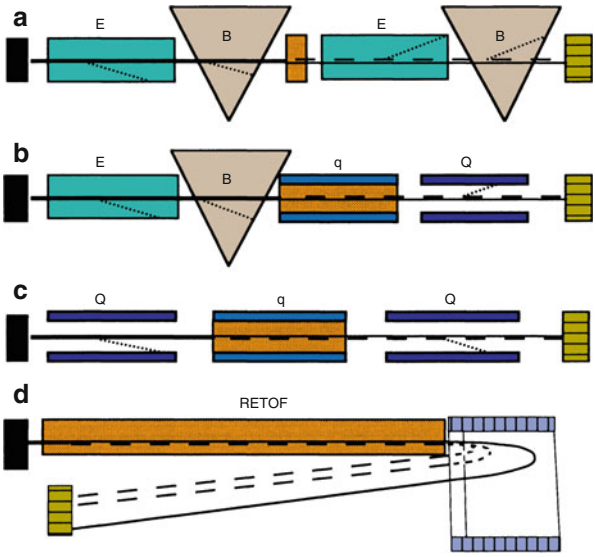

Fig. 9.2 Tandem-in-space setups for different beam instruments: (**a**) magnetic four-sector instrument of EB-EB geometry, (**b**) magnetic sector–quadrupole hybrid of EB-qQ geometry, (**c**) triple quadrupole (includes QqQ, QhQ, QoQ setups), and (**d**) ReTOF instrument. The line styles indicate —— stable precursor ions, - - - transmitted ions, and ····· non-transmitted fragment ions. *Orange* areas show the region of analytically useful ion dissociations (Adapted from Ref. [6] with permission. © Elsevier Science, 1994)

9.1.2 Pictograms for Tandem MS

To facilitate the evaluation of tandem mass spectra, the particular type of experiment can be described by pictograms. Following a simplistic notation [7, 10, 11], the chosen analyzer (or stage of experiment) may be indicated by ●, a scanning analyzer (or stage of experiment) by ○. Information such as precursor ion mass, type of ion activation, or neutral loss may be indicated as required (Table 9.1).

Dissociations in transit through the mass analyzer may either occur spontaneously (*metastable*, Sect. 9.2) or can result from intentionally supplied additional activation, typically from collisions with neutrals (Sect. 9.3). Below follows a description of methods for activating or reacting otherwise stable ions in the *field-free region* (FFR) between the first stage, *m*/*z*-selection (MS1), and product ion analysis (MS2).

Thus, to include ionization mode, type of mass analyzers, scan mode, and conditions of ion activation, a more elaborate set of pictograms has been suggested by Lehmann (Fig. 9.3) [12]. Since then, such pictorial presentations of basic experimental parameters are occasionally given along with tandem mass spectra. Unfortunately, neither an authorized "character set" nor an update to include current equipment and modes are available.

Table 9.1 Pictogram symbols for tandem MS experiments [7]

Mode	Product ion mode	Product ion mode	Precursor ion mode	Neutral loss scan
Level	MS^2	MS^3	MS^2	MS^2
Pictogram	● ↓ ○	● 228 ↓ ● 200 ↓ ○	○ ↓ CID ●	○ ↓ 32 ○
Notes		The *m*/*z* values of the selected ions may be noted	Conditions for activation may be added to arrow	Neutral loss can be indicated on arrow

product ion analysis of m/z 465 generated by negative ion CI in a hybrid instrument, He as collision gas at 800 V offset

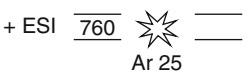

positive ion ESI, product (daughter) scan of m/z 760 with Ar as collision gas at 25 V offset using a triple-stage quadrupole

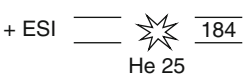

positive ion ESI, precursor (parent) scan of m/z 184, with He as collision gas at 25 V offset using a triple-stage quadrupole

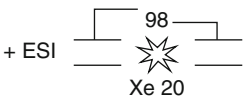

positive ion ESI, neutral loss scan for loss of 98 D, with Xe as collision gas at 20 V offset using a triple-stage quadrupole

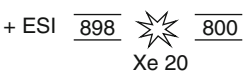

positive ion ESI, selected reaction monitoring (SRM) for the fragmentation m/z 898 -> m/z 800 with Xe as collision gas at 20 V offset using a triple-stage quadrupole

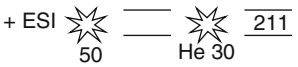

positive ion ESI, sCID at 50 V offset plus precursor ion scan for m/z 211 with He as collision gas and 30 V offset using a triple-stage quadrupole

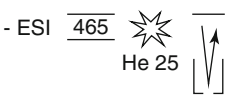

negative ion ESI, product ion analysis of m/z 465 with He as collision gas at 25 V offset using a quadrupol/orthogonal extraction TOF analyzer combination

positive ion ESI, product ion analysis of m/z 1000 using an ion trap

positive ion ESI, product ion analysis of m/z 902, formed by CID of m/z 1000, using an ion trap

Fig. 9.3 Pictograms for tandem MS (Reproduced from Ref. [12] with permission. © Elsevier Science Inc., 1997)

Tandem MS modes are defined by mass analyzers
There is a close relationship between the type of mass analyzer and choice of method of ion activation that can be applied to the respective instrumental platform. It is therefore unfavorable to strictly separate the discussion of ion activation from that of instrumental setups and their modes of operation. Thus, the following passages of this chapter will reflect these mutual dependences by alternating discussions of activation methods and instrumental details in a way that is supposed to deliver convenient access to the subject matter.

9.1.3 Terminology for Tandem Mass Spectrometry

Here are the basic terminological conventions for tandem mass spectrometry [4]:

- The term tandem *mass spectrometry* or *mass spectrometry/mass spectrometry* collectively describes mass spectrometric experiments where mass-analyzed ions are subjected to fragmentations or ion–molecule reactions and the products thereof are collected and mass-analyzed by a second stage.
- Instruments are accordingly referred to as *tandem mass spectrometers*; their stages are denoted MS1, MS2 etc.
- Tandem MS is often abbreviated as MS/MS or MS^2. Tandem MS experiments of higher order are referred to as MS^3, MS^4, . . . or generally as MS^n.
- Ions emerging from MS1 are termed *precursor ions*, those entering MS2 are called *product ions*; in higher-order experiments, one may refer to them as *n*th generation product ions. (The old terms *parent ion* and *daughter ion* are deprecated.)
- Spectra are called *tandem mass spectra* (never MS/MS spectra).

9.2 Metastable Ion Dissociation

The success of any tandem mass spectrometric experiment depends on the occurrence of some kind of reaction between the consecutive steps of precursor ion selection and product ion analysis. This demands that ions entering the zone and/or period for reaction either possess or receive sufficient internal energy for doing so; alternatively, a partner for reaction may be presented.

As dealt with in Sect. 2.6, ions reacting sufficiently fast to dissociate while transiting the analyzer are termed *metastable ions* [13]. In classical beam instruments, this is correlated to lifetimes of roughly 10^{-6}–10^{-5} s, and thus, requires

rate constants of unimolecular dissociation in the order of 10^6–10^5 s^{-1}. EI, CI, and MALDI can provide a respectable fraction of ions, as to say in the afterglow of the ion source, falling into this range of internal energy and therefore into the lifetime of metastable decomposition. The fraction of metastable ion dissociations occurring in the *field-free region* (FFR) between MS1 and MS2 is accessible by means of tandem MS. Ions fragmenting during the very step of mass analysis are lost.

It is a generally accepted assumption that metastable ions possess internal energy only slightly above threshold of ion dissociation. Interestingly, there are still differences even among metastable ion populations, depending on whether they are observed in close proximity to the ion source (1.FFR) or further away (2.FFR). Metastable ion spectra represent one of the indispensable tools for studying the mechanism and thermochemistry of ion dissociations [13, 14]. Examples are given in the section on tandem MS on magnetic sector instruments.

9.3 Collision-Induced Dissociation

Even though collisions of ions with neutral gas atoms or molecules appear contradictory to the conditions of high vacuum, most mass spectrometers are equipped (or can be upgraded) to allow for their study. Consequently, fundamental and analytical studies make use of activating or reactive collisions within the mass spectrometer. The most prominent collision technique is *collision-induced dissociation* (CID) [15, 16]; the terms *collisionally activated dissociation* (CAD) or *collisional activation* (CA) are also being used. CID allows for the fragmentation of gaseous ions that were otherwise perfectly stable. Thus, CID is especially useful for elucidating the structure of ions of low internal energy as for those created by soft ionization methods.

9.3.1 Effecting Collisions in a Mass Spectrometer

CID is generally realized by passing an ion beam through a *collision cell* where the collision gas (He, N_2, Ar) is set to a pressure considerably above that of the surrounding high vacuum. This can be achieved by introducing the gas via a needle valve into a comparatively tight compartment with narrow entrance and exit slits for the ion beam (Fig. 9.4). A nearby vacuum pump removes effusing gas, thereby creating a *differentially pumped* region, due to the lack of laminar flow at some 10^{-4} Pa. Instead, expansion of the gas is diffusion-controlled. The reading of a pressure gauge can serve to reproduce the pressure adjustment, but it does not show the actual pressure inside the cell [17].

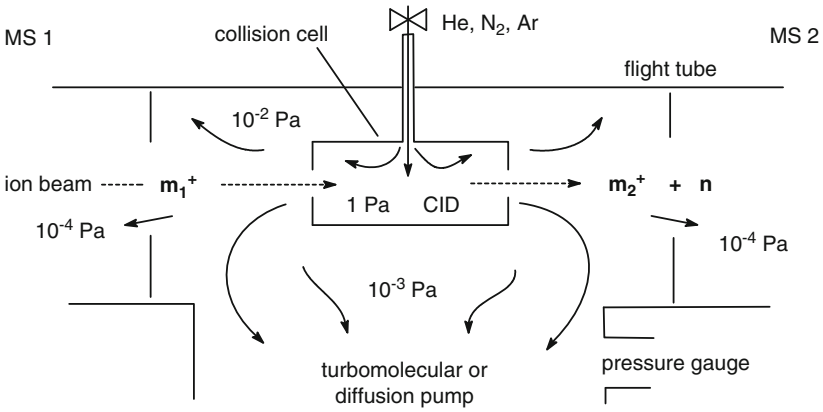

Fig. 9.4 Schematic of a collision cell for CID experiments in a beam instrument. Ions mass-selected in MS1 enter from the left

9.3.2 Energy Transfer During Collisions

The collision of an ion AB^+ carrying some kiloelectronvolts of kinetic energy with a neutral N takes about 10^{-15} s. This allows to apply the assumptions of QET analogously to electron ionization (Sect. 2.1) [14, 18–21]. The collision-induced dissociation of AB^+ can therefore be regarded as a two-step process [22]. First, the activated species AB^{+*} is formed. Second, after randomization of the internal energy has occurred, AB^{+*} will dissociate along any fragmentation pathway available at this specific level of internal energy:

$$AB^+ + N \rightarrow AB^{+*} + N \rightarrow A^+ + B + N \tag{9.3}$$

The internal energy E_{AB+*} is composed of the internal energy prior to the collision, E_{AB+}, and of the amount of energy Q transferred during the collision:

$$E_{AB+*} = E_{AB+} + Q \tag{9.4}$$

Thus, the collision marks a restart of the time scale for the activated ion. As $Q > E_{AB+}$ generally holds, the internal energy prior to the collision is of minor relevance – though not generally negligible – for the behavior of the activated ion. As may be expected, the CID spectra of stable molecular ions exhibit marked similarity to the 70-eV EI spectra of the respective compounds [15, 16].

CID causes vibrational excitation Except for the intensities relative to the precursor ion, the B/E-linked scan CID spectrum of the toluene molecular ion, m/z 92, closely resembles the 70-eV EI mass spectrum (Fig. 9.5; for EI cf. Sect. 6.4.3). Here, all fragments are due to CID because the molecular ion was generated by field ionization and did not show any metastable decomposition, i.e., $E_{AB+} = 0$ and $E_{AB+*} = Q$.

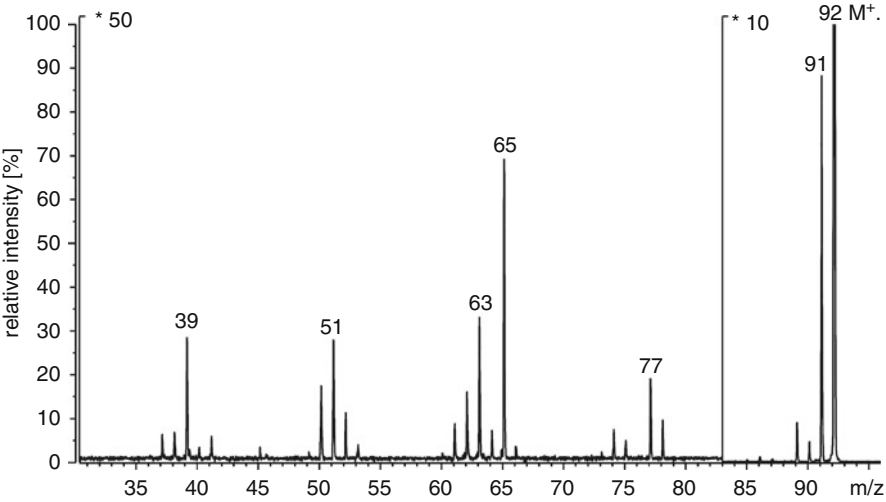

Fig. 9.5 CID spectrum of toluene molecular ion, *m/z* 92 ($E_{lab} = 10$ keV, B/E = *const.* linked scan on magnetic sector instrument (cf. Sect. 9.6.4), collision gas He at about 50% transmission)

The absolute upper limit for the value of Q is defined by the *center-of-mass collision energy*, E_{CM} [18, 19],

$$E_{CM} = E_{LAB} \frac{m_N}{m_N + m_{AB}} \tag{9.5}$$

where m_N is the mass of the neutral, m_{AB} the mass of the ion, and E_{LAB}, the *ion kinetic energy in the laboratory frame of reference*.

Laboratory frame of reference

E_{LAB}, the ion kinetic energy in the laboratory frame of reference, simply represents the kinetic energy of the ion as received from passing through an acceleration stage that defines its kinetic energy, e.g., a singly charged ion initially at rest will have $E_{LAB} = 10$ eV after passing through a potential of 10 V. The collision event of the ion–neutral pair, however, is also determined by both ion mass, m_{AB}, and neutral mass, m_N, as expressed by the ratio $m_N / (m_N + m_{AB})$. The neutral is commonly treated as being at rest, which is a good approximation for the collision gas at thermal energy.

For a polyatomic ion consisting of both the atom B actually, involved in the collision process, and the remainder A, the maximum of Q is calculated to have a lower value than E_{CM}. Assuming central collisions we obtain [19]:

$$E_{\text{int max}} = 4E_{LAB}\, m_A\, m_B \left(\frac{m_N}{m_{AB}\,(m_B + m_N)} \right)^2 \tag{9.6}$$

However, most collisions are not "head-on", but occur at some angle θ. Increasing m_{AB} makes $E_{\text{int max}}$ decrease, whereas larger m_N is beneficial for energy transfer. In CID-MIKES the center of the peak is shifted to the low mass side, i.e., to the low ion translational energy side, because the uptake Q originates from a loss in E_{LAB} [23–28]. The relationship between ΔE_{LAB} and Q can be expressed as [25]:

$$Q = \frac{\Delta E_{LAB}(m_{AB} + m_N)}{m_N} - \left[\left(\frac{2m_{AB}E_{LAB}}{m_N}\right)\left(1 - \sqrt{\frac{E_{LAB} - \Delta E_{LAB}}{E_{LAB}}}\cos\theta\right)\right] \quad (9.7)$$

Several conclusions can be drawn from Eq. 9.7:

- Q has a broad distribution (0–15 eV) due to variations in θ and typically is in the order of some electronvolts [29].
- Up to a certain ionic mass, the neutral penetrates the incident ion, i.e., the activated ion leaves the neutral behind (forward-scattered ion), but beyond the limit ($> 10^2$ atoms) the neutral is expelled in the direction of ion motion (backward-scattered ion) [25].
- At about m/z 1500 the translational energy loss is fully converted into vibrational excitation of the ion ($\Delta E_{LAB} = Q$).
- Q decreases beyond m/z 1500, thus explaining the difficulties in fragmenting heavy singly charged ions by CID (Fig. 9.6) [21, 25, 30].

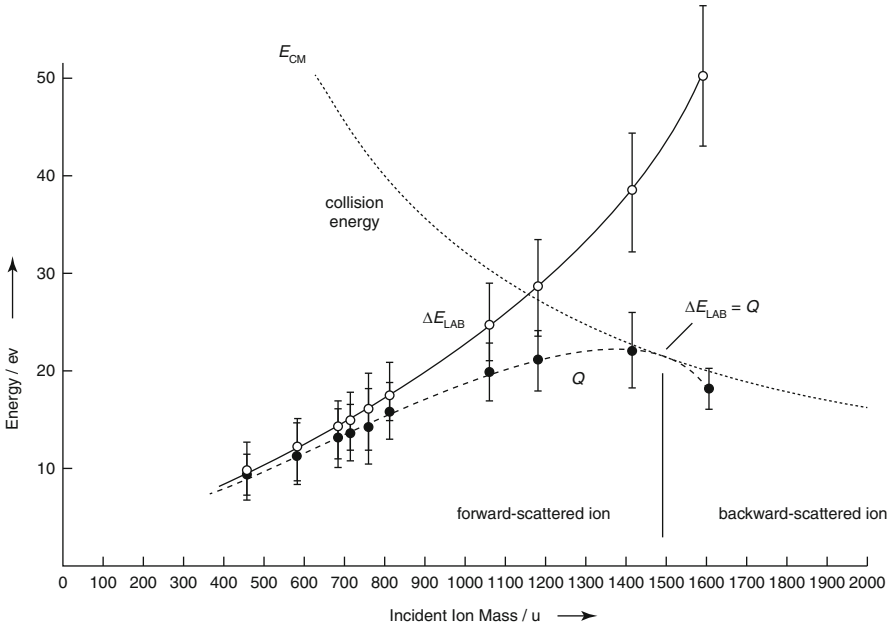

Fig. 9.6 The relationship between E_{CM}, ΔE_{LAB}, and Q (Adapted from Ref. [25] with permission. © Verlag der Zeitschrift für Naturforschung, 1984)

Selection of collision gases
In magnetic sector and TOF instruments, He is typically used as the collision gas because $E_{\text{int max}}$ from *high-energy collisions* (keV) is still comparatively large, and He reduces the risk of charge transfer due to its high *IE*. In the *low collision energy regime* [19] of quadrupole and ion trapping instruments (1–200 eV), heavier gases are frequently employed (N_2, Ar, Xe) to make CID more effective.

9.3.3 Single and Multiple Collisions in CID

Generally, the collision gas pressure is indirectly adjusted via the attenuation of the beam of mass-selected ions undergoing collisions. As the so-called *main beam* becomes increasingly attenuated, the probability for multiple collisions rises and so does the yield of fragments resulting from high activation energy processes. In a typical high-energy collision experiment a transmission of 90% for the main beam translates into 95% of the colliding ions to undergo single collisions while only about 5% encounter double collisions. At 50% transmission, about 68% of the colliding ions encounter a single, 23% two, and the remaining even three and four collisions (Fig. 9.7) [17]. To achieve sufficient activation of the ions in the low-energy collision regime, elongated collision cells are employed where Q is accumulated from numerous collision events.

In beam-type analyzers, the collision event leading to ion activation can be considered in terms of the Lambert-Beer law, because the precursor ion beam flux $[M_p]_0$ is exponentially reduced when passing through a collision chamber of length l containing gas at target number density n

$$\left[M_p\right] = \left[M_p\right]_0 \times e^{-n\sigma l} \tag{9.8}$$

where σ is the collision cross section of the event [31].

In tandem-in-time experiments as performed in trapping instruments a description in terms of rate constants and reaction times is more appropriate, which leads to the expression

$$\left[M_p\right]_t = \left[M_p\right]_0 \times e^{-nkt} \tag{9.9}$$

where t is the activation time span, and k sums the rate constants of all processes leading to reduction in $[M_p]_0$, i.e., it includes fragmentation and scattering losses.

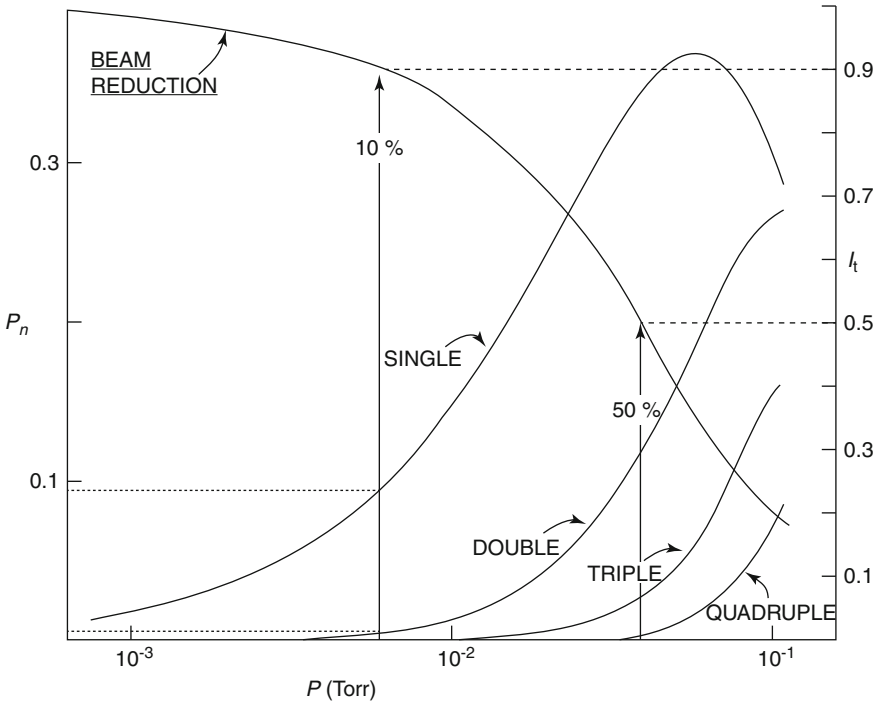

Fig. 9.7 Total collision probability P_n (*left* ordinate) and fractions of single, double, triple, and quadruple collisions vs. collision gas pressure. The transmission of the main beam I_t is given on the *right* ordinate. *Dotted lines* mark beam transmission and collision probabilities for 90% and 50% transmission, respectively. Values are calculated for an ion of collision cross section 5×10^{-16} cm^2 and 1 cm collision path; 10^{-2} Torr = 1.33 Pa (Adapted from Ref. [17] with permission. © John Wiley & Sons, 1985)

Adjusting the collision gas pressure
It has turned out that medium transmission is optimal for structure elucidation. Too strong reduction of the main beam favors ion losses due to scattering, charge exchange ($M^{+\bullet} + N \rightarrow M + N^{+\bullet}$) or charge stripping processes ($M^{+\bullet} + N \rightarrow M^{2+} + N^{+\bullet}$) instead of delivering additional structural information.

9.3.4 Time Scale of Ion Activating Processes

Collisions of energetic ions with gaseous molecules are very fast. Nonetheless, there is a considerable variation of the effective activation period, i.e., single collisions of ions of keV energy occur in the femtosecond range while those at

eV energies tend to take picoseconds. If multiple collisions occur within one activation stage, the time scale is extended, because the span between collisions is then ruling the overall duration. Other activation techniques go along with even millisecond to second time spans (Fig. 9.8) [31]; most of these techniques will be addressed in this chapter [3]. While the fast ones can be treated by QET analogous to the event of electron ionization, the slower processes (SORI-CID, IRMPD, BIRD) tend to achieve an equilibrium of ion internal energy prior to dissociation.

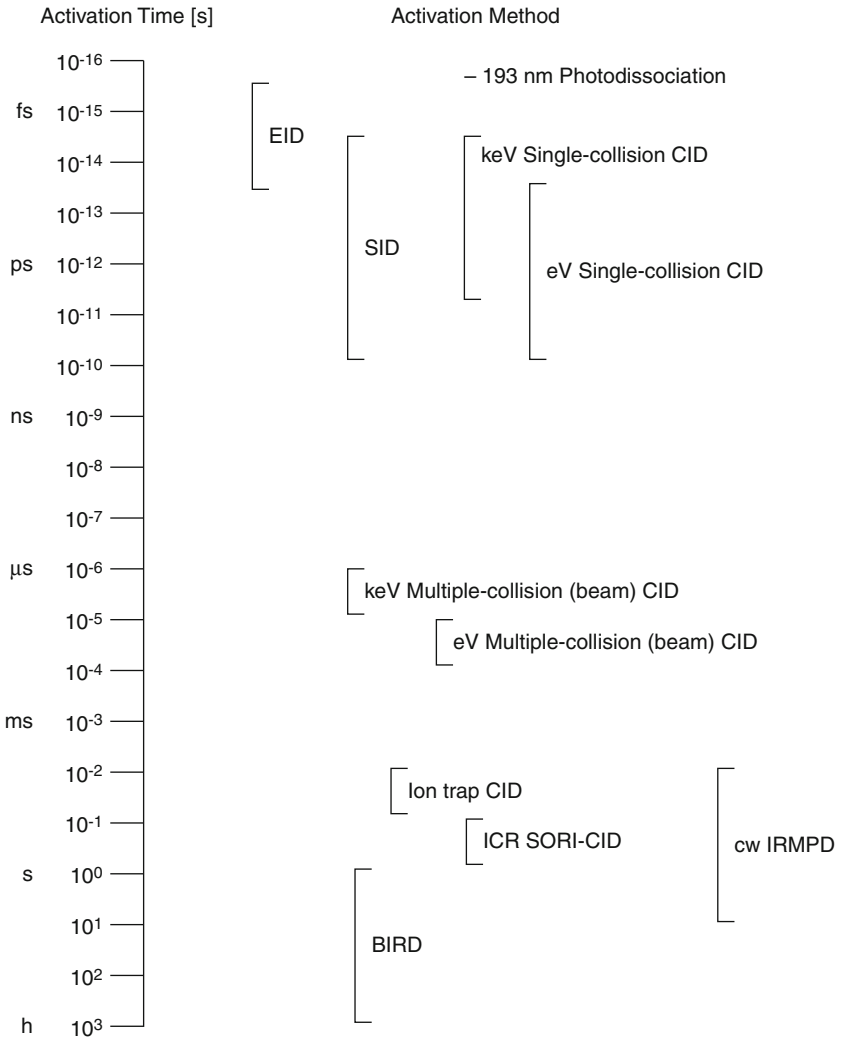

Fig. 9.8 Time scale of ion activation processes for tandem mass spectrometry (Adapted from Ref. [31] with permission. © Wiley & Sons, Ltd., 1997)

9.4 Surface-Induced Dissociation

Collisions with solid surfaces can be employed to induce dissociation of the incident ions similar to collisions with gaseous collision partners. This technique has become known as *surface-induced dissociation* (SID) [32, 33]. In SID, ions of some tens to a hundred electronvolts of kinetic energy are collided with a solid surface at an angle of about 45°. By variation of the SID target potential, the SID setup allows to control the energy of the incident ions, and therefore to adjust the degree of fragmentation. The first SID setup employed a linear quadrupole mass analyzer at right angles to the incident ion beam for fragment ion analysis (Fig. 9.9) [32, 34, 35].

SID conditions can be tuned to deliver spectra resembling either high- or low-energy CID spectra [32]. The absence of collision gas presents an advantage of SID over CID because losses of resolution due to high background pressure are avoided. However, apart from the quadrupole ion trap [36], SID requires substantial modifications of the instrumental hardware.

Fluorinated self-assembled monolayers (FSAM) are frequently employed surfaces for SID which are prepared on thin gold layers applied onto glass slides [37]. The perfluorinated alkyl groups in the top layer of the SID target serve to reduce ion losses by neutralization and improve energy transfer to the incident ions.

SID was never commercialized, and thus, SID lags behind the countless applications of CID. Nonetheless, SID is still developed further and implemented in modern instruments [37–41]. The Waters Synapt G2 may serve as an example (Fig. 9.10 and Sect. 4.10.4). In this particular instrument, the original transfer

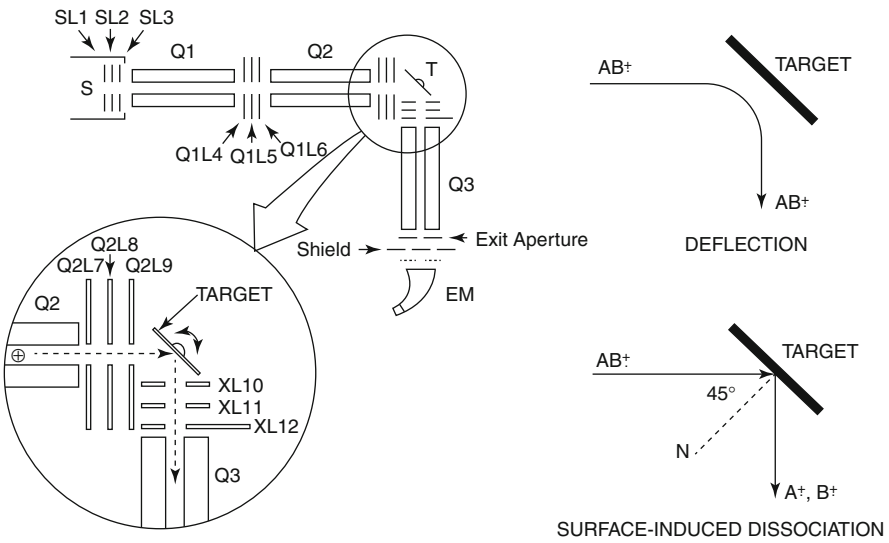

Fig. 9.9 Apparatus (*left*) and modes of operation (*right*) for SID with a modified triple quadrupole mass spectrometer (Reproduced from Ref. [34] with permission. © Elsevier Science, 1987)

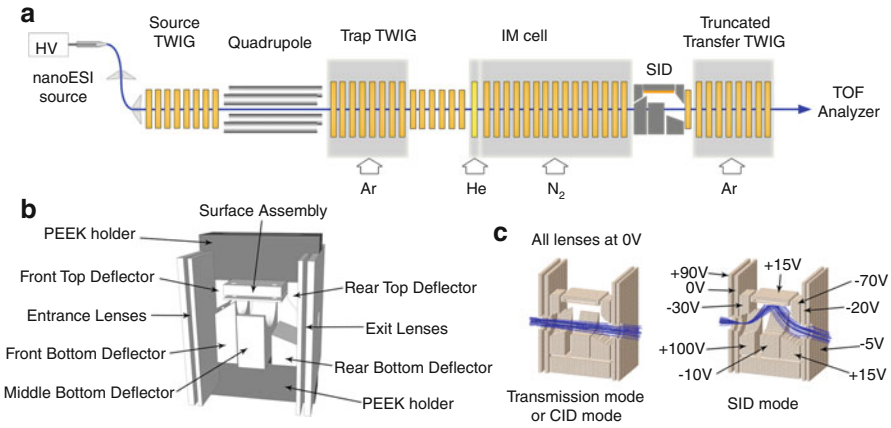

Fig. 9.10 Waters Synapt G2 modified to incorporate a SID device in front of the transfer TWIG. (**a**) Setup of the instrument (dimensions of the ion optics are not to scale). (**b**) 3D perspective view of the SID device assembly. (**c**) Cutaway views of a SIMION simulation showing the ion paths in transmission mode versus SID mode. The voltages on the SID lenses are given relative to the potential on the transfer TWIG (Reproduced from Ref. [40] with permission. © American Chemical Society, 2012)

TWIG (Sect. 4.10.3) was truncated to accommodate the SID device. The SID device itself comprises several compact electrodes to focus and deflect the entering ion beam onto the collision surface that is aligned parallel to the beam. The optimal voltages in SID experiments vary at different collision energies [40]. Switching off the deflection voltage also allows for transmitting ions through the SID device without collisions to the surface.

The reason for prefering SID over CID lays in the different processes of energy transfer to the precursor ions. Low-energy CID as used in modern hybrid instruments leads to vibrational excitation of the precursor ion via multiple collisions. SID, in contrast, causes energy to be impacted during a single fast event [37, 38]. The simplified reaction pathway for dissociation of a noncovalent protein complex via CID or SID illustrates how in CID multistep activation permits time for structural rearrangement, finally resulting in the formation of an unfolded subunit (Fig. 9.11). In SID, rapid energy deposition is proposed to induce dissociation faster than protein unfolding via different dissociation pathways [37].

Such differences in product ion formation are always observed when switching from very fast energy uptake (EI, high-energy CID, ECD) to slow heating (low-energy CID, SORI-CID, IRMPD, Sect. 9.3.4) [42]. Generally, pathways having high activation barriers are only accessibly by fast energy transfer, while slow heating fosters the selection of low-energy transition states.

Subunits of human serum amyloid P Human serum amyloid P (SAP) is a glycoprotein with an oligomerization behavior that is strongly dependent on the conditions in solution. It occurs in both a compact and a less compact SAP decamer

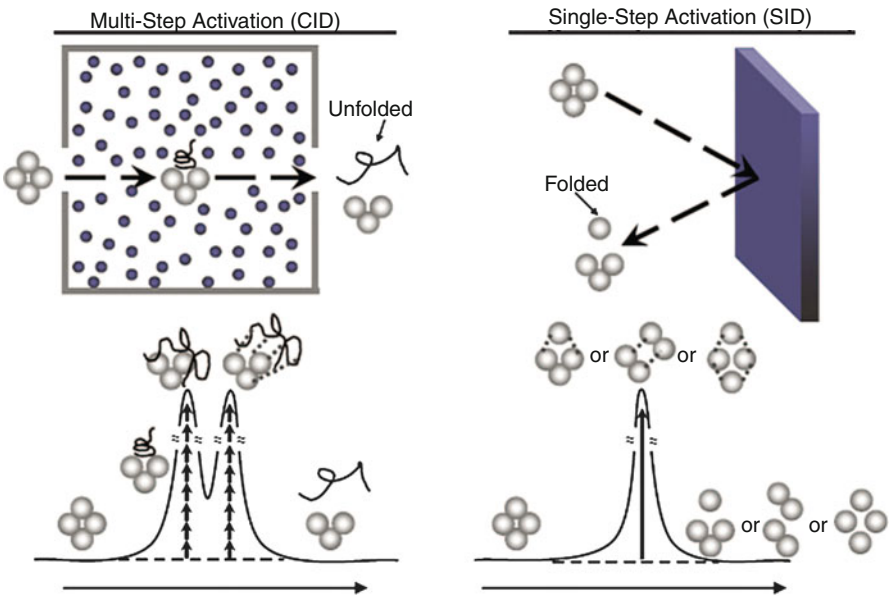

Fig. 9.11 Comparison of CID and SID experiments illustrating the differences in energy uptake (*top*) and the effect on fragmentation of a noncovalent protein complex. The reaction coordinate (*bottom*, *x* axis) is plotted versus energy (*y* axis). The actual energies needed and achieved, and numbers of rearrangements or of noncovalent bonds broken are, of course, unknown (Reproduced from Ref. [37] with permission. © American Chemical Society, 2009)

protein complex. These SAP decamers have been examined by CID at 160 V collision offset and by SID at 120 V offset. CID and SID spectra using the instrument shown in Fig. 9.10 reveal different product ion distributions (Fig. 9.12) [40]. However, the CID spectra of the two decamers are almost identical while their SID spectra show marked differences that help in distinguishing the complexes.

9.5 Tandem MS on TOF Instruments

9.5.1 Utilizing a ReTOF for Tandem MS

Consider an ion m_1^+ decomposing in transit through a field-free region. Its kinetic energy is distributed among the product ion m_2^+ and the neutral fragment n according to their relative contribution to the mass of the precursor ion:

$$E_{kin(m2+)} = E_{kin(m1+)}\frac{m_{i2}}{m_{i1}} \quad \text{and} \quad E_{kin(n)} = E_{kin(m1+)}\left(1 - \frac{m_{i2}}{m_{i1}}\right) \tag{9.10}$$

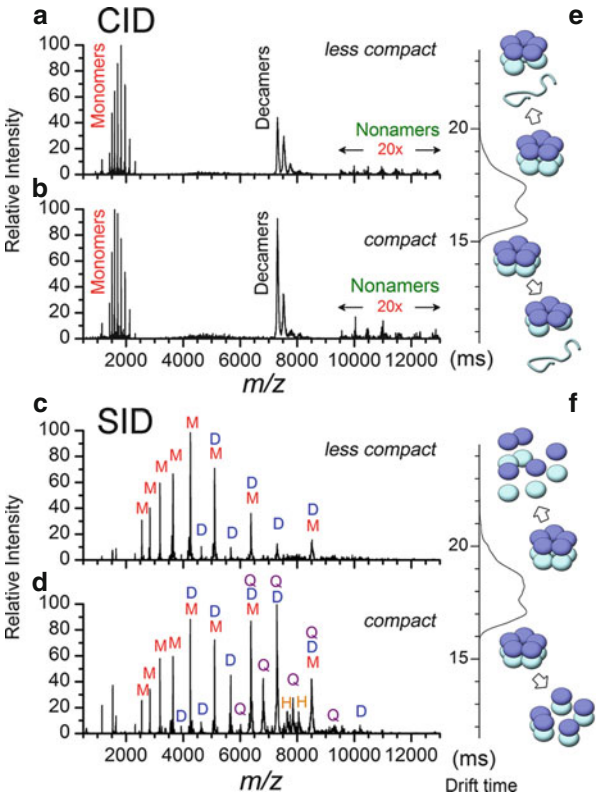

Fig. 9.12 Fragment ion spectra of SAP decamers. (**a**) CID of the less compact and (**b**) the compact decamer at 160 V. (**c**) SID of the less compact and (**d**) the compact decamer at 120 V. Major peaks are labeled in the spectra (*M* monomer; *D* dimer, *Q* tetramer, *H* hexamer). Parts (**e**) and (**f**) show the corresponding IMS drift time distributions with some separation of CID or SID products from less compact and compact SAP decamers and schematic representations for plausible dissociation pathways (Reproduced from Ref. [40] with permission. © American Chemical Society, 2012)

Fragment ions generated on the flight from the ion source to the reflector will have kinetic energies lower than intact precursor ions (Fig. 9.13). While the kinetic energy changes upon dissociation, the ion velocity remains constant, as already noted in the discussion on linear TOF (Sect. 4.2.3). A reflector is capable of handling ions bearing down to 70–90% of the energy to which it has been adjusted (0.7–0.9 × $E_{\mathrm{kin(m1+)}}$). Stepwise reduction of the reflector potential allows acquisition of partial fragment ion spectra each covering several percent of the precursor ion mass [6, 43, 44]. Piecing the data together yields a spectrum of the product ions formed by metastable dissociation of m_1^+. To cover the range from m_1 to 0.1 × m_{i1} the reflector must be stepped down from its potential V_0 to 0.1 × V_0 in some 10–20 increments.

For tandem MS, the ReTOF analyzer itself only provides the field-free region and MS2 of the setup. Without further modification, the metastable dissociations of all potential precursor ion species leaving the ion source would be detected simultaneously and overlapping.

The precursor ion selection (MS1) follows a simple – although technically demanding – principle, i.e., a deflector electrode is placed adjacent to the flight

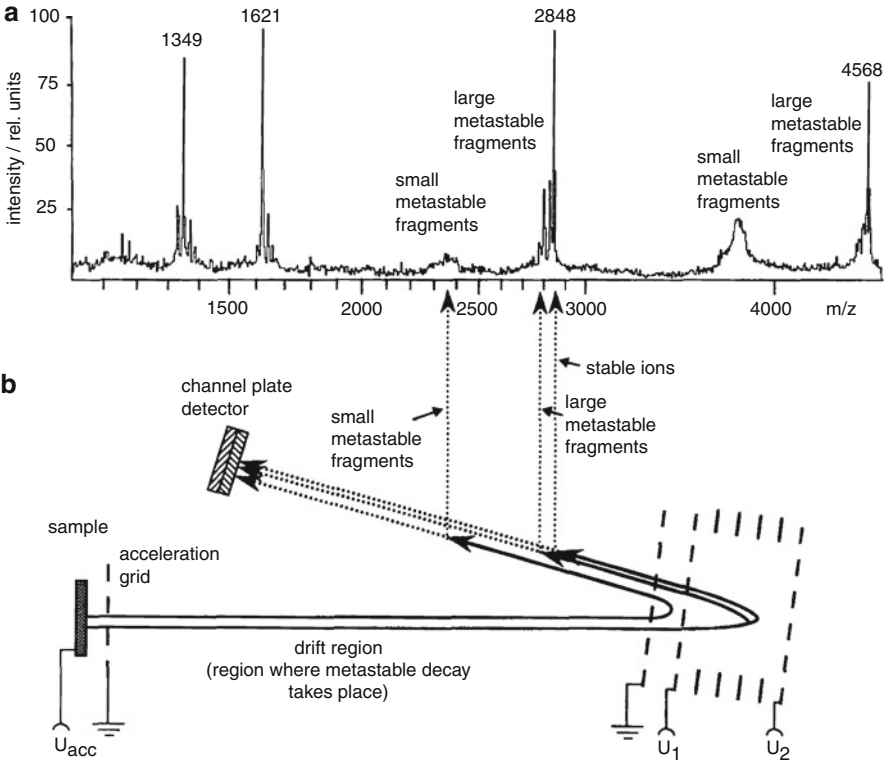

Fig. 9.13 Explanation of PSD fragments in MALDI-ReTOF spectra. (**a**) The occurrence of peaks due to ions of different origin is indicated above the schematic in the MADLI spectrum of a mixture showing $[M+H]^+$ ions of substance P, *m*/*z* 1348, bombesin, *m*/*z* 1621, melittin, *m*/*z* 2848, and ACTH, *m*/*z* 4568. (**b**) The PSD mode translates the diffuse fragment ion peaks into analytically useful signals. While the precursor ion and fragments of closely related mass penetrate deep into the reflector, those ions resulting from larger neutral losses return in the fringe field close to the reflector entry and are not properly focused onto the detector. To make these ions enter the useful reflector region, the reflector potential needs to be stepped down to successively lower values (Reproduced from Ref. [43] with permission. © John Wiley & Sons, Ltd. 1992)

path. To select precursor ions, ions below the selected precursor *m*/*z* value are electrostatically deflected, then the deflector is briefly turned off to transmit the precursor ions, and finally the high voltage is switched on again to deflect ions of higher *m*/*z*. As the deflector gate is located rather close to the ion source, it acts as a short TOF analyzer providing only moderate precursor ion resolution. An early velocity-dependent ion selector has been introduced by Bradbury and Nielsen, thus often called *Bradbury-Nielsen gate* [45]. In modern instrumentation the term *timed ion selector* (TIS) is commonly used for the precursor ion-selecting device. The entire procedure has become known as *fragment analysis and structural TOF* (FAST) [6, 43, 44].

Despite the comparatively poor precursor ion resolution and being a time- and sample-consuming FAST procedure, MS/MS of *post-source decay* (PSD) ions on the ReTOF has been one of the major tools of early MALDI biomolecule sequencing for ions in the m/z 500–3000 range. However, since the advent of tandem TOF instruments, the application of the FAST methodology has become rather rare.

Odd terminology
In particular the MALDI-TOF community has coined some sort of own terminology, e.g., *in-source decay* (ISD) for all fragmentations occurring within the ion source, *post-source decay* (PSD) instead of metastable ion dissociation, and *fragment analysis and structural TOF* (FAST) for the specific mode of operation of a ReTOF to detect metastable ions.

Historic remark on metastable ions in ReTOFs
Methods for the detection of metastable ion dissociations in ReTOF-MS in combination with *secondary ion mass spectrometry* (SIMS) and ^{252}Cf *plasma desorption* (^{252}Cf-PD) mass spectrometry were known before the advent of MALDI [46–49].

9.5.2 Curved-Field Reflectron

The laborious stepwise acquisition of PSD spectra can be avoided by using by the *curved-field reflectron* [50–53]. It offers advantages in speed and simplicity of operation when metastable fragmentations are to be studied, as in peptide sequencing by MALDI-TOF. Shimadzu employs curved-field reflectrons in the Axima series of MALDI-TOF instruments.

The curved-field reflectron extends over a long section of the flight tube, where it creates a nonlinear electric field that increases with its depth by steadily increasing the voltage difference between a comparatively large number of lenses. This type of ion reflector is capable of simultaneously focusing PSD fragments over the entire range of kinetic energies from 0.1–1.0 $\times$ $E_{\mathrm{kin(m1+)}}$. As it acts as a divergent ion mirror, it causes more ion losses as compared to two-stage reflectors.

The curved-field reflectron of a coaxial ReTOF instrument occupies a large portion (D) of the total flight path ($s = l_1 + D$). A prototype instrument used 86 lens elements whose voltages were set by 85 precision potentiometers located between them (Fig. 9.14) [52]. The distance l_1 between ion source and reflector entrance provided a sufficiently field-free flight path for metastable dissociations. To enhance fragmentation of precursor ions via CID, a collision cell can be placed anywhere in the short flight path in front of the precursor ion-selecting gate [53].

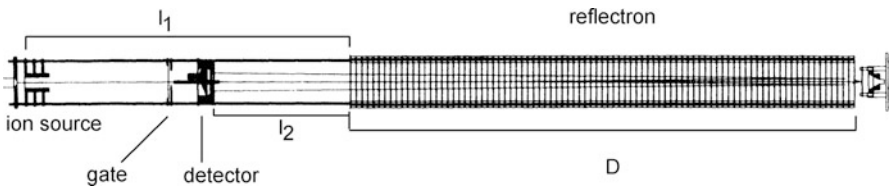

Fig. 9.14 Coaxial curved-field reflectron TOF spectrometer. The total length is about 1 m (Adapted from Ref. [52] with permission. © John Wiley & Sons, 1995)

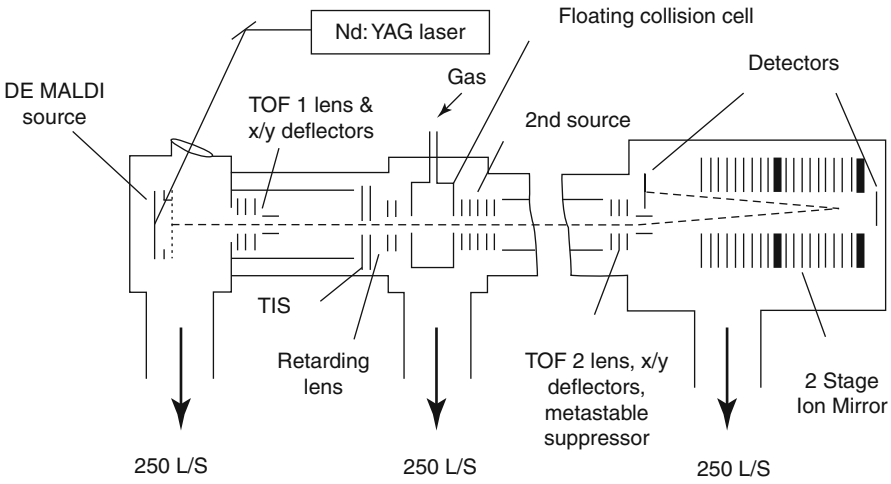

Fig. 9.15 Tandem TOF analyzer with linear TOF1 and ReTOF2. The ions from TOF1 are *m*/*z*-selected by a timed ion selector, decelerated, fragmented by CID, accelerated, and then passed into ReTOF2 (Reproduced from Ref. [54] with permission. © Elsevier Science, 2002)

9.5.3 Tandem MS on True Tandem TOF Instruments

Both limited precursor ion resolution and the need for stepwise acquisition of tandem mass spectra have driven the development of TOF/TOF instrumentation. Here, the MS1 functionality is achieved by a distinguished short linear TOF analyzer delivering ions *m*/*z*-selected by a *timed ion selector* (TIS) to a collision cell from where fragments are accelerated in a well-defined manner into the second flight tube that belongs to a ReTOF system. The first commercial TOF/TOF instruments of that class were available from Applied Biosystems [54] and Bruker Daltonik [55, 56]. Although differing in detail, the basic idea of these TOF/TOF instruments is to operate TOF1 at comparatively low acceleration voltage and to accelerate fragment ions into a high-resolving ReTOF acting as MS2 designed to analyze ions of 20–27 keV kinetic energy (Fig. 9.15).

The lower velocity of precursor ions in TOF1 does not only simplify the operation of the TIS, it also permits sufficient time for the ions to dissociate

(10–20 μs) [56] and it results in a narrow spread of the kinetic energies of the fragment ions arising thereof. After fragmentation, typically enforced by CID [57], the ions are passed into a second acceleration stage located behind the collision cell. By "lifting" all ions by a certain amount of kinetic energy, their relative spread in kinetic energy is reduced. For example, a precursor ion of 5 keV might yield fragments having 0.5–5 keV. Addition of another 15 keV to all fragment ions lifts them to 15.5–20 keV. In fact, the assembly comprising collision cell and acceleration lenses acts like a second DE ion source. Given a reflector of sufficient energy acceptance they can be analyzed without tedious stepping of the reflector voltage. The Bruker system employs 8-keV ions in TOF1 that are accelerated by another 19 kV after collision. For standard MALDI-MS operation, the ions are fully accelerated in the ion source and the TIS–collision cell–LIFT assembly is switched off (grounded). The Applied Biosystems instruments decelerate mass-analyzed ions to 1–2 keV prior to CID and then accelerate them to 20 keV for the ReTOF. Both concepts make use of delayed extraction for each stage and both require a metastable ion suppressor in the tube between collision cell and reflector. The metastable ion suppressor deflects precursor ions having survived the CID cell analogous to the TIS operation, because the 2.FFR metastable ions would otherwise interfere with the spectrum in the same way as shown in Fig. 9.13 [53, 57].

9.6 Tandem MS with Magnetic Sector Instruments

There are multiple ways of detecting metastable and collision-induced dissociations with magnetic sector instruments [13]. In fact, the whole phenomenon of so-called "diffuse peaks" in mass spectra was discovered with this particular type of mass analyzer (Sect. 4.3.2). In the mid-1940s, these broad signals were correctly interpreted as ions decomposing in transit [58, 59]. Metastable ion spectra still represent one of the indispensable tools for studying the mechanism and thermochemistry of ion dissociations [1, 2, 13, 14].

9.6.1 Dissociations in the FFR Preceding the Magnetic Sector

Peaks from metastable ion decompositions are detected at non-integral m/z values. Instead, the peak corresponding to a fragment m_2^+ formed from m_1^+ upon decomposition in the field-free region in front of the magnetic sector is located at a magnet setting m* which is described by the relationship $m^* = m_2^2/m_1$ [58, 59]. This is because dissociation in a *field-free region* (FFR) not only causes partitioning of ion kinetic energy (Eq. 9.10), but also goes with partitioning of momentum p

$$p_{(m2+)} = p_{(m1+)}\frac{m_{i2}}{m_{i1}} \tag{9.11}$$

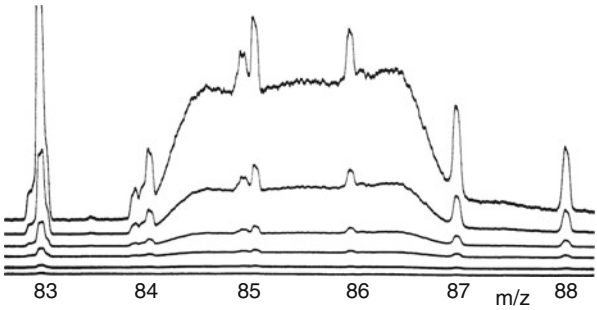

Fig. 9.16 Peak due to metastable NO loss of the *o*-nitrophenol molecular ion. The multiple traces correspond to different amplifier settings of a multi-channel recorder (Adapted from Ref. [60] with permission. © Verlag der Zeitschrift für Naturforschung, 1965)

Due to conservation of velocity, i.e., $v_1 = v_2 \equiv v$, the momentum of a fragment ion m_2^+ formed in a FFR preceding the magnetic sector is different from that of such a fragment ion arising from the ion source. The ion formed by metastable ion dissociation thus passes the magnet as if it had the virtual mass m*

$$m* = \frac{{m_2}^2}{m_1} \tag{9.12}$$

This explains "diffuse" peaks at fractional m/z values in the B scan spectra of B and EB instruments as a result of metastable ion dissociations [58, 59]. In turn, the mass spectra obtained from BE instruments do not show any metastable ion peaks in normal operation.

Observation of a very broad peak The metastable decay of the *o*-nitrophenol molecular ion, m/z 139, by loss of NO to yield the $[M–NO]^+$ ion, m/z 109, has been studied on a single-focusing magnetic sector instrument (Fig. 9.16) [60]. The mass spectrum shows a flat-topped peak of low intensity expanding over three mass units. Some minor and narrow "regular" peaks corresponding to fragment ions formed within the ion source are observed beside and on top of it. The peak due to the metastable dissociation is centered at m/z 85.5 which can be explained by the simple calculation $m* = {m_2}^2/m_1 = 109^2/139 = 85.5$.

9.6.2 Mass-analyzed Ion Kinetic Energy Spectra

Mass-analyzed ion kinetic energy spectra (MIKES) [61, 62] can be measured on BE geometry instruments only. The precursor ion is selected by the magnet and the fragments from dissociations of m_1^+ in the 2.FFR are analyzed by the ESA due to their kinetic energy. This is possible because the kinetic energy of the precursor is distributed among the product ion and the neutral. Derived from Eq. 9.10 we have

$$\frac{E_2}{E_1} = \frac{m_{i2}}{m_{i1}} = \frac{m_{i2}v^2}{m_{i1}v^2} \tag{9.13}$$

Thus, scanning of the electric field (E scan) yields an energy spectrum which allows for the determination of the *kinetic energy release* (KER) from the peak width. The MIKE technique provides good precursor ion resolution, but poor product ion resolution due to the influence of KER on peak shapes.

Abscissa of MIKE spectra
In MIKES E_1 represents the full electric field necessary to transmit the precursor ion m_1^+ through the ESA, and E_1 is often denoted as starting value E_0. Then, the abscissa of MIKE spectra is divided into units of $E/E_0 = m_2/m_1$.

9.6.3 Determination of Kinetic Energy Release

We just saw that peaks due to metastable ion dissociations are much broader than "regular" peaks (Fig. 9.16). In Sect. 2.8 we dealt with the *activation energy of the reverse reaction*, E_{or}, and *energy partitioning* as the thermochemical reasons for the occurrence of *kinetic energy release* (KER). The peak broadening is caused by the kinetic energy from KER grafted onto the kinetic energy of the ion beam as it passes through the mass analyzer. Due to the free rotation of the dissociating ion, there is no preferred orientation of this superimposed motion. Given a suitable experimental setup of the analyzer system that allows to obtain a kinetic energy spectrum, the x-component of KER, i.e., along the flight axis, can be calculated from the peak width of metastable ion decompositions. *Mass-analyzed ion kinetic energy spectrometry* (MIKES) is an established technique for doing so (Fig. 9.17). The peak width at half height is related to KER by [13, 14]:

$$T = \frac{m_2 U_b \ e}{16n} \left(\frac{\Delta E}{E}\right)^2 \tag{9.14}$$

where T is the average kinetic energy released, m_2 is mass of the fragment ion, n the mass of the neutral, U_b the acceleration voltage, e the electron charge, E gives the position and ΔE the width of the peak on the kinetic energy scale. Correction of the width of the metastable peak, w_{50meta}, for the width of the main beam, w_{50main}, should be applied for smaller values of T [63, 64]:

$$w_{50corr} = \sqrt{{w_{50meta}}^2 - {w_{50main}}^2} \tag{9.15}$$

KER of McLafferty rearrangements The observed KER values and also peak shapes may change dramatically as E_{0r} decreases (Fig. 9.17). In the McLafferty rearrangement of immonium ions (Sect. 6.12.1) the leaving alkene grows from

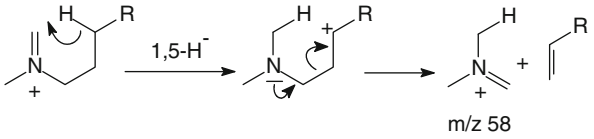

Scheme 9.1

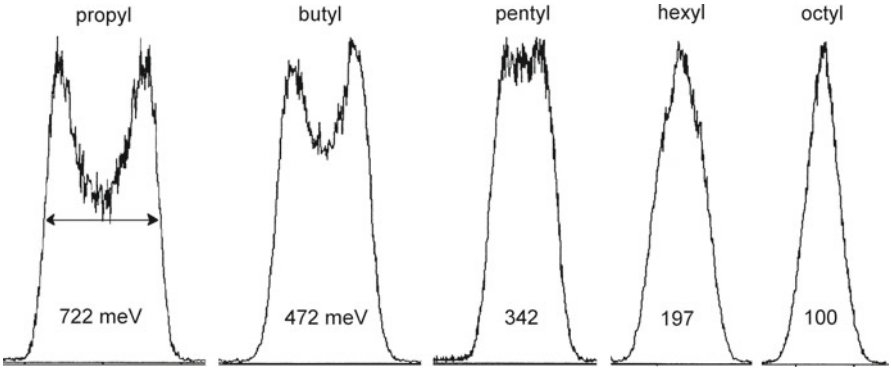

Fig. 9.17 Effect of decreasing E_{0r} on KER. The peaks from MIKE measurements result from the m/z 58 ion product ion of alkene loss via McL (ethene to hexene) from homologous iminium ions. The KER is determined from peak width at half height

ethene to hexene as the substituent varies from propyl to octyl. Nonetheless, the mechanism of the reaction by which the product ion at m/z 58 is formed remains unaffected [65] (Scheme 9.1).

Adjusting to an established standard
Before performing KER measurements, a "calibration" of the instrument (al parameters) against a well-established standard is recommended. Allylmethylether molecular ions, for example, decompose to yield three peaks of different shape and position in the spectrum [65–67].

9.6.4 B/E = *Const.* Linked Scan

Ions decomposing in the 1.FFR of BE and EB instruments can be detected using the $B/E = const.$ linked scan [68]. Due to the proportionality of B and p ($r_m = mv_i/qB$) ions are transmitted through the magnet if

$$\frac{B_2}{B_1} = \frac{m_2 v}{m_1 v} = \frac{p_2}{p_1} = \frac{m_2}{m_1} \tag{9.16}$$

where m_1 and m_2 denote the masses of the precursor and the product ion and v is their equal velocity. For their subsequent passage through the ESA, Eq. 9.13 has to be satisfied. Therefore, we have for the passage through both fields

$$\frac{B_2}{B_1} = \frac{E_2}{E_1} = \frac{m_2}{m_1} \tag{9.17}$$

which defines the conditions for a scan as $B/E = const.$ Thus, B and E have to be scanned together, i.e., in a *linked* fashion. The $B/E = const.$ linked scan provides good fragment ion resolution (R ≈ 1000) but poor precursor ion resolution (R ≈ 200). As with all linked scans, there is a risk of artefact peaks [69–72] because linked scan techniques represent no true tandem MS where MS1 and MS2 are clearly separate. The use of two complementary scan modes is therefore suggested to avoid ambiguities [70].

9.6.5 Additional Linked Scan Functions

Whereas TOF instruments solely allow for the detection of product ions of a selected precursor, sector instruments offer additional modes of operation: (*i*) to exclusively identify product ions of a particular precursor ion, so-called *precursor ion scans* [73, 74], or (*ii*) to detect only ions formed by loss of a specific neutral mass, so-called *constant neutral loss* (CNL) scan [75]. This can be achieved by some technically more demanding linked scans (Table 9.2) [76–79].

Table 9.2 Common scan laws for the detection of metastable ion dissociations on magnetic sector mass spectrometers

Selected mass	Scan law	KER from peak width?	Analyzer and FFR	Properties
m_1	$B = B_{m1}$, and $E/E_0 = m_2/m_1$	Yes	BE 2.FFR	Mass-analyzed ion kinetic energy spectrum (MIKES), E is scanned
m_1	$B/E = B_{0(1)}/E_0$ i.e., $B/E = const.$	No	BE or EB 1.FFR	Linked scan, poor precursor but good product ion resolution
m_2	$B^2/E = B_2{}^2/E_0$ i.e., $B^2/E = const.$	Yes	BE or EB 1.FFR	Linked scan, poor product but good precursor ion resolution, demands precise control of B
m_2	$B^2 \times E = B_{0(2)} \times E_0$ i.e., $B^2 \times E = const.$	No	BE 2.FFR	Linked scan, resolution controlled by that of B, needs precise control of B
m_n	$(B/E) \times [1–(E/E_0)]^{1/2}$ i.e., $E/E_0 = m_2/m_1 = 1–(m_n/m_1)$	No	BE or EB 1.FFR	Constant neutral loss (CNL), linked scan

All scans listed use constant acceleration voltage U. Scanning of U offers additional scan modes. However, scanning of U over a wide range causes detuning of the ion source

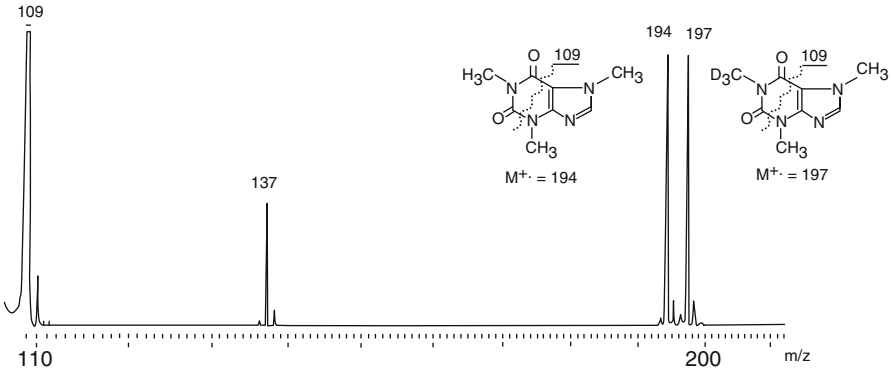

Fig. 9.18 CID B^2E spectrum of the ion m/z 109 of a caffeinated softdrink (cola) with $[D_3]$caffeine as internal standard. Different brands yielded 73–158 mg l^{-1} (Adapted from Ref. [80] with permission. © John Wiley & Sons, 1983)

Analytical use of the $B^2E = const.$ linked scan The $B^2E = const.$ linked scan [74] has been employed to quantify the caffeine content of coffee, black tea, and caffeinated softdrinks [80]. Caffeine, $M^{+\bullet} = 194$, was determined by spiking the sample with a known concentration of $[D_3]$caffeine, $M^{+\bullet} = 197$, as internal standard. Both molecular ions dissociate to form a fragment ion at m/z 109 which was selected as m_2^+. Then, the precursor ion scan showed both molecular ion, m_1^+ and $[D_3]m_1^+$, as precursor of the ion at m/z 109. The ratio of peak intensities was taken as a measure for the relative concentration of analyte and labeled standard (Fig. 9.18). A modern approach would certainly involve a triple quadrupole instrument (Sect. 9.7).

Scan into the past?
Precursor ion scanning suggests some sort of measuring into the past. One should be aware that also in precursor ion scans the product ions are detected, but this is accomplished in a way that only fragments of a selected precursor ion mass can reach the detector, hence the term.

9.6.6 Multi-sector Instruments

Multi-sector instruments, typically four-sector machines, were developed in the 1980s to combine high precursor ion resolution with high fragment ion resolution [81, 82]. Their major field of application was sequencing of biomolecules by

FAB-CID-MS/MS. Commercial representatives are (were) the JEOL HX110/HX110A (EBEB), the JEOL MStation-T (BEBE), or the Micromass AutospecT (EBEBE). Today, all types of hybrid instruments have replaced these impressing "dinosaurs" weighing some 4–5 tons and having about 3 × 5 m footprint. A few custom-built four-sector instruments are still being used in laboratories devoted to gas-phase ion chemistry [83].

FAB and peptide sequencing The FAB-CID-MS/MS spectrum of thymosin-T1 $[M+H]^+$ ions, m/z 1427.7, as obtained from a magnetic four-sector instrument [84] shows numerous fragment ions due to *N*-terminal, *C*-terminal, and internal fragmentations (Fig. 9.19) [85]. It would be almost impossible to obtain sequence information from such a spectrum without generalizing rules to follow [86–91]. The most abundant ions obtained from the fragmenting peptide ion usually belong to six series named **a**, **b**, and **c** if the proton (charge) is kept in the *N*-terminus or **x**, **y**, and **z**, respectively, where the proton is located in the *C*-terminal part. Within each series the mass difference should only be one amino acid. Ideally, one can then count down the amino acids.

Tandem MS for mixtures
One of the advantages of MS/MS techniques is that they do not require the full isolation of all compounds of interest, because the precursor ion selection of MS1 excludes accompanying ions from contributing to the CID spectrum of the actually selected precursor ion as acquired by MS2 (Sect. 14.7).

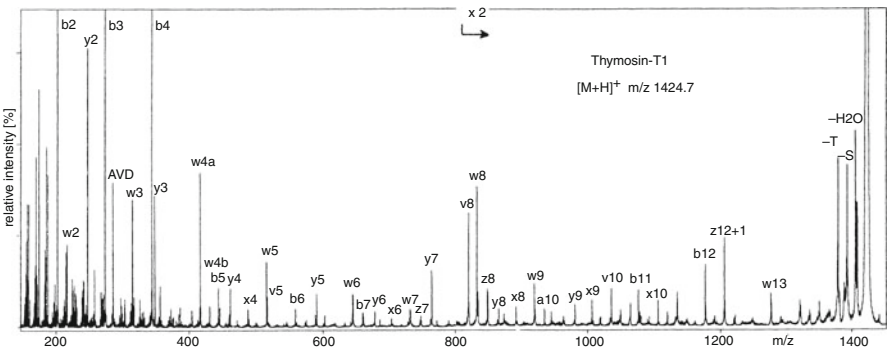

Fig. 9.19 FAB-CID tandem mass spectrum of thymosin-T1 $[M+H]^+$ ions, m/z 1427.7 (Reproduced from Ref. [85] by permission. © American Chemical Society, 1993)

9.7 Tandem MS with Linear Quadrupole Analyzers

9.7.1 Triple Quadrupole Mass Spectrometers

Triple quadrupole mass spectrometers, QqQ, are becoming a standard analytical tool for GC-MS/MS and LC-MS/MS applications, in particular for cases where accurate quantitation is desired (Sect. 14.3). Ever since their introduction [92–94], they have continuously been improved in terms of mass range, resolution, and sensitivity [95–97]. In early triple quadrupole mass spectrometers, Q_1 served as MS1, followed by an intermediate RF-only quadrupole, q_2, acting as "field-free region" with ion-guiding capabilities for metastable dissociations or more often as collision cell for CID experiments, and finally Q_3 to analyze the fragment ions exiting from q_2 (Fig. 9.20). The transition of ions through the QqQ instrument is normally supported by Einzel lenses in the gaps separating the quadrupoles [98, 99].

Guidance requested
Collision cells of simple short tube design like in tandem TOF or magnetic sector instruments (Sect. 9.3.1) cannot be combined with quadrupoles since the ions are rather dispersed at the exit and would be lost upon further collisional scattering.

In recent instruments, the collision region between MS1 and MS2 is not anymore an RF-only quadrupole, but a hexapole or octapole due to their steeper potential well (Sect. 4.4.4), which greatly improves their ion-guiding capabilities as compared to a true quadrupole. Today, most "triple quadrupole instruments" essentially

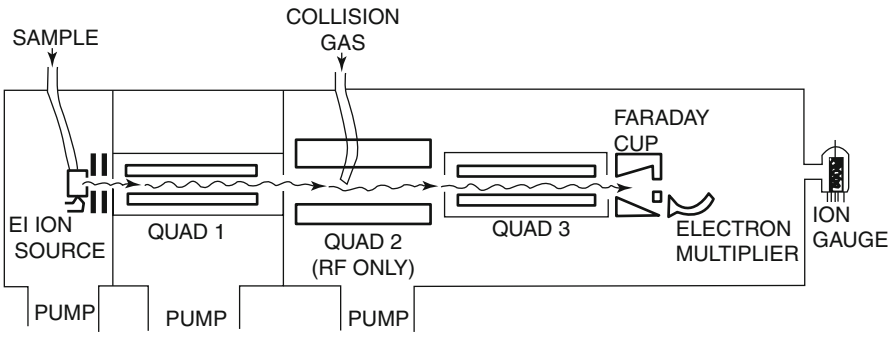

Fig. 9.20 Schematic of an early triple quadrupole mass spectrometer (QqQ) (Reproduced from Ref. [93] with permission. © Elsevier Science, 1979)

present QhQ or QoQ designs. Since the introduction of the *traveling wave ion guide* (TWIG, Sect. 4.10.2), there are also instruments featuring a Q-TWIG-Q geometry like the Waters Xevo TQ-XS or the Waters Vion IMS-Q-TOF.

In MS/MS operation, the mass-selected ions emerging from Q_1 are accelerated into the ion guide collision cell by a potential offset of typically 5–50 V where the collision gas (N_2, Ar) is provided at a pressure of 0.1–0.3 Pa. Careful optimization of all parameters allows for major improvements of CID efficiency and resolution [100]. If MS/MS is not intended, either Q_1 or Q_3 may be set to RF-only mode, thereby reducing its function to that of a simple flight tube with ion-guiding capabilities. The instrument then behaves as though it was a single quadrupole mass spectrometer.

QqQ in "normal" scanning
At first sight, there is no difference whether Q_1 or Q_3 is switched to RF-only for MS mode. However, for EI it seems better to operate Q_3 in RF-only mode. Otherwise, the ion source would effectively extend up to the entrance of Q_3 making fragment ions more abundant due to elongated time for dissociations. Soft ionization methods do not show such differences.

9.7.2 Scan Modes for Tandem MS with Triple Quadrupole Instruments

In triple quadrupole instruments Q_1 and Q_3 are operated independently as MS1 and MS2, respectively, making MS/MS straightforward. The experimental setups for product ion, precursor ion, and neutral loss scanning are summarized in Table 9.3 and depicted in Fig. 9.21. Definitely, this instrument class offers the most easily understandable tandem MS modes of operation.

Table 9.3 Scan modes of triple quadrupole instruments

Scan mode[a]	Operation of Q_1	Operation of q_2	Operation of Q_3
Product ion, define m_1	No scan, select m_1	Metastable or CID	Scan up to m_1 to collect its fragments
Precursor ion, define m_2	Scan from m_2 upwards to cover potential precursors	Metastable or CID	No scan, select m_2
Constant neutral loss, define n	Scan desired range	Metastable or CID	Scan range shifted by Δm to low mass

[a]Masses for reaction $m_1^+ \rightarrow m_2^+ + n$

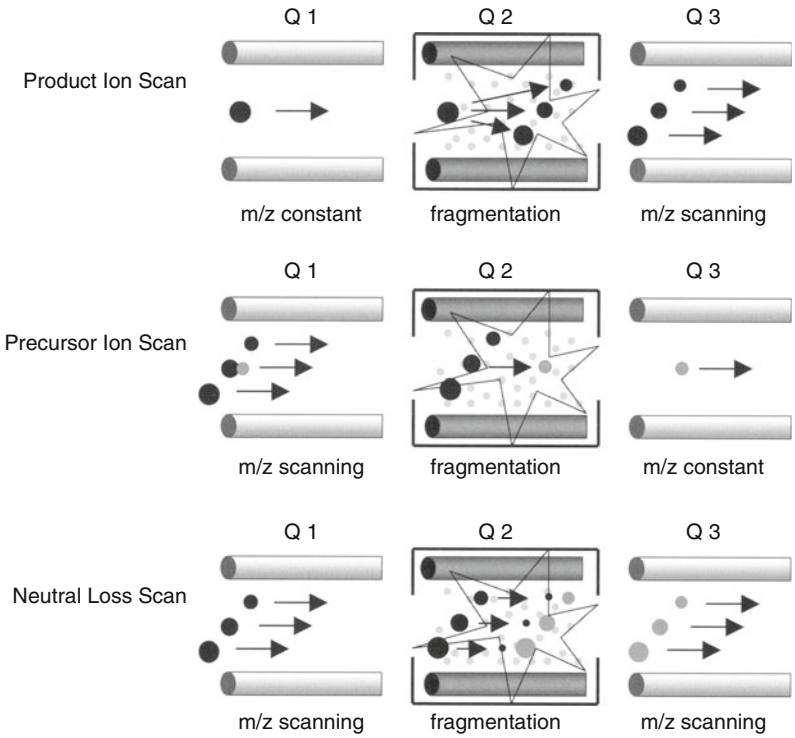

Fig. 9.21 Scan modes of triple quadrupole mass spectrometers (Adapted from Ref. [101] with permission. © Springer-Verlag, 2004)

9.7.3 Penta Quadrupole Instruments

The concept of the triple quadrupole instrument may be expanded by adding another RF-only quadrupole and a third mass-analyzing quadrupole to build a QqQqQ instrument. The penta quadrupole represents one of the rare tandem-in-space concepts to achieve MS^3. A commercial penta quadrupole instrument has once been offered by Extrel, but remained fairly exotic. Nonetheless, the penta quadrupole instrument may serve as a versatile tool for the study of gas phase ion chemistry and in particular ion–molecule reactions [102–105]. For the latter application the effective spatial separation of the zone with neutral reagent from that of preparation of the *m*/*z*-selected precursor ion presents a clear advantage over tandem-in-time concepts.

9.8 Tandem MS with the Quadrupole Ion Trap

Ion traps are *tandem-in-time* instruments, i.e., they perform the steps of precursor ion selection, ion activation, and acquisition of fragment ion spectra in the very same place. This advantageous property allows the multiple use of a single QIT to perform not only MS^2 but also MS^3 and higher order MS^n experiments – indeed a very economic concept. Depending on the abundance of the initial precursor ion, its fragmentation behavior – and of course, on the performance of the QIT – MS^6 experiments are possible [106].

In the QIT, MS^n is accomplished by using appropriate scan functions for the fundamental RF and the auxiliary modulation voltage (Sect. 4.6.7) [106–108]. At a sufficient level of sophistication, e.g., by combining slow and fast forward and reverse RF voltage scans with suitable settings of the auxiliary voltage, monoisotopic precursor ions can even be isolated in case of triply charged ions (Figs. 9.22 and 9.23) [109]. The resonance excitation provided by moderate

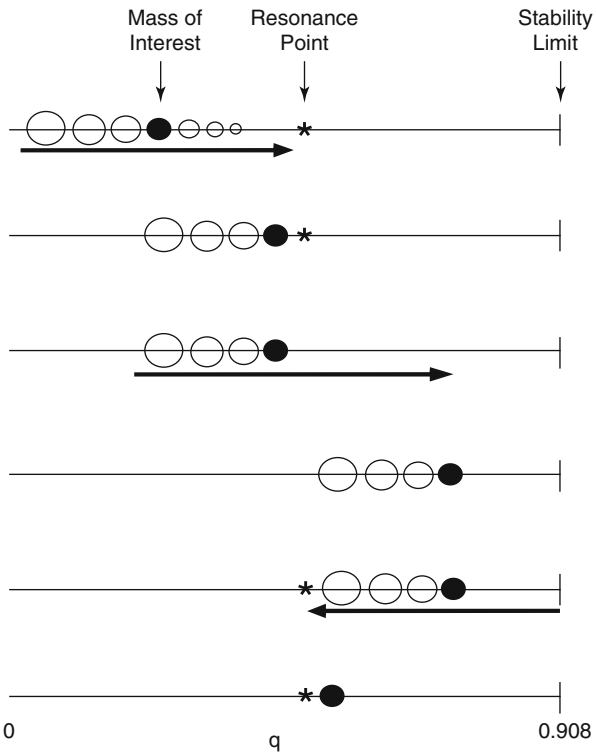

Fig. 9.22 The principle of isolation of a precursor ion by using forward and reverse scanning of a QIT. Ions smaller than the precursor are ejected by exciting them above the stability limit at $q = 0.908$, then settings are changed so that reduction of the RF amplitude causes ejection of the heavier ions (Reproduced from Ref. [109] with permission. © John Wiley & Sons, 1992)

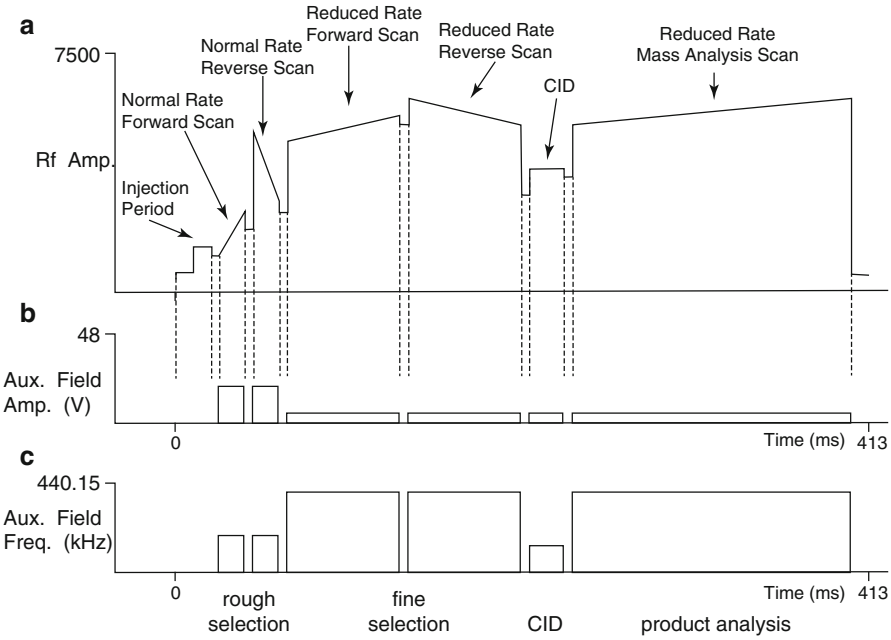

Fig. 9.23 Sequence of changes of (**a**) RF amplitude, (**b**) auxiliary voltage amplitude, and (**c**) auxiliary voltage frequency to first achieve a rough precursor ion selection, then a fine selection by repetition at slow rates, followed by CID, and product ion scan (Adapted from Ref. [109] with permission. © John Wiley & Sons, 1992)

auxiliary voltages can be employed to effect low-energy CID of the trapped ions due to activating collisions with the buffer gas [110], i.e., no additional collision gas is required in a QIT. A full description of the numerous approaches to continuously improving scans can be found in the literature [109, 111–116].

Unfortunately, there is one major disadvantage of QITs for fragment ion analysis in that they cannot simultaneously store ions over the full *m*/*z* range. It is a commonly accepted property of QITs to loose ions below an *m*/*z* value of about one third of the precursor ion. This phenomenon is known as *low-mass cutoff* (LMCO) [116].

Tandem MS on a QIT The positive-ion electrospray tandem mass spectrum of the $[M+2H]^{2+}$ ion of the β-casein tryptic phosphopeptide FQpSEEQQQTEDELQDK was obtained on a Bruker Esquire 3000 quadrupole ion trap (Fig. 9.24) [101]. Sequential amino acid residue losses from both terminal ends of the peptide are labeled according to the b- and y-ion nomenclature. Due to the phosphoserine, the C- and N-terminal peptide ions ($b_3 - b_{15}$ and $y - y_{14}$) exhibit an increase of 80 u

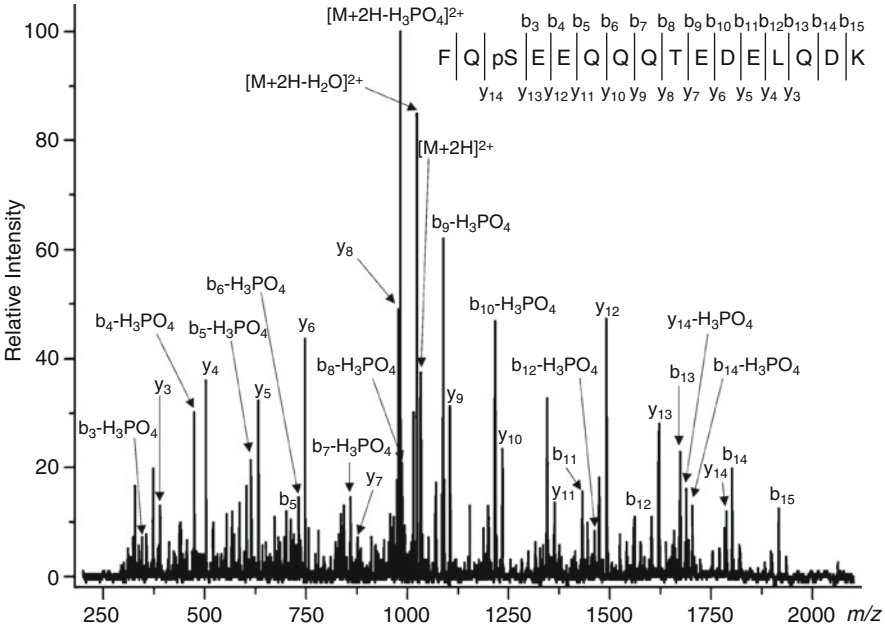

Fig. 9.24 Positive-ion electrospray tandem mass spectrum of the $[M+2H]^{2+}$ ion of the β-casein tryptic phosphopeptide FQpSEEQQQTEDELQDK as obtained upon HPLC coupling to a quadrupole ion trap (Reproduced from Ref. [101] with permission. © Springer-Verlag, 2004)

in mass as compared to the unphosphorylated form. In addition, most ions are accompanied by the corresponding fragments from H_3PO_4 loss (98 u).

QIT for MS^n MS^4 on a QIT was used for the identification of beauverolides, cyclic peptides from the fermentation broth of *Beauveria bassiana*, a pathogenic fungus of insects [117]. All MS^n (ESI-CID-QIT) experiments started from singly charged $[M+H]^+$ precursor ions (Fig. 9.25).

Limitation of tandem-in-time

In contrast to tandem-in-space instruments, tandem-in-time instruments neither support precursor ion nor constant neutral loss scanning. While product ion scans just need a precursor to be isolated prior to its fragmentation, both precursor ion and constant neutral loss scan rely on the simultaneous application of selection plus scanning or double scanning, respectively. Fulfilling two criteria at the same time requires two distinct analyzers at work.

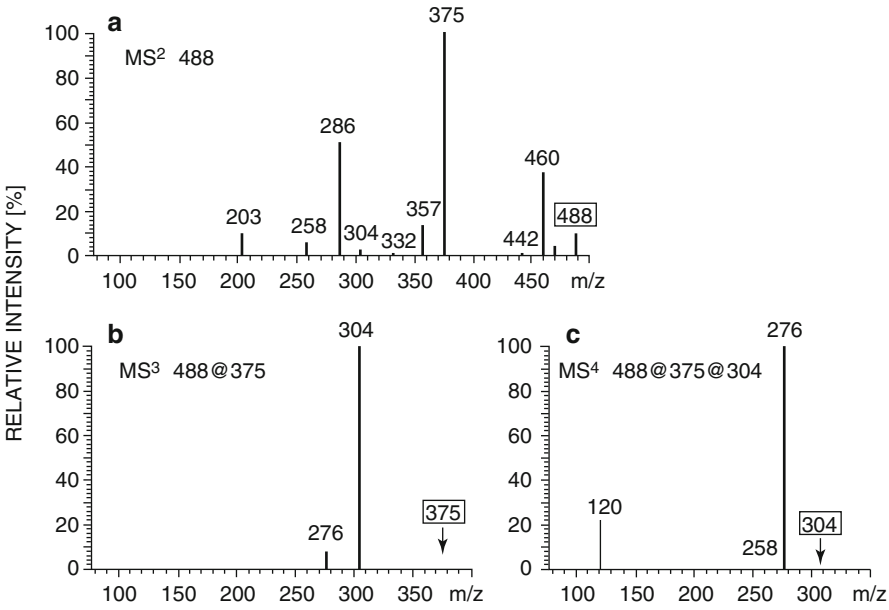

Fig. 9.25 Sequence of ESI-CID-QIT mass spectra of a beauverolide: (**a**) MS^2 of $[M+H]^+$, *m/z* 488, selected out of a full scan spectrum, (**b**) MS^3 of *m/z* 375 selected from (**a**), and (**c**) MS^4 of *m/z* 304 selected from (**b**) (Adapted from Ref. [117] by permission. © John Wiley & Sons, 2001)

9.9 Tandem MS with Linear Quadrupole Ion Traps

Mass spectrometers incorporating a linear quadrupole ion trap are highly flexible instruments. As discussed in Sect. 4.5, there are two competing concepts available on the market, one employing a LIT with axial ejection as part of a hybrid instrument [118], and another, featuring a pure LIT design with radial ejection [119, 120].

9.9.1 Tandem MS on QqLIT Instruments

The QqLIT design basically presents a triple quadrupole instrument having Q3 exchanged for a linear ion trap. As such, it offers all scan modes and properties typical for QqQ instruments (Sect. 9.7) plus those additional ones that are enabled by the LIT, i.e., higher-order tandem MS and combinations of ion accumulation and subsequent scanning for enhanced sensitivity (Fig. 9.26) [118, 121–123].

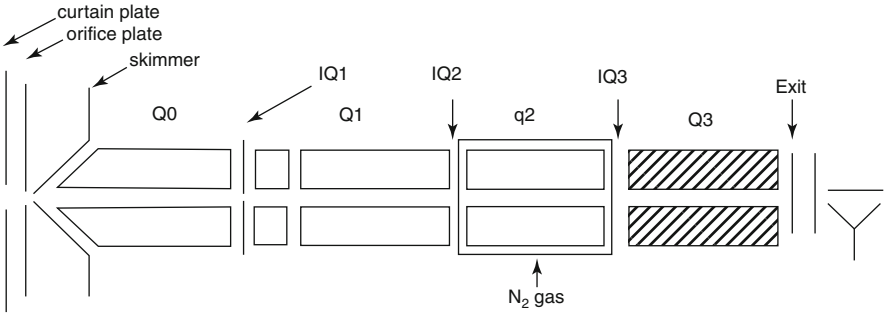

Scan Type	Q1	q2	Q3
Q1 Scan	Resolving (Scan)	RF-only	RF-only
Q3 Scan	RF-only	RF-only	Resolving (Scan)
Product Ion Scan (PIS)	Resolving (Fixed)	Fragment	Resolving (Scan)
Precursor Ion Scan (PI)	Resolving (Scan)	Fragment	Resolving (Fixed)
Neutral Loss Scan (NL)	Resolving (Scan)	Fragment	Resolving (Scan Offset)
Selected Reaction Monitoring mode (SRM)	Resolving (Fixed)	Fragment	Resolving (Fixed)
Enhanced Product Ion (EPI)	Resolving (Fixed)	Fragment	Trap/scan
MS3	Resolving (Fixed)	Fragment	Isolation/frag trap/scan
Time delayed frag capture Product Ion (TDF)	Resolving (Fixed)	Trap/No frag	Frag/trap/scan
Enhanced Q3 Single MS (EMS)	RF-only	No frag	Trap/scan
Enhanced Resolution Q3 Single MS (ERMS)	RF-only	No frag	Trap/scan
Enhanced Multiply Charge (EMC)	RF-only	No frag	Trap/empty/scan

Fig. 9.26 Correlation of the instrumental setup of a QqLIT instrument (Applied Biosystems Q-Trap series) with the description of its various scan modes. The *upper part* of the table lists scan modes that are identical to triple quadrupole instruments, whereas the *lower part* contains those unique to the specific instrument design (Reproduced from Ref. [118] with permission. © John Wiley and Sons, Ltd., 2003)

Elucidating fragmentation pathways The fragmentation pathways of ions of Trocade™, an anti-rheumatoid drug, $[\text{trocade+H}]^+$, m/z 437, were elucidated by sequential tandem MS up to MS^4 on a QqLIT instrument (Fig. 9.27). The protonated molecule first eliminates hydroxylamine, 33 u, to yield the acylium ion fragment at m/z 404, which in turn cleaves off the imidazolidinedione substituent at the α-carbon prior to loss of CO from the fragment ion at m/z 262 [118].

9.9.2 Tandem MS on LITs with Radial Ejection

A single LIT alone offers tandem MS along the tandem-in-time route. Improved trapping efficiency, more effective fragmentation, and trapping can be achieved when the LIT is operated with a higher buffer gas pressure, while higher scan rates

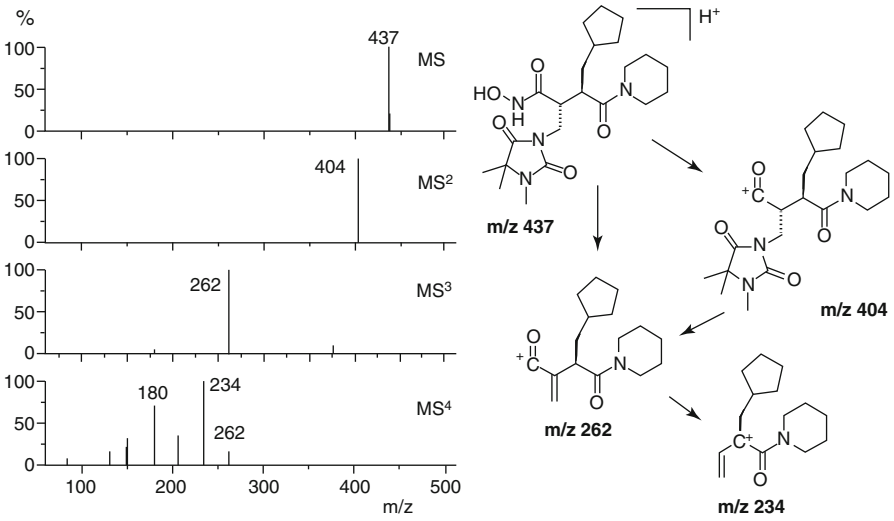

Fig. 9.27 Fragmentation pathways of $[trocade+H]^+$ ions, *m/z* 437, as elucidated by sequential tandem mass spectrometry up to MS^4 on a QqLIT instrument (Adapted from Ref. [118] with permission. © John Wiley and Sons, Ltd., 2003)

and resolving power are obtained at lower pressure. The recent *dual-LIT* design introduced by the Thermo Fisher LTQ Velos™ series unites these requirements by operating two identical LITs in tandem that are connected to the same RF and auxiliary AC power supplies, whereas the DC offset for trapping is delivered separately. Admission of the helium buffer gas into the high-pressure LIT allows to reduce its pressure in the neighboring mass-analyzing LIT (Fig. 9.28) [119]. The functional separation between the LITs not only allows to maintain unit resolution up to a scan rate of 33,000 u s^{-1}, it also more than doubles resolving power of the single-LIT version up to 25,000 when operated at very slow scan rates over a narrow *m/z* range. Such a dual-LIT design has also been incorporated in other hybrid instruments of this manufacturer that make use of LITs as MS1 (LTQ-Orbitrap Velos™ [124], LTQ-FT Velos™).

In space or in time?
With the introduction of QqLIT and dual-LIT instruments, even the concepts of tandem-in-space and tandem-in-time MS start to intermingle, because both tandem characteristics are part of each of these instruments. Once more, this demonstrates the ongoing highly dynamic development of mass spectrometry instrumentation.

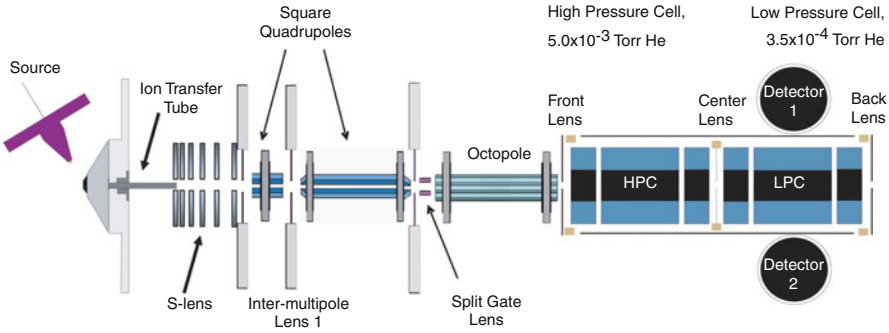

Fig. 9.28 The Thermo Fisher LTQ Velos instruments have a dual linear ion trap, the first section of which is operated at higher pressure (HPC), the second is run at lower pressure to achieve better resolving power (LPC). The dual LIT design also increases the speed of operation, because the first LIT can already prepare ions for the second while this is still mass-analyzing fragments from the previous cycle (Reprinted from Ref. [119] with permission. © American Chemical Society, 2009)

9.10 Tandem MS with Orbitrap Instruments

The Orbitrap analyzer itself does not provide for a mode of tandem MS operation. Instead, the steps of precursor ion isolation and dissociation are performed in a dedicated LIT as MS1 (Sect. 4.8.4) prior to high-resolution and accurate mass analysis of the fragments by the Orbitrap. Multiple-collision CID (Sect. 9.3) in the LIT of the LTQ-Orbitrap instrument is sometimes not hard enough to achieve fragmentation of comparatively stable precursor ions, e.g., it can be insufficient to generate immonium ion fragments from protonated peptides.

9.10.1 Higher-Energy C-Trap Dissociation

One approach towards harsher CID is to use the C-trap as a collision cell simply by raising the RF voltage from the standard setting of 1500 V peak-to-peak to 2500 V. The nitrogen present at about 1.3×10^{-3} mbar is sufficient to serve as the collision gas. After several oscillations, most of the precursor ions have undergone dissociating fragmentation, and all ions accumulate in the middle of the C-trap being confined by voltages on the gate aperture and trapping plate. This procedure has been termed *higher-energy C-trap dissociation* (HCD, Fig. 9.29a) [125]. An increase in RF voltage of the C-trap unfortunately goes along with a decrease in the m/z range that can be stored simultaneously in the C-trap.

These disadvantages are avoided by attaching an RF-only octopole collision cell with nitrogen at 5 mbar to the back end of the C-trap. To use this collision cell the C-trap passes through the ions from the LIT rather than ejecting them directly into the Orbitrap. This octopole collision cell provides fragment trapping over a

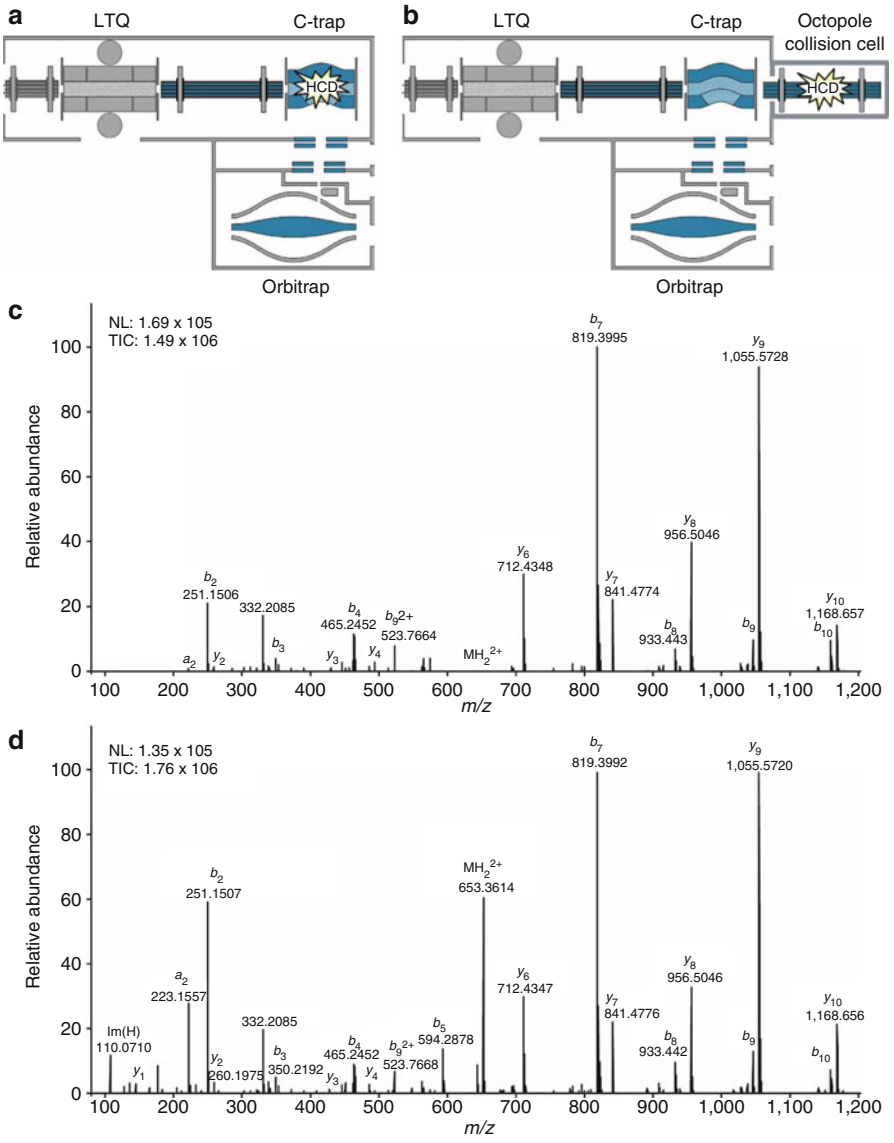

Fig. 9.29 Schematic of the hybrid LIT–Orbitrap instrument indicating the electrostatic potentials used in HCD and comparison of CID spectra. (**a**) HCD operation of the C-trap; (**b**) with an additional dedicated octopole collision cell; (**c**) CID spectrum of peptide $[HLVDEPQNLIK+2H]^{2+}$ ions from HCD as in (**a**); (**d**) spectrum as obtained by setup (**b**). NL: intensity in counts normalized to 1 s; TIC: total ion current (Reproduced from Ref. [125] with permission. © Nature Publishing Group, London, 2007)

wide m/z range. The fragments generated are then filled back into the C-trap, thermalized, and transferred into the Orbitrap for final m/z analysis (Fig. 9.29b) [125]. Such an instrument geometry is being offered as LTQ-OrbitrapXL™.

HCD for peptide ions Peptide ions, $[HLVDEPQNLIK+2H]^{2+}$, m/z 653.36, were selected as precursor ions, accumulated and isolated in the LIT until 10^5 ions were reached. With HCD setup (**a**) spectrum (**c**) was obtained. Using the dedicated octopole collision cell as depicted in (**b**) delivered the spectrum shown as (**d**) that exhibits stronger and more fragment ion signals in the lower m/z range. In particular, the immonium fragment ion of histidine can be observed at m/z 110 (Fig. 9.29) [126].

9.10.2 Extended LIT-Orbitrap Hybrid Instruments

It makes sense to extend the HCD geometry towards the dual-LIT MS1 to arrive at an advanced hybrid instrument design that combines MS^n in several modes with a powerful final m/z analysis [124]. Such an instrument has become available in the form of the Thermo Fisher LTQ Orbitrap Velos (Fig. 9.30). One of the most important advantages of this instrumentation is speed for proteomics analysis, e.g., within 1.0 s the dual-LIT can deliver five complete tandem mass spectra simultaneously with the Orbitrap running one high-resolution accurate mass scan of the whole m/z range.

Parallelized tandem MS in proteomics The coverage of the analyzed proteome and the identification of peptides have been strongly coupled to the detection limits and spectral acquisition rates of mass spectrometers. The spectral acquisition rate is primarily limited by the duration of the ion accumulation and analysis steps. Extensive parallelization of the acquisition process using a Q-Orbitrap-tandem LIT analyzer (Orbitrap Fusion tribrid, Sect. 4.9) significantly increases the spectral acquisition rate [127, 128]. The instrument's architecture permits a multitude of

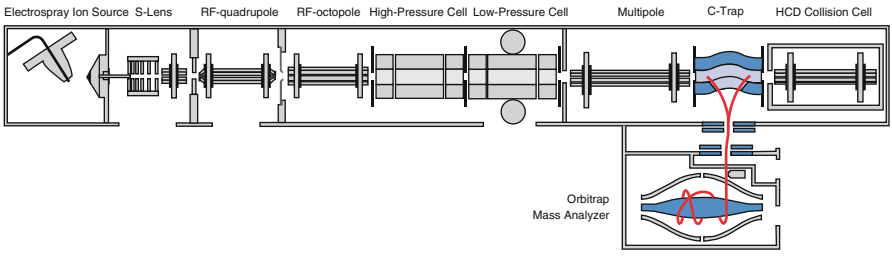

Fig. 9.30 Schematic of the Thermo Scientific LTQ Orbitrap Velos hybrid FT mass spectrometer combining dual-LIT and HCD with an Orbitrap analyzer (Courtesy of Thermo Fisher Scientific, Bremen)

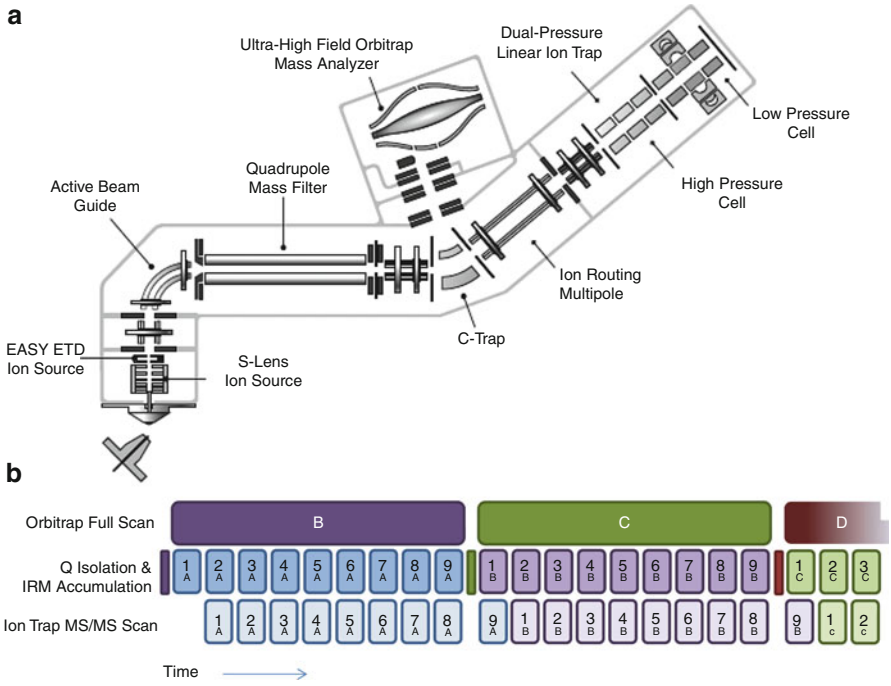

Fig. 9.31 Three processes running in parallel on the Orbitrap Fusion Lumos tribrid mass spectrometer. (**a**) Schematic of the instrument, (**b**) parallelized operation of three modes. The high-resolution accurate mass full scan of the Orbitrap takes several times longer (0.5 s) than precursor ion selection by the quadrupole and subsequent fragmentation plus fragment ion analysis in the tandem LIT (each ca. 0.06 s). The *darker-colored narrow* bars in the second row mark the ion accumulation for the Orbitrap, whereas ion accumulation for MS/MS takes longer to provide a larger precursor ion population to the tandem LIT (Reprinted with kind permission from Thermo Fisher. © Thermo Fisher Scientific, Bremen, 2015)

operational modes that allow tandem MS experiments to be run in parallel while a full range survey scan delivers accurate mass data of the next package of precursors to be interrogated (Fig. 9.31). This mode delivers survey spectra at about 2 Hz and tandem mass spectra of selected precursor ions at 15–20 Hz.

9.11 Tandem MS with FT-ICR Instruments – Part I

As ion trapping devices, FT-ICR mass spectrometers belong to the *tandem-in-time* class of instruments. Precursor ion selection (MS1) is accomplished by selectively storing the ions of interest, whereas all others are ejected by means of a suitably tailored excitation pulse. For this purpose, the SWIFT technique [129] or *correlated sweep excitation* (CHEF) [130, 131] are used (Sect. 4.7.7). Both methods generate

tailored waveforms that cause excitation of all but the selected ions. Like QITs and LITs, FT-ICR analyzers are also capable of MS^n.

Although hybrid designs such as Qh-FT-ICR or LIT-FT-ICR are prevalent in modern FT-ICR instrumentation (Sects. 4.7.11 and 4.9.1), there is still the need for tandem MS experiments inside the ICR cell. Its dedicated abilities of very precise precursor ion selection, elongated ion storage in the order of tens of seconds, and possibility to admit gaseous reactants to perform even slow ion-molecule reactions make the ICR cell a unique tool [3].

9.11.1 Sustained Off-Resonance Irradiation-CID in ICR Cells

CID still is widely used as an activation technique for tandem MS in FT-ICR instruments. The collision gas is admitted into the ICR cell through a pulsed valve. To avoid detrimental effects of the collision gas on the ultra-high vacuum of the ICR cell ($\approx 10^{-10}$ mbar) the gas is admitted from a low pressure vessel ($\approx$10 mbar) in short pulses (5–50 ms). While the admitted gas causes the cell pressure to rise ($\approx 10^{-8}$ mbar), this still does not diminish the resolving power and mass accuracy of FT-ICR to an extent that would negatively affect this type of experiment. To further reduce the interference with collision gas, a pump delay (1–5 s) can be inserted between CID and m/z analysis. Generally, a set of such cycles is accumulated to obtain a spectrum.

For effective dissociation, CID requires that the ions collide sufficiently fast with the collision gas. The increase in ion kinetic energy is classically effected by short (0.1–0.5 ms) excitation at the cyclotron frequency of the precursor ion [132, 133]. This is known as *resonance excitation* (RE). The uptake of kinetic energy by resonance excitation occurs very fast, and thus, care has to be taken to avoid ion ejection from the cell. On the other hand, RE offers access to fragmentation channels requiring comparatively high activation energy.

Nowadays, *sustained off-resonance irradiation* (SORI) has established as the standard CID method in FT-ICR [134, 135], although there are others of comparable effect [136, 137]. Irradiating slightly off resonance ($\Delta\nu \approx 1\%$ or 500–1500 Hz) makes ions undergo acceleration–deceleration cycles throughout the duration of the RF pulse (Fig. 9.32). The principle behind off-resonance irradiation is the occurrence of a beat frequency f_b induced by the alternating positive and negative interference of cyclotron frequency f_c and excitation frequency f_{exc} as given by

$$f_b = f_{exc} - f_c \tag{9.18}$$

As a consequence, the orbit does not exceed the cell dimensions but still maintains a high average translational energy for an extended activation period during which only small increments of internal energy are transferred to the ions. The ions can therefore be irradiated for a sustained period (0.1–1 s) without causing ejection, that otherwise at f_c was unavoidable. SORI-CID results in sequential

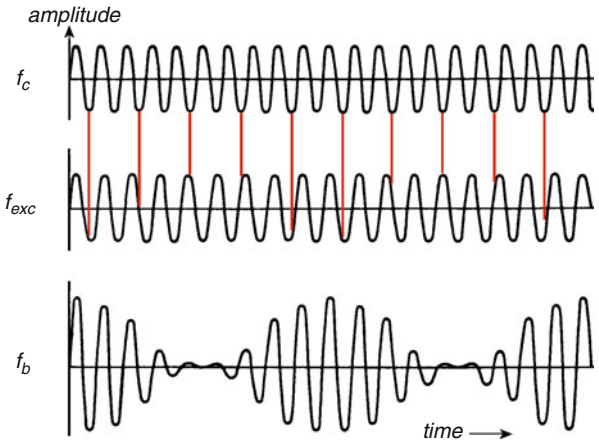

Fig. 9.32 Generation of an oscillation of ion kinetic energy as defined by a beat frequency due to off-resonance excitation; vertical connections are to locate points of positive and negative interferences, respectively. The larger the amplitude of f_b the more kinetic energy is contained in the circulating ions. One SORI-CID experiment consists of hundreds of beats

activation of ions by multiple collisions of low (<10 eV) kinetic energy ions with the collision gas, i.e., SORI-CID exploits slow internal heating of the ions [138]. Hence, SORI-CID addresses those fragmentation routes requiring rather low activation energy but benefit from sufficient reaction time.

Selective precursor ion activation
Both, RE-CID and SORI-CID are highly selective in precursor ion *m*/*z*, and therefore, activate only the precursor ion itself, normally even just a selected isotopolog. As a result, special pulse shapes are required to achieve activation of all isotopologs to preserve isotopic information in the fragment ion spectra. Furthermore, the high *m*/*z* selectivity causes only the precursor ion to dissociate while fragment ions do not receive any further energy to trigger second-generation cleavages.

SORI at work MALDI-SORI-FT-ICR spectra of the 2-aminobenzamide derivative of an unknown oligosaccharide were used for structure elucidation. First, the $[M+Na]^+$ ion, *m*/*z* 1240.5, was selected and fragmented (MS^2, Fig. 9.33a), then selected fragments thereof were subjected to further dissociation; to illustrate the principle, only one of these has been included here (MS^3, Fig. 9.33b). The frequency for SORI was chosen at 1.5% distant from the respective precursor ion's cyclotron frequency and supplied with an amplitude $V_{SORI} = 10$ V [138].

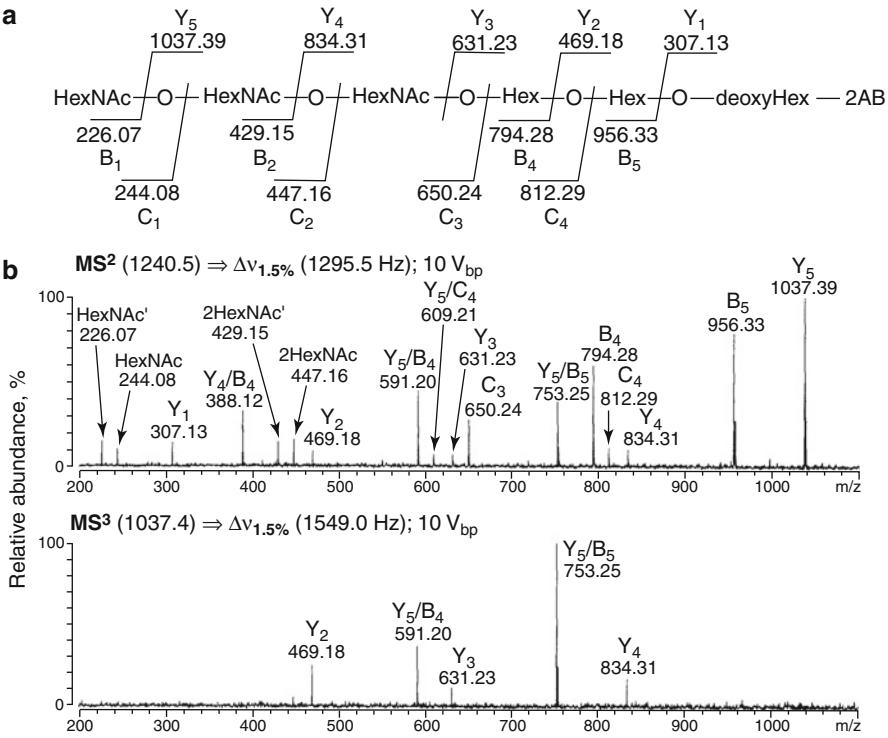

Fig. 9.33 MALDI-SORI-FT-ICR spectra of the $[M+Na]^+$ ion, *m/z* 1240.5, of the 2-aminobenzamide derivative of an unknown oligosaccharide (MS^2, **a**), and of the fragment at *m/z* 1037.4 obtained thereof (MS^3, **b**) (Adapted from Ref. [139] with permission. © Elsevier Science Publishers, 2002)

Dosing gas into ICR cells

CID can rather easily be implemented on FT-ICR instruments because it only demands for a pulse valve and a reservoir. Although the collision gas in SORI-CID can be easily handled, its use is nonetheless in contradiction to the high vacuum requirements of the ICR cell. Thus, alternative ion activation techniques without the use of gas are desirable.

9.12 Infrared Multiphoton Dissociation

The energy received from multiple photon absorption may also be used to activate and dissociate otherwise stable gaseous ions [140]:

$$m_1^+ + x \times h\nu \rightarrow m_2^+ + n \tag{9.19}$$

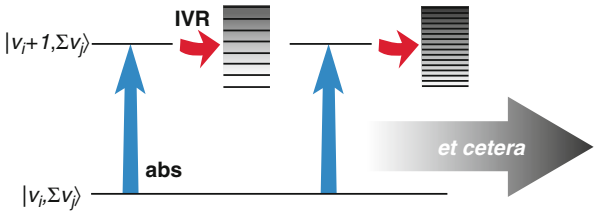

Fig. 9.34 IRMPD mechanism involving intramolecular vibrational relaxation (IVR) (Reproduced from Ref. [144] with permission. © John Wiley Periodicals, Inc., 2009)

Infrared multiphoton dissociation (IRMPD) was first described along with the dissociation of weakly bound protonated diethylether cluster ions [140]:

$$\left[(Et_2O)_2 + H\right]^+ + x\,h\nu \rightarrow \left[Et_2O + H\right]^+ + Et_2O \tag{9.20}$$

IRMPD is a technique that can be conveniently applied to trapped ions as is the case in ICR cells. IRMPD normally employs a continuous wave carbon dioxide laser of 10.6 μm wavelength (2.83×10^{13} Hz) having a power of 25–40 W which is passed into the ICR cell through a ZnSe or BaF_2 window [141, 142]. It is advantageous to combine FT-ICR with IRMPD because the amount of energy applied to the ions can be varied via the duration of laser irradiation, typically in the range of 5–300 ms [143]. This allows for the application of IRMPD to small ions [140] as well as to medium-sized [143] or high-mass ions [142].

Absorption of photon energy by a single normal mode of the ion is usually followed by dissipation among other vibrational modes, i.e., by *intramolecular vibrational relaxation* (IVR). The initial absorbing mode thereby returns to its ground state and gets ready to absorb another IR photon and so on (Fig. 9.34) [144]. IRMPD is regarded as a *slow heating method* because a large number of IR photons must be absorbed to effect fragmentation. In case of the usual carbon dioxide laser the energy of a single photon is just 0.116 eV, i.e., per electronvolt the absorption of nine photons is required [145, 146].

Safety note
For IRMPD, care must be taken to block the IR laser from abandoning its assigned optical path. The IR laser is extremely powerful and can instantaneously ignite objects or cause injuries from burns.

9.12.1 IRMPD in QITs and LITs

IRMPD is a valuable tool for gas phase ion studies and analytical applications that often do not require the full power of a highly expensive FT-ICR instrument. Therefore, efforts have been made to implement IRMPD on three-dimensional (Fig. 9.35) [145–148] and linear quadrupole ion traps [149–152].

Collisional cooling by the buffer gas required for quadrupole ion trap operation counteracts the accumulation of the ion internal energy by slow collisional

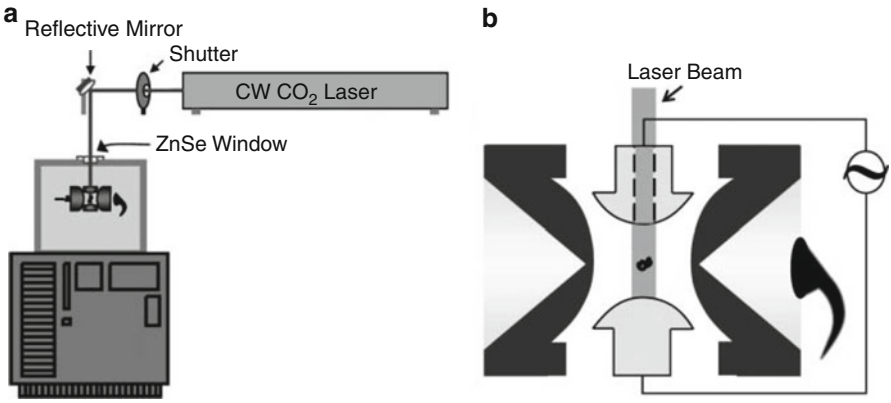

Fig. 9.35 IRMPD in a quadrupole ion trap (**a**) relative to the entire instrument and (**b**) with beam passage through a hole in the ring electrode of the QIT (Reproduced from Ref. [145] with permission. © John Wiley Periodicals, 2009)

activation. To avoid this problem, a dynamic pressure operation mode has been developed for IRMPD in QITs where initial ion storage and precursor ion selection are run at standard QIT pressure (3×10^{-2} mbar) while the buffer gas flow is interrupted several milliseconds prior to IRMPD ($<10^{-4}$ mbar) and subsequent product ion scanning [42, 146]. Alternatively, the energy drain by collisional cooling is strongly reduced by IRMPD in a tandem linear ion trap as in the Thermo LTQ Velos instruments (Fig. 9.30). The low-pressure cell is then employed for IRMPD, while the high-pressure cell only serves for CID [150].

9.13 Electron Capture Dissociation

9.13.1 Principles of Electron Capture Dissociation

For an ion, the cross section for *electron capture* (EC) roughly increases with the square of the ionic charge [153]. This makes multiply charged ions as produced by *electrospray ionization* (ESI, Chap. 12) the ideal targets for this process. When a UV laser of 193 nm wavelength (6.4 eV per photon) in the course of *ultraviolet photon dissociation* (UVPD) experiments erroneously hit a metal surface, electrons were deliberated inside the ICR cell. Electron capture by the formed multiply charged protein ions shifted their charge state from 11^+ to 10^+ without affecting mass [153]:

$$[\mathrm{M}+11\mathrm{H}]^{11+} + \mathrm{e}^- \rightarrow [\mathrm{M}+11\mathrm{H}]^{10+\bullet} \tag{9.21}$$

The product of EC is a radical ion (Fig. 9.36). The energy from neutralization of one ionic charge (5–7 eV) is transformed into ion internal energy that causes immediate fragmentation, so-called *electron capture dissociation* (ECD).

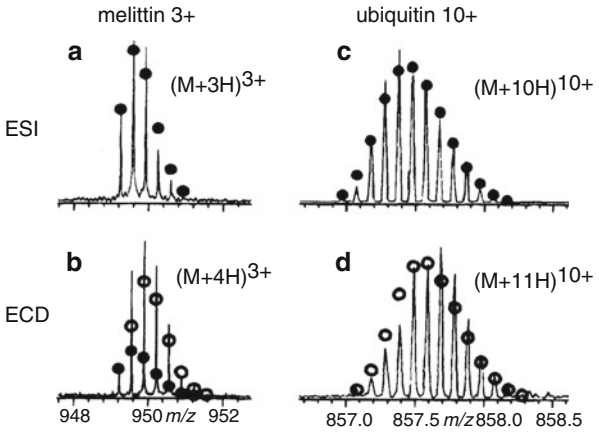

Fig. 9.36 Discovery of ECD by comparison of electrospray ionization (ESI) mass spectra of protein ions with those obtained when the UV laser was switched on to generate thermal electrons from the inner walls of the ICR cell. *Closed circles* mark the theoretically predicted isotopic abundances for the closed-shell ions of n^+ charge state, while *open circles* show those for the $(n–1)^{+\bullet}$ radical ions. The experimental patterns clearly show superimpositions of both (Reproduced from Ref. [153] with permission. © American Chemical Society, 1998)

Again, ECD is a technique for trapped ions only. To effectively achieve ECD the electrons must have energies <0.2 eV. Therefore, they are supplied analogously to EI from a carefully regulated heated filament [154] externally mounted to the ICR cell. Although a rather recent discovery [153, 155], ECD is now widely applied in biomolecule sequencing by means of ESI-FT-ICR-MS [154, 156]. The motivation for those numerous ECD applications is due to the fact that ECD yields information complementary to CID [157] and IRMPD [141].

ECD requires multiply charged precursors
As one electron charge is neutralized upon EC, the precursor ion for ECD must at least be a doubly charged positive even-electron ion to yield a singly charged radical ion for subsequent dissociation.

9.13.2 Peptide Ion Cleavages Upon ECD

In contrast to the prevalent generation of *b*- and *y*-type fragment ions from slow-heating activation methods, the fragmentation patterns in ECD contain mostly *c*- and *z*-type ions. These are generated by cleavage of an amine bond (N–C_α bond cleavage). Assuming a peptide ion $[M+zH]^{z+}$ having a lysine (Lys) residue, one can write the mechanism of ECD-induced peptide cleavage as depicted in Fig. 9.37 [158]. This scheme follows the most widely used model for the ECD mechanism,

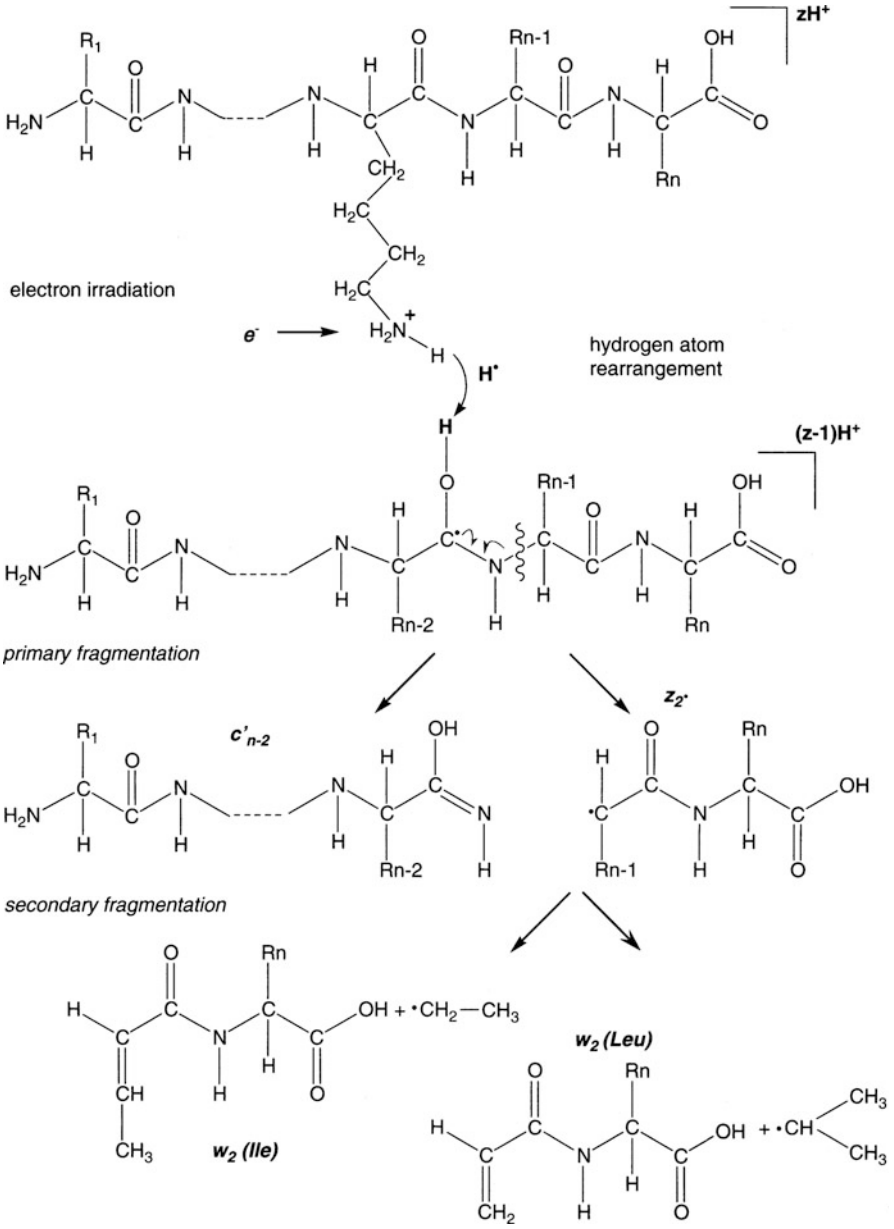

Fig. 9.37 Mechanism of fragmentation upon ECD following the hot hydrogen atom model. In this example, a protonated lysine residue captures the electron and immediately transfers a hydrogen atom to its neighboring carbonyl-O. Primary and secondary fragmentation pathways of the peptide ions are shown (Adapted from Ref. [158] with permission. © John Wiley & Sons, Ltd., 2004)

the so-called *hot hydrogen atom model*, which states that the electron is captured in a high Rydberg state by action of a charged site in the ion. Typically, the charges reside on basic amino acid residues, i.e., on arginine (Arg), lysine (Lys), or histidine (His), or on *N*-terminal amino groups. The primary odd-electron ion immediately cleaves off a hydrogen radical by N–H bond cleavage, thereby creating a hydrogen atom with an excess energy of about 6 eV. This "hot" hydrogen atom may be transferred along the peptide chain to any amide carbonyl group or to disulfide groups [159, 160]. Now, one of the electrons of the carbonyl-carbon atom is unpaired. Due to the excess energy this radical can dissociate by N–C_α bond cleavage. Thus, the amine-terminal peptide fragments are forming *c*-type fragment ions while the carboxylate-terminal fragments belong to the *z*-type fragment ion series.

The mechanism of peptide fragmentation upon ECD is still a matter of debate [160–162]. In particular, there is a discussion as to whether the ECD process is *nonergodic* (so fast that there is no internal equilibration of energy prior to dissociation) [153, 155] or ergodic (following QET) [162].

Annotating a H shift
Peptide fragments formed after transfer of a hydrogen (atom) are marked by a prime after the letter, e.g., the fragments from ECD are c' and z' ions [160].

9.14 Tandem MS with FT-ICR Instruments – Part II

As obvious from the preceding pages, both IRMPD and ECD are intimately connected with FT-ICR instrumentation. Now having considered these methods for ion activation in some detail we may focus our attention on their practical realization on the FT-ICR platform and some illustrative applications.

9.14.1 IRMPD in FT-ICR-MS

In contrast to CID conditions, the absence of a collision gas maintains the ultra-high vacuum inside the ICR cell, and thus, avoids time-consuming pump delays in the sequence of an experiment. The ultra-high vacuum environment also cancels collisional cooling as observed in QITs or LITs (Sect. 9.12.1). IRMPD was optionally available on the Bruker Apex series of FT-ICR instruments, while it has been abandoned on the more recent Solarix series, seemingly for safety of operation. Thermo LTQ-FT and LTQ-FT Ultra FT-ICR instruments still are optionally equipped with IRMPD.

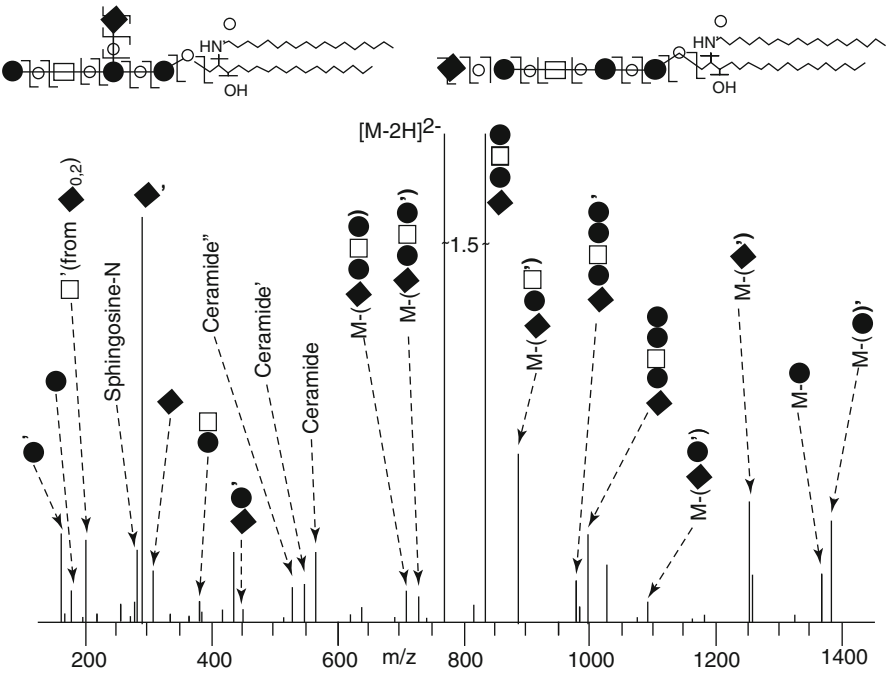

Fig. 9.38 IRMPD (200 ms, 14 W, 100 scans) spectrum of doubly deprotonated ganglioside GM1, $[M–2H]^{2–}$, occurring in two isomeric forms (Reproduced from Ref. [163] with permission. © Elsevier Science Publishers, 2005)

IRMPD application Gangliosides such as GM1 contain a hydrophobic ceramide moiety that consists of sphingosine, a long-chain amino alcohol, which is acylated with a fatty acid on the amino group. The molecule has a polar oligosaccharide head that contains sialic acid. GM1 exists as two isomeric forms, GM1a and GM1b, differing in that the sialic acid is in branched or terminal position, respectively. The negative-ion IRMPD (200 ms, 14 W, 100 scans) spectrum of doubly deprotonated ganglioside GM1, $[M–2H]^{2–}$, exhibits a cleavage within the ceramide moiety that causes loss of the fatty acid. The presence of GM1b as a minor component is evident from (*i*) the fragment ion peak at *m*/*z* 1091.722, which corresponds to a loss of the disaccharide HexNeuAc' from the precursor and (*ii*) its complementary peak at *m*/*z* 452.141 due to the disaccharide (Fig. 9.38) [163].

9.14.2 Infrared Photodissociation Spectroscopy

Provided a tunable laser light source is available, the IRMPD experiment can be performed in a wavelength-dependent manner to reveal the absorption characteristics of gaseous ions. Different from IR spectroscopy of condensed

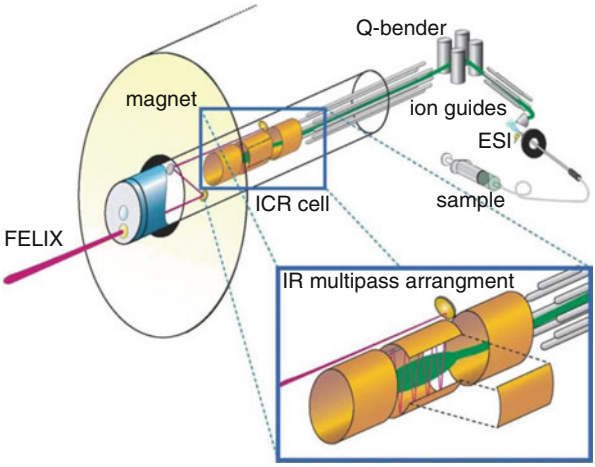

Fig. 9.39 Setup for infrared photodissociation spectroscopy. In this particular setup (FELIX at Utrecht, Netherlands) the light from a free-electron laser is guided into an open cylindrical ICR cell in a way that the IR light undergoes multiple reflections on the inner surfaces to extend its path for absorption by the ions inside the cell (Reproduced from Ref. [144] with permission. © John Wiley Periodicals, Inc., 2009)

phase samples, in mass spectrometry the occurrence of IR absorption is observed by detection of specific fragment ions and their abundances as a function of laser wavelength. This technique is known as *infrared photodissociation spectroscopy* (IRPD) [144, 164].

Unfortunately, powerful IR lasers tunable over a significant frequency range are difficult to obtain. Currently, the most effective but highly demanding approach to this end is represented by the *free-electron laser* (FEL). FEL facilities are limited and offer access for researchers to perform their experiments at dedicated ports on a tight schedule (Fig. 9.39). Alternatively, *optical parametric oscillator/amplifiers* (OPO/As) can serve as tunable IR light sources [144, 164].

9.14.3 Blackbody Infrared Radiative Dissociation

Even under essentially perfect vacuum where collisional activation is virtually absent ($<10^{-9}$ mbar) ions can undergo slow unimolecular dissociation. As the energy for these fragmentations is provided by the emission of infrared photons by blackbody radiation of the vacuum housing, this process is termed *blackbody infrared radiative dissociation* (BIRD) [165]. Blackbody infrared radiation is always present above non-zero temperatures. BIRD dissociations are characterized by reaction times in the order of several seconds to even minutes. Therefore, ICR cells provide the most suitable environment for their study. To vary the wavelength and intensity of IR radiation both the ICR cell and the surrounding vacuum manifold have to be uniformly heated. Typically, temperatures up to about 250 °C can be reached in dedicated instruments. This allows to study reaction kinetics where bonds of low to moderate strength are involved [165].

BIRD is quite exotic
Routine FT-ICR instruments are not suited for BIRD studies because of restrictions in heat resistance of electronic circuitry in proximity to the ICR cell and complications with the superconducting cryomagnet. BIRD requires wide-bore magnets (160 mm) that can accommodate the heated ICR cell housing plus a water-cooled mantle around it to prevent dissipation of heat to the magnet.

9.14.4 ECD for Tandem FT-ICR-MS

The implementation of ECD on ICR cells is nicely compatible with IRMPD. One approach is to use a hollow cathode [166] instead of a filament to deliver electrons for ECD. The hollow cathode also offers a wide electron beam that enlarges the volume where ECD can occur within the ICR cell. The IR laser then may pass through the central hole – a setup that exerts some restrictions to the ICR radii where ions can interact with the laser beam. Several cathode designs are in use (Figs. 9.40 and 9.41) [167].

ECD to locate postranslational peptide modifications The direct bond cleavages upon ECD can be used to locate postranslational peptide modifications that would be disguised in CID or IRMPD spectra. The difference between CID and IRMPD on one side and ECD on the other arises from the loss of most posttranslational modifications prior to backbone cleavage to from *b*- and *y*-type ions, while in ECD the chain is immediately cleaved to yield *c*- and *z*-type ions, independent of the peptide sequence [168]. Thus, the neutral loss reflects the mass of the modification, e.g., additional 80 u (HPO_3) in case of the phosphorylation that can be identified to occur at the tyrosine of the peptide RLpYIFSCFR (Fig. 9.42)

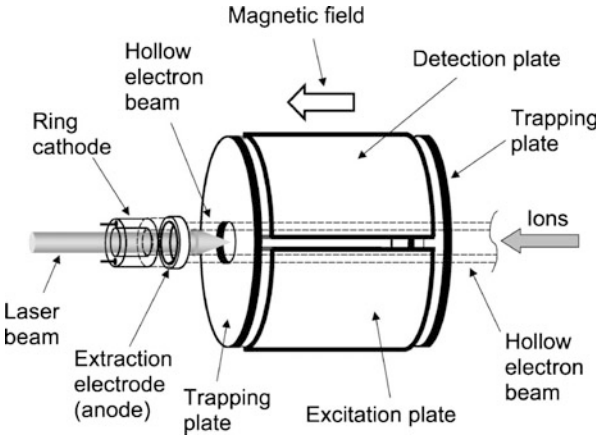

Fig. 9.40 A combined ECD and IRMPD setup for FT-ICR-MS. The IR laser is transmitted into the cell via the central hole of indirectly heated ring dispenser cathode mounted to the rear trapping plate of an ICR cell (Reproduced from Ref. [167] by permission. © John Wiley & Sons, 2003)

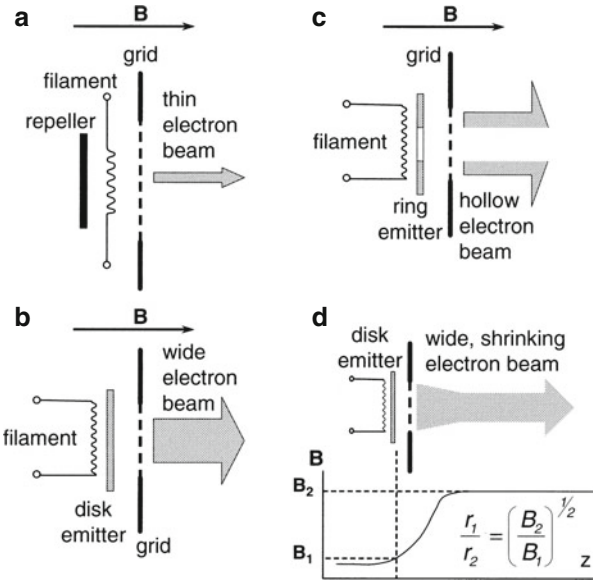

Fig. 9.41 Electron injection systems for ECD-FT-ICR instruments: (**a**) directly heated filament in homogeneous magnetic field, (**b**) disk-shaped indirectly heated cathode in homogeneous magnetic field, (**c**) ring-shaped indirectly heated cathode, and (**d**) cathode in fringing magnetic field region with beam collimation (Reproduced from Ref. [158] with permission. © John Wiley & Sons, Ltd., 2004)

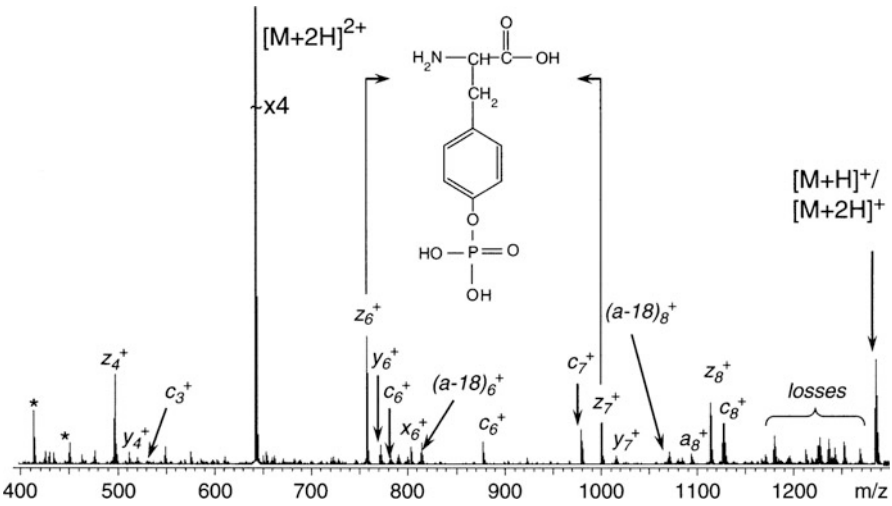

Fig. 9.42 Upon ECD, the $[M+2H]^{2+}$ ion of the peptide RLpYIFSCFR exhibits an increased mass difference of 80 u between its z_6^+ and z_7^+ fragments due to tyrosine phosphorylation (Adapted from Ref. [158] with permission. © John Wiley & Sons, Ltd., 2004)

[158]. The opportunity to obtain complementary peptide sequence information is the reason why CID or IRMPD spectra are sometimes combined with ECD spectra for structure elucidation of peptides [141, 157, 169].

9.15 Electron Transfer Dissociation

ECD can only take place in the ultra-high vacuum of FT-ICR mass spectrometers, while it is not possible to simultaneously store thermal electrons and peptide cations in quadrupole ion traps that utilize RF fields for ion manipulation and trapping. Furthermore, thermal electrons absorb energy from the RF field within milliseconds to become energetic. On the other hand, LITs can be operated as to store oppositely charged ions. Attempts for applying the advantages of ECD to LITs therefore make use of electron transfer via cation–anion reactions. In contrast to ECD, electron transfer may then occur at relatively high pressures ($\approx 10^{-3}$ mbar) [170]. This technique is termed *electron-transfer dissociation* (ETD) [168].

Anthracene radical anions as obtained by electron capture in a chemical ionization source with methane reagent gas were formerly employed as anions [168, 171]. Meanwhile, fluoranthene has become more widely used (Scheme 9.2) [172, 173].

Thus, ETD lends the capabilities of ECD to linear ion trap mass spectrometers. The individual steps involved in the operation of an LTQ instrument in ETD mode (Fig. 9.43) are: injection of multiply protonated peptides as delivered by an ESI source; application of a DC offset to store these ions in the front section of the LIT followed by injection of reagent anions from the CI source into the center of the LIT. Then all but the peptide precursor ions and the electron-donor reagent ions are ejected. Next the DC potential well is switched off and a secondary RF voltage is applied to the end lens plates of the LIT causing positive and negative ion populations to mix and react. The reaction period is ended by axial ejection of reagent anions while positive product ions are retained in the center section of the LIT. Finally, mass-selective radial ejection as usual yields the ETD spectrum

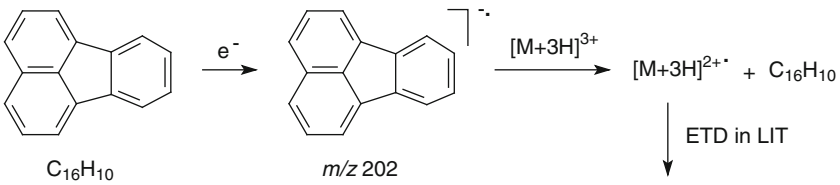

Scheme 9.2

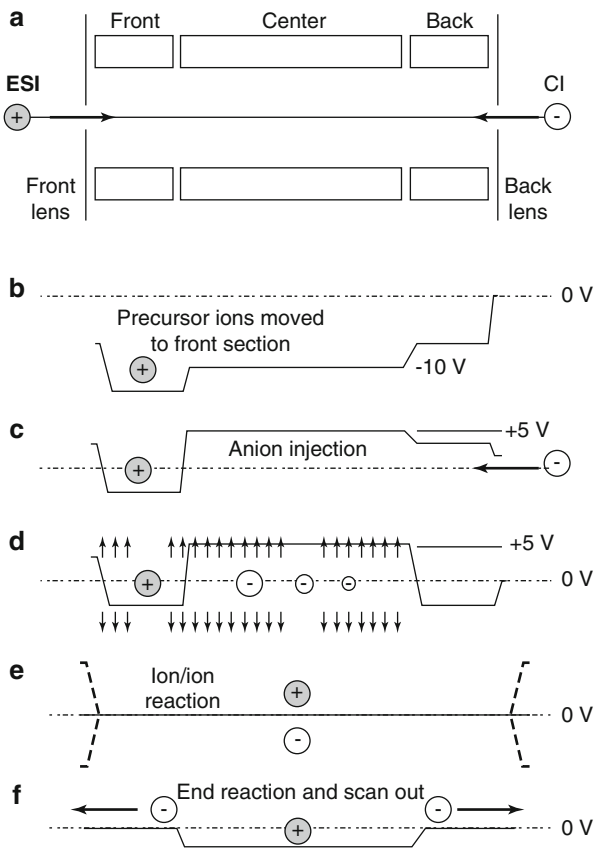

Fig. 9.43 Sequence of events to trap both positive peptide ions and reagent anions in a LIT, to react them, and to obtain an ETD spectrum showing the product ions. (**a**) Setup of the segmented LIT for ETD, (**b**) trapping of precursor ions in the front section, (**c**) admitting negative reagent ions, (**d**) anion storage in the center, (**e**) ETD reaction, and (**f**) scan for product ions (Reproduced from Ref. [168] with permission. © The National Academy of Sciences of the USA, 2004)

[168]. The attractive ETD technique has also been implemented on LITs with axial ejection [151, 174] and on LIT-Orbitrap hybrids [175–177].

Unfortunately, ETD has limited applicability to doubly protonated peptide precursor ions, $[M+2H]^{2+}$, while triply protonated ions fragment to reveal the full sequence due to the higher exothermicity of the electron capture (Fig. 9.44) [170].

9.16 Electron Detachment Dissociation

Both ECD and ETD cause direct backbone cleavages in multiply positive peptide ions to deliver *c*- and *z*-type fragments which are highly informative for mass spectral sequencing. Especially when occurring more than once on a molecule, post-translational modifications like phosphorylation or sulfonation, reduce its tendency to form multiply protonated ions. Such analytes are best studied as negative ions, which are of course not amenable to ECD [178]. If the primary

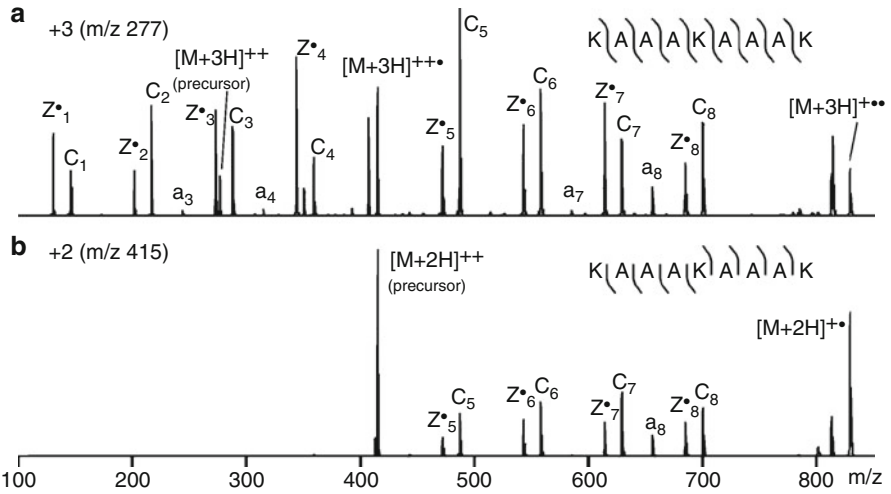

Fig. 9.44 Effect of precursor ion charge state on ETD product ion spectra of (**a**) the triply protonated peptide ion $[KAAAKAAAK+H]^{3+}$ and (**b**) the doubly protonated ion of the same peptide which only produces half of the possible *c*- and *z*-type fragments (Reproduced from Ref. [170] with permission. © American Chemical Society, 2007)

electrons are energetic (about 20 eV) rather than thermal, there is a substantial chance to promote *electron detachment* from the anion [179]. In fact, the overall process can be regarded as electron ionization of an anion, which leads+ to formation of a neutral radical site (Sect. 6.3.1).

$$[M - nH]^{n-} + e^- \rightarrow [M - nH]^{(n-1)-\bullet} + 2e^- \tag{9.22}$$

Alternatively, electron ionization can occur anywhere along a polypeptide chain to locally form a positive radical ion that also may be regarded as an electron hole. This will attract an excess electron from one of the anionic sites of the ion and end up in mutual neutralization. The released energy effects electronic excitation, that, in turn, causes backbone cleavage [179]. This technique is termed *electron detachment dissociation* (EDD, Scheme 9.3) [178–181].

EDD is not only useful for acidic peptides but also for oligonucleotides [182] and other analytes [160]. EDD has also been adapted to QITs [180]. Nonetheless, EDD is clearly less relevant in bioanalytical work than ECD or ETD.

A variation of EDD, termed *negative electron transfer dissociation* (NETD) employs fluoranthene, $C_{16}H_{10}^{+\bullet}$, or $Xe^{+\bullet}$ ions instead of energetic electrons to induce radical cationic sites by charge transfer rather than by electron ionization [183]. NETD yields selective backbone cleavage at the C_α–C bonds, similar to EDD, but leaves the phosphorylation sites intact, thereby enabling the localization of posttranslational modifications (PTMs).

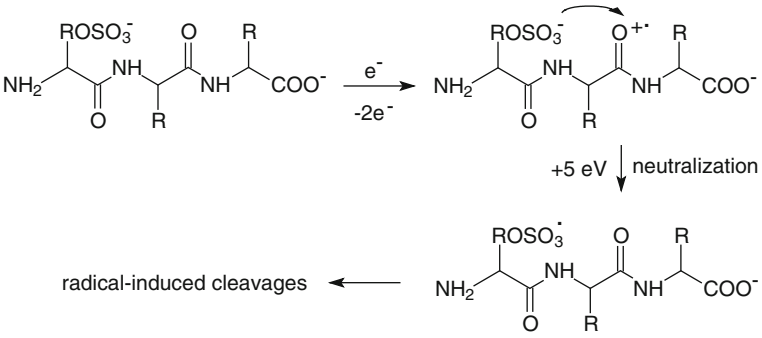

Scheme 9.3

9.17 Special Applications of Tandem MS

Bimolecular reactions may take place when gaseous ions collide with neutrals at *thermal energy* rather than at multi- or even kiloelectronvolt energy. Proton transfer is one of the prominent representatives of an *ion–molecule reaction* in the gas phase. It is employed for the determination of *GB*s and *PA*s as described below. More sophisticated studies are enabled by reactions of gaseous ions with more complex reagents in the gas phase and the immediate mass spectral analysis of the reaction products [3].

9.17.1 Ion–Molecule Reactions in Catalytic Studies

The catalytic activities of a large pool of transition-metal carbene complexes have been screened by means of ion–molecule reactions in tandem-MS experiments [184–186]. Reactions of bare or solvated metal ions with organic molecules have been studied using mass spectrometers as reaction vessels [187–190]. In contrast to the concepts and methods discussed so far, the latter experiments are not designed to study the fundamentals of mass spectrometry. Instead, sophisticated methods of modern mass spectrometry are now employed to reveal the secrets of other complex chemical systems.

Activation of methane Reaction of mass-selected $[Ni(H)(OH)]^+$ ions, m/z 76, with methane at 0 eV collision energy in the laboratory frame of reference yields a CH_2 insertion product, $[Ni(CH_3)(OH)]^+$, m/z 90. The experiments were carried out by using a QhQ mass spectrometer with an electrospray ion source. $[NiL]^+$ reactand ions were produced by ESI from solutions of NiL_2 (L = F, Cl, Br, I) in pure methanol and $[NiOH]^+$ ions from NiI_2 in H_2O. For the methane-activation study, the ions containing ^{58}Ni were mass selected in Q1 and reacted at thermal

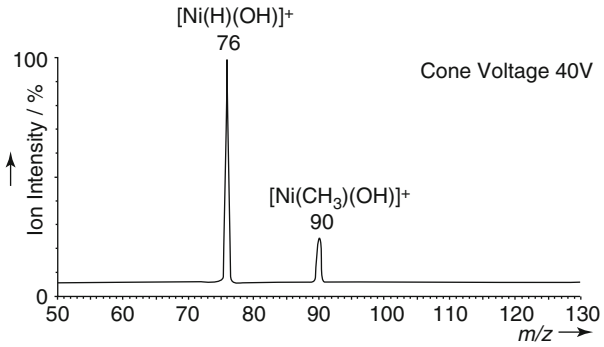

Fig. 9.45 Reaction of mass-selected $[Ni(H)(OH)]^+$ ions, *m*/*z* 76, with methane at 0 eV collision energy in the laboratory frame of reference yields a CH_2 insertion product, *m*/*z* 90. The cone voltage refers to the ESI conditions to produce optimum precursor ion abundance from Ni salt solutions (Reproduced from Ref. [190] with permission. © Wiley-VCH Verlag, Weinheim, 2007)

energy with methane in the RF-only hexapole at about 10^{-4} mbar. The ionic products were then detected by Q2 (Fig. 9.45) [190].

9.17.2 Gas Phase Hydrogen–Deuterium Exchange

Deuterium and other isotopic labeling prior to mass spectrometric analysis has been known from the early days of mass spectrometry (Sects. 2.9 and 3.3). Modern methodology even allows labeling of gaseous ions, thereby yielding insight into mechanistic details of reactions in a much more convenient way than by complicated synthetic routes. Furthermore, the gas phase exchange of hydrogen for deuterium can be applied to transient species that would otherwise remain inaccessible. So *hydrogen–deuterium exchange* (HDX) can be accomplished not only in solution (Chaps. 6 and 7 in [191]), e.g., prior to analysis by electrospray ionization, but also in the gas phase. This is best achieved on ion traps of any kind as these provide extended and easily variable reaction times – circumstances that also enable kinetic studies.

HDX in peptide fragmentation Gas phase HDX has been used to probe complete parent and fragment ion populations generated by CID of multiply charged protonated peptides [192]. The peptide ions were monoisotopically selected, dissociated by SORI-CID, and then subjected to HDX by repeated pulsed admission of CD_3OD to the ICR cell. Finally, the products were analyzed by FT-ICR-MS. HDX for variable reaction times revealed distinguished exchange kinetics for different types of ions, which allowed to deduce information on their structures. For example, *b*-type ions exhibited fast HDX while *a*-type ions showed only restricted exchange even at longer reaction times (Fig. 9.46) [192, 193]. The

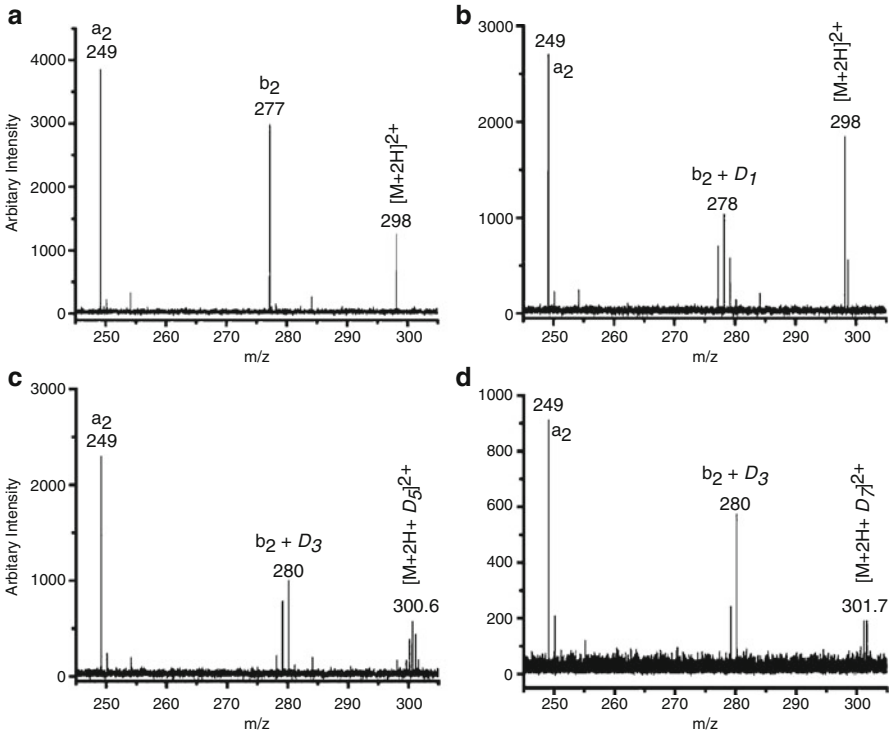

Fig. 9.46 The a_2-b_2 region of the product ion spectrum of doubly protonated YIGSR after (**a**) 0 s, (**b**) 1 s, (**c**) 10 s, and (**d**) 60 s gas phase HDX in an ICR cell. The uptake of deuterium is denoted by D_n in the formulas (Reproduced from Ref. [193] with permission. © Elsevier Science Publishers, 2009).

observed exchange behavior was used to argue in favor of a oxazolone structure of the b_2 ions.

9.17.3 Determination of Gas Phase Basicities and Proton Affinities

The methods for the determination of *GB*s and *PA*s (Sect. 2.12) make use of their relation to K_{eq} (Eq. 9.23) and the shift of K_{eq} upon change of $[AH]^+$ or B, respectively [194, 195]. Basically, the value of *GB* or *PA* is bracketed by measuring K_{eq} with a series of several reference bases ranging from lower to higher *GB* than the unknown. There are two methods we should address in brief, a detailed treatment of the topic being beyond the scope of the present book, however. The *kinetic method* makes use of the dissociation of proton-bound heterodimers, and the

thermokinetic method determines the equilibrium constant of the acid-base reaction of gaseous ions. In general, proton transfer plays a crucial role in the formation of protonated molecules, e.g., in positive-ion chemical ionization mass spectrometry (Chap. 7).

The *kinetic method* [196–199] compares the relative rates of the competitive dissociations of a proton-bound adduct $[A–H–B]^+$ formed by admitting a mixture of A and B to a CI ion source [196, 197]. There, the proton-bound adduct $[A–H–B]^+$ is generated amongst other products such as $[AH]^+$ and $[BH]^+$. Using standard tandem MS techniques, e.g., MIKES, the cluster ion $[A–H–B_{ref}]^+$ is selected and allowed to undergo metastable decomposition:

$$[AH]^+ + B_{ref} \leftarrow [A - H - B_{ref}]^+ \rightarrow A + [B_{ref}H]^+ \tag{9.23}$$

The relative intensities of the products $[AH]^+$ and $[B_{ref}H]^+$ are then used as a measure of relative rate constants of the competing reactions. In case the *PA* of the unknown was equal to that of the reference, both peaks would be of equal intensity. As this will almost never be the case, a series of reference bases is employed instead, and *PA* is determined by interpolation. The value of $PA_{(A)}$ is obtained from a plot of $\ln[AH]^+/[B_{ref}H]^+$ versus $PA_{(B)}$ at $\ln[AH]^+/[B_{ref}H]^+ = 0$.

The *thermokinetic method* [200, 201] uses the measurement of the forward rate constant of the equilibrium

$$[AH]^+ + B_{ref} \rightleftharpoons A + [B_{ref}H]^+ \tag{9.24}$$

The thermokinetic method takes advantage of the correlation observed between k_{exp} and $\Delta G_2{}^0$ through the relationship

$$\frac{k_{exp}}{k_{coll}} = \frac{1}{1 + \exp\left[\left(\Delta G_2^0 + \Delta G_a^0\right)/RT\right]} \tag{9.25}$$

where k_{coll} is the collision rate constant and $\Delta G_a{}^0$ a term close to *RT*. The *GB* of the unknown is then obtained from $\Delta G_2{}^0 = GB - GB_{ref}$. The task to establish a proper value of the reaction efficiency, $R_{eff} = k_{exp}/k_{coll}$, is solved by plotting the experimental values of R_{eff} versus $GB_{(B)}$ and interpolating these points with a parametric function. Although this can be done with high accuracy, it is still a matter of debate as to which value of R_{eff} yields the most realistic *GB*, suggestions being $R_{eff} =$ 0.1–0.5 [194].

Determination of *GB* and *PA* *GB* and *PA* of cyclohexanecarboxamide were determined by both experimental methods. The kinetic method based on both metastable dissociation and CID yielded $GB = 862 \pm 7$ kJ mol^{-1} and $PA = 896 \pm$ 5 kJ mol^{-1}, while the thermokinetic method gave $GB = 860 \pm 5$ kJ mol^{-1} and $PA =$ 891 ± 5 kJ mol^{-1}, i.e., both methods yield comparable results (Fig. 9.47).

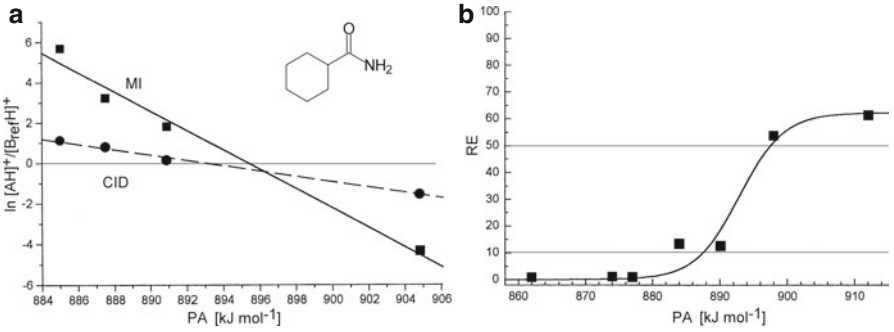

Fig. 9.47 Determination of the proton affinity of cyclohexanecarboxamide (**a**) by the kinetic method, and (**b**) by the thermokinetic method. The *horizontal lines* show the indicative values ln $[AH]^+/[B_{ref}H]^+ = 0$ in (**a**) and *RE*s according to different authors in (**b**) [194] (Adapted from Ref. [202] by permission. © IM Publications, 2003)

9.17.4 Neutralization-Reionization Mass Spectrometry

In CID, charge exchange between the ions and the collision gas is an unwanted side reaction. However, it may become useful when employed in combination with a subsequent reionization step as in *neutralization-reionization mass spectrometry* (NR-MS) [203–211]. In NR-MS, the precursor ion of some kiloelectronvolts of kinetic energy is mass-selected in MS1 and passed through a first collision cell containing a reducing collision gas. A certain fraction of these ions will be reduced by charge exchange to become neutrals. As these neutrals basically retain their initial kinetic energy and direction, they leave the first collision cell along with the precursor ion beam. Remaining ions can then be removed from the beam by electrostatic deflection. Having traveled for some microseconds along a short path through the field-free region, the neutrals are subjected to ionizing collisions in a second collision cell. Finally, the mass spectrum of the reionized species is detected by means of MS2.

For neutralization one can employ:

- noble gases of low *IE* such as Xe (12.1 eV) [205],
- metal vapors effusing from an oven, e.g., Hg (10.4 eV), Zn (9.3 eV), and Cd (9.0 eV) [203, 212],
- volatile organic molecules, e.g., benzene (9.2 eV) or triphenylamine (6.8 eV) [213].

Reionization of the neutrals in the second collision cell can be achieved using:

- O_2 (12.1 eV) or He (24.6 eV) [212, 213],
- ionization methods such as electron ionization or field ionization [207].

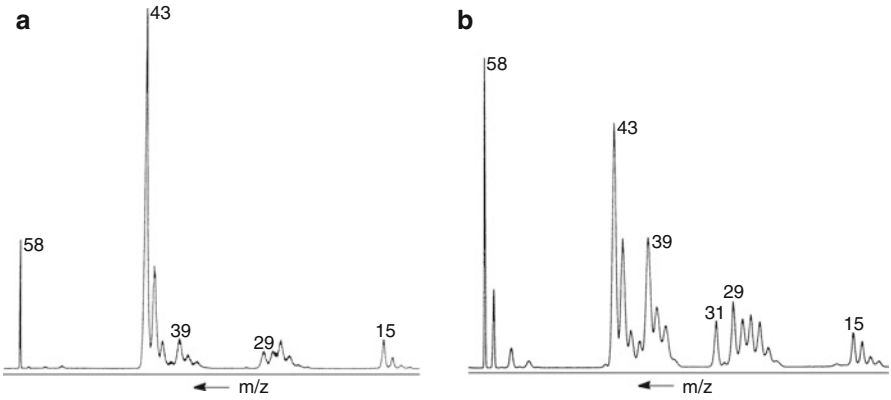

Fig. 9.48 NR-MS (Xe–He) of acetone (**a**) and its enol (**b**) from neutralization of the corresponding ions (Adapted from Ref. [205] with permission. © Elsevier Science, 1985)

NR-MS is applied in numerous ways [208, 213–215]. In particular, NR-MS is a powerful tool where the existence of short-lived and otherwise unstable species has to be proven [216–218].

NR-MS of acetone The NR mass spectrum of acetone closely resembles its 70-eV EI mass spectrum (Sect. 6.2.1), thereby demonstrating that the molecular ion basically retains the structure of the neutral (Fig. 9.48) [205]. However, the isomeric $C_3H_6O^{+\bullet}$ ions formed by McLafferty rearrangement of 2-hexanone molecular ion are expected to have enol structure (Sect. 6.8.1), and thus the corresponding NR mass spectrum is easily distinguished from that of acetone.

9.18 Tandem Mass Spectrometry Condensed

Terminology in Tandem Mass Spectrometry
The terms *tandem mass spectrometry*, also *mass spectrometry/mass spectrometry*, collectively describes mass spectrometric experiments where ions that are mass-analyzed in MS1 are subjected to fragmentations or ion–molecule reactions and the products thereof are collected and analyzed by a second stage, MS2. Tandem MS is often abbreviated as MS/MS or MS^2. Tandem MS experiments of higher order are referred to as MS^3, MS^4, . . . or generally as MS^n.
Ions emerging from MS1 are termed *precursor ions*, those entering MS2 are called *product ions*; in higher-order experiments, one may refer to them as n^{th} generation product ions.

Mass Analyzers for Tandem MS
A tandem mass spectrometer can either be composed of – mostly independent – mass analyzers in serial connection or can be achieved by operating the same analyzer to sequentially perform the stages of the tandem MS experiment. The

first mode of tandem MS is described as *tandem MS in space*, the second as *tandem MS in time*. Beam instruments (BE, EB, QqQ, ReTOF, QqTOF, TOF/TOF) provide tandem MS in space, ion trap analyzers (QIT, LIT, FT-ICR) yield tandem MS in time. Orbitraps cannot be operated in a tandem MS mode; they exclusively serve as MS2 to analyze fragment ions delivered by a Q- or LIT-type MS1.

Ion Activation Techniques

Ideally, a single all-purpose ion activation method would suffice to generate fragment ions for structure elucidation of any compound class. Moreover, the charge state of the precursor ion, its mass, and other characteristics would not interfere. In reality, however, no such method exists [170]. In case of peptides, for example, there is no single successful activation technique for delivering a sufficient number of sequence-informative product ions for sequence identification; instead, the amino acid composition and posttranslational modifications exhibit a strong influence on the fragmentation pattern – justifying all the previous methods. Commonly available ion activation techniques are summarized and briefly described in Table 9.4 [31, 219].

Table 9.4 Common ion activation techniques for tandem MS

Method	Instrumental platforms	Ionic charge and species accessible	Description and properties
CID	BE, ReTOF, TOF-TOF	+/− Precursor and fragments	Collisions at keV-energies with inert gas. Several eV energy transfer in single collision within a femtosecond
	QqQ, QqTOF, QqLIT, etc.	+/− Precursor and fragments	Tens of eV-collisions with inert gas About eV energy transfer per collision; several events within about a millisecond
	FT-ICR	+/− Selected precursor only	Several eV-collisions with inert gas; about eV energy transfer per collision; several events within a second.
SID	QqQ, IMS-QqTOF etc.	+/− Selected precursor only	Single collision at several tens of eV with inert surface within some picoseconds
IRMPD	FT-ICR (QIT)	+/− Precursor and fragments	Rather low-energy activation by IR laser; compatible with ECD
BIRD	FT-ICR	+/− Precursor and fragments	Slow, low-energy activation by IR blackbody radiation close to equilibrium; to study kinetics and thermodynamics
ECD	FT-ICR	Multiply + Precursor and fragments	Energy from partial neutralization by thermal electrons; extremely fast process causes radical ion cleavages
ETD	LIT and hybrids with LIT	Multiply + Precursor and fragments	Energy from partial neutralization transferred by cation–anion reaction; result similar to ECD
EDD	FT-ICR	Multiply – Precursor and fragments	Energy from partial neutralization delivered by electron detachment; results like “ECD for anions”

Applications

Tandem MS was initially developed as a tool for gas phase ion chemistry to track dissociation pathways and to determine thermodynamic properties of gaseous ions. Then, structure elucidation started to also play a role in analytical mass spectrometry. Step by step, tandem MS instruments were constructed and modes of operation were developed that allowed to use almost any type of mass analyzer.

The tremendous commercial success of all sorts of hybrid instruments is due to their effectivity in tandem MS. Today, tandem MS has a plethora of applications, mostly in biomolecule sequencing and in trace analysis to increase selectivity for the detection and eventually quantification of target compounds (Sects. 14.2 and 14.3).

References

1. McLafferty FW (ed) (1983) Tandem Mass Spectrometry. John Wiley & Sons, New York
2. Busch KL, Glish GL, McLuckey SA (1988) Mass Spectrometry/Mass Spectrometry. Wiley VCH, New York
3. Schalley CA, Springer A (2009) Mass Spectrometry and Gas-Phase Chemistry of Non-Covalent Complexes. John Wiley & Sons, Hoboken
4. Murray KK, Boyd RK, Eberlin MN, Langley GJ, Li L, Naito Y (2013) Definitions of Terms Relating to Mass Spectrometry (IUPAC Recommendations 2013). Pure Appl Chem 85:1515–1609. doi:10.1351/PAC-REC-06-04-06
5. Johnson JV, Yost RA, Kelley PE, Bradford DC (1990) Tandem-in-Space and Tandem-in-Time Mass Spectrometry: Triple Quadrupoles and Quadrupole Ion Traps. Anal Chem 62:2162–2172. doi:10.1021/ac00219a003
6. Kaufmann R, Kirsch D, Spengler B (1994) Sequencing of Peptides in a Time-of-Flight Mass Spectrometer: Evaluation of Postsource Decay Following Matrix-Assisted Laser Desorption Ionization (MALDI). Int J Mass Spectrom Ion Proc 131:355–385. doi:10.1016/0168-1176(93)03876-N
7. Glish GL (1994) Multiple Stage Mass Spectrometry: The Next Generation Tandem Mass Spectrometry Experiment. Analyst 119:533–537. doi:10.1039/AN9941900533
8. Glish G (1991) Letter to the Editor [Concerning Terms in Mass Spectrometry]. J Am Soc Mass Spectrom 2:349. doi:10.1016/1044-0305(91)80026-4
9. Thorne GC, Ballard KD, Gaskell SJ (1990) Metastable Decomposition of Peptide $[M+H]^+$ Ions via Rearrangement Involving Loss of C-Terminal Amino Acid Residue. J Am Soc Mass Spectrom 1:249–257. doi:10.1016/1044-0305(90)85042-K
10. Louris JN, Wright LG, Cooks RG, Schoen AE (1985) New Scan Modes Accessed with a Hybrid Mass Spectrometer. Anal Chem 57:2918–2924. doi:10.1021/ac00291a039
11. Glish GL, Burinsky DJ (2008) Hybrid Mass Spectrometers for Tandem Mass Spectrometry. J Am Soc Mass Spectrom 19:161–172. doi:10.1016/j.jasms.2007.11.013
12. Lehmann WD (1997) Pictograms for Experimental Parameters in Mass Spectrometry. J Am Soc Mass Spectrom 8:756–759. doi:10.1016/S1044-0305(97)00028-7
13. Cooks RG, Beynon JH, Caprioli RM (1973) Metastable Ions. Elsevier, Amsterdam
14. Levsen K (1978) Fundamental Aspects of Organic Mass Spectrometry. Weinheim, Verlag Chemie
15. McLafferty FW, Bente PFI, Kornfeld R, Tsai SC, Howe I (1973) Collisional Activation Spectra of Organic Ions. J Am Chem Soc 95:2120–2129. doi:10.1021/ja00788a007
16. Levsen K, Schwarz H (1976) Collisional Activation Mass Spectrometry – A New Probe for Structure Determination of Ions in the Gaseous Phase. Angew Chem 88:589–601. doi:10.1002/ange.19760881802

17. Holmes JL (1985) Assigning Structures to Ions in the Gas Phase. Org Mass Spectrom 20:169–183. doi:10.1002/oms.1210200302
18. Levsen K, Schwarz H (1983) Gas-Phase Chemistry of Collisionally Activated Ions. Mass Spectrom Rev 2:77–148. doi:10.1002/mas.1280020104
19. Bordas-Nagy J, Jennings KR (1990) Collision-Induced Decomposition of Ions. Int J Mass Spectrom Ion Proc 100:105–131. doi:10.1016/0168-1176(90)85071-9
20. McLuckey SA (1992) Principles of Collisional Activation in Analytical Mass Spectrometry. J Am Soc Mass Spectrom 3:599–614. doi:10.1016/1044-0305(92)85001-Z
21. Shukla AK, Futrell JH (2000) Tandem Mass Spectrometry: Dissociation of Ions by Collisional Activation. J Mass Spectrom 35:1069–1090. doi:10.1002/1096-9888(200009)35:9<1069::AID-JMS54>3.0.CO;2-C
22. Guevremont R, Boyd RK (1988) Are Derrick Shifts Real? An Investigation by Tandem Mass Spectrometry. Rapid Commun Mass Spectrom 2:1–5. doi:10.1002/rcm.1290020102
23. Bradley CD, Derrick PJ (1991) Collision-Induced Decomposition of Peptides. An Investigation into the Effect of Collision Gas Pressure on Translational Energy Losses. Org Mass Spectrom 26:395–401. doi:10.1002/oms.1210260507
24. Bradley CD, Derrick PJ (1993) Collision-Induced Decomposition of Large Organic Ions and Inorganic Cluster Ions. Effects of Pressure on Energy Losses. Org Mass Spectrom 28:390–394. doi:10.1002/oms.1210280421
25. Neumann GM, Sheil MM, Derrick PJ (1984) Collision-Induced Decomposition of Multiatomic Ions. Z Naturforsch A 39:584–592. doi:10.1515/zna-1984-0612
26. Alexander AJ, Thibault P, Boyd RK (1990) Target Gas Excitation in Collision-Induced Dissociation: A Reinvestigation of Energy Loss in Collisional Activation of Molecular Ions of Chlorophyll-a. J Am Chem Soc 112:2484–2491. doi:10.1021/ja00163a003
27. Kim BJ, Kim MS (1990) Peak Shape Analysis for Collisionally Activated Dissociation in Mass-Analyzed Ion Kinetic Energy Spectrometry. Int J Mass Spectrom Ion Proc 98:193–207. doi:10.1016/0168-1176(90)80001-J
28. Vékey K, Czira G (1993) Large Translational Energy Loss and Scattering in Collision-Induced Dissociation Processes. Org Mass Spectrom 28:546–551. doi:10.1002/oms.1210280513
29. Wysocki VH, Kenttämaa H, Cooks RG (1987) Internal Energy Distributions of Isolated Ions After Activation by Various Methods. Int J Mass Spectrom Ion Proc 75:181–208. doi:10.1016/0168-1176(87)83054-9
30. Bradley CD, Curtis JM, Derrick PJ, Wright B (1992) Tandem Mass Spectrometry of Peptides Using a Magnetic Sector/Quadrupole Hybrid-the Case for Higher Collision Energy and Higher Radio-Frequency Power. Anal Chem 64:2628–2635. doi:10.1021/ac00045a028
31. McLuckey SA, Goeringer DE (1997) Slow Heating Methods in Tandem Mass Spectrometry. J Mass Spectrom 32:461–474. doi:10.1002/(SICI)1096-9888(199705)32:5<461::AID-JMS515>3.0.CO;2-H
32. Mabud MA, Dekrey MJ, Cooks RG (1985) Surface-Induced Dissociation of Molecular Ions. Int J Mass Spectrom Ion Proc 67:285–294. doi:10.1016/0168-1176(85)83024-X
33. Cooks RG, Hoke SH II, Morand KL, Lammert SA (1992) Mass Spectrometers: Instrumentation. Int J Mass Spectrom Ion Proc 118-119:1–36. doi:10.1016/0168-1176(92)85057-7
34. Bier ME, Amy JW, Cooks RG, Syka JEP, Ceja P, Stafford G (1987) A Tandem Quadrupole Mass Spectrometer for the Study of Surface-Induced Dissociation. Int J Mass Spectrom Ion Proc 77:31–47. doi:10.1016/0168-1176(87)83022-7
35. Wysocki VH, Ding JM, Jones JL, Callahan JH, King FL (1992) Surface-Induced Dissociation in Tandem Quadrupole Mass Spectrometers: a Comparison of Three Designs. J Am Soc Mass Spectrom 3:27–32. doi:10.1016/1044-0305(92)85015-C
36. Lammert SA, Cooks RG (1991) Surface-Induced Dissociation of Molecular Ions in a Quadrupole Ion Trap Mass Spectrometer. J Am Soc Mass Spectrom 2:487–491. doi:10.1016/1044-0305(91)80036-7
37. Beardsley RL, Jones CM, Galhena AS, Wysocki VH (2009) Noncovalent Protein Tetramers and Pentamers with "n" Charges Yield Monomers with n/4 and n/5 Charges. Anal Chem 81:1347–1356. doi:10.1021/ac801883k

38. Laskin J (2004) Energetics and Dynamics of Peptide Fragmentation from Multiple-Collision Activation and Surface-Induced Dissociation Studies. Eur J Mass Spectrom 10:259–267. doi:10.1255/ejms.641
39. Wysocki VH, Joyce KE, Jones CM, Beardsley RL (2008) Surface-Induced Dissociation of Small Molecules, Peptides, and Non-Covalent Protein Complexes. J Am Soc Mass Spectrom 19:190–208. doi:10.1016/j.jasms.2007.11.005
40. Zhou M, Huang C, Wysocki VH (2012) Surface-Induced Dissociation of Ion Mobility-Separated Noncovalent Complexes in a Quadrupole/Time-of-Flight Mass Spectrometer. Anal Chem 84:6016–6023. doi:10.1021/ac300810u
41. Zhou M, Wysocki VH (2014) Surface Induced Dissociation: Dissecting Noncovalent Protein Complexes in the Gas Phase. Acc Chem Res 47:1010–1018. doi:10.1021/ar400223t
42. Brodbelt JS (2016) Ion Activation Methods for Peptides and Proteins. Anal Chem 88:30–51. doi:10.1021/acs.analchem.5b04563
43. Spengler B, Kirsch D, Kaufmann R, Jaeger E (1992) Peptide Sequencing by Matrix-Assisted Laser-Desorption Mass Spectrometry. Rapid Commun Mass Spectrom 6:105–108. doi:10.1002/rcm.1290060207
44. Boesl U, Weinkauf R, Schlag E (1992) Reflectron Time-of-Flight Mass Spectrometry and Laser Excitation for the Analysis of Neutrals, Ionized Molecules and Secondary Fragments. Int J Mass Spectrom Ion Proc 112:121–166. doi:10.1016/0168-1176(92)80001-H
45. Bradbury NE, Nielsen RA (1936) Absolute Values of the Electron Mobility in Hydrogen. Phys Rev 49:388–393. doi:10.1103/PhysRev.49.388
46. Tang X, Ens W, Standing KG, Westmore JB (1988) Daughter Ion Mass Spectra from Cationized Molecules of Small Oligopeptides in a Reflecting Time-of-Flight Mass Spectrometer. Anal Chem 60:1791–1799. doi:10.1021/ac00168a029
47. Tang X, Ens W, Mayer F, Standing KG, Westmore JB (1989) Measurement of Unimolecular Decay in Peptides of Masses Greater Than 1200 Units by a Reflecting Time-of-Flight Mass Spectrometer. Rapid Commun Mass Spectrom 3:443–448. doi:10.1002/rcm.1290031210
48. Schueler B, Beavis R, Ens W, Main DE, Tang X, Standing KG (1989) Unimolecular Decay Measurements of Secondary Ions from Organic Molecules by Time-of-Flight Mass Spectrometry. Int J Mass Spectrom Ion Proc 92:185–194. doi:10.1016/0168-1176(89)83027-7
49. Brunelle A, Della-Negra S, Depauw J, Joret H, LeBeyec Y (1991) Time-of-Flight Mass Spectrometry with a Compact Two-Stage Electrostatic Mirror: Metastable-Ion Studies with High Mass Resolution and Ion Emission from Thick Insulators. Rapid Commun Mass Spectrom 5:40–43. doi:10.1002/rcm.1290050112
50. Cornish TJ, Cotter RJ (1993) A Curved-Field Reflectron for Improved Energy Focusing of Product Ions in Time-of-Flight Mass Spectrometry. Rapid Commun Mass Spectrom 7:1037–1040. doi:10.1002/rcm.1290071114
51. Cornish TJ, Cotter RJ (1994) A Curved Field Reflection Time-of-Flight Mass Spectrometer for the Simultaneous Focusing of Metastable Product Ions. Rapid Commun Mass Spectrom 8:781–785. doi:10.1002/rcm.1290080924
52. Cordero MM, Cornish TJ, Cotter RJ, Lys IA (1995) Sequencing Peptides Without Scanning the Reflectron: Post-Source Decay with a Curved-Field Reflectron Time-of-Flight Spectrometer. Rapid Commun Mass Spectrom 9:1356–1361. doi:10.1002/rcm.1290091407
53. Cotter RJ, Gardner BD, Iltchenko S, English RD (2004) Tandem Time-of-Flight Mass Spectrometry with a Curved Field Reflectron. Anal Chem 76:1976–1981. doi:10.1021/ac0349431
54. Yergey AL, Coorssen JR, Backlund PS, Blank PS, Humphrey GA, Zimmerberg J, Campbell JM, Vestal ML (2002) De Novo Sequencing of Peptides Using MALDI/TOF-TOF. J Am Soc Mass Spectrom 13:784–791. doi:10.1016/S1044-0305(02)00393-8
55. Schnaible V, Wefing S, Resemann A, Suckau D, Bücker A, Wolf-Kümmeth S, Hoffmann D (2002) Screening for Disulfide Bonds in Proteins by MALDI In-Source Decay and LIFT-TOF/TOF-MS. Anal Chem 74:4980–4988. doi:10.1021/ac025807j

56. Suckau D, Resemann A, Schuerenberg M, Hufnagel P, Franzen J, Holle A (2003) A Novel MALDI LIFT-TOF/TOF Mass Spectrometer for Proteomics. Anal Bioanal Chem 376:952–965. doi:10.1007/s00216-003-2057-0
57. Moneti G, Francese S, Mastrobuoni G, Pieraccini G, Seraglia R, Valitutti G, Traldi P (2007) Do Collisions Inside the Collision Cell Play a Relevant Role in CID-LIFT Experiments? J Mass Spectrom 42:117–126. doi:10.1002/jms.1151
58. Hipple JA, Condon EU (1945) Detection of Metastable Ions with the Mass Spectrometer. Phys Rev 68:54–55. doi:10.1103/PhysRev.68.54
59. Hipple JA, Fox RE, Condon EU (1946) Metastable Ions Formed by Electron Impact in Hydrocarbon Gases. Phys Rev 69:347–356. doi:10.1103/PhysRev.69.347
60. Beynon JH, Saunders RA, Williams AE (1965) Formation of Metastable Ions in Mass Spectrometers with Release of Internal Energy. Z Naturforsch A 20:180–183. doi:10.1515/zna-1965-0203
61. Beynon JH, Cooks RG, Amy JW, Baitinger WE, Ridley TY (1973) Design and Performance of a Mass-Analyzed Ion Kinetic Energy (MIKE) Spectrometer. Anal Chem 45:1023A–1031A. doi:10.1021/ac60334a763
62. Amy JW, Baitinger WE, Cooks RG (1990) Building Mass Spectrometers and a Philosophy of Research. J Am Soc Mass Spectrom 1:119–128. doi:10.1016/1044-0305(90)85047-P
63. Ottinger C (1965) Fragmentation Energies of Metastable Organic Ions. Phys Lett 17:269–271. doi:10.1016/0031-9163(65)90526-3
64. Baldwin MA, Derrick PJ, Morgan RP (1976) Correction of Metastable Peak Shapes to Allow for Instrumental Broadening and the Translational Energy Spread of the Parent Ion. Org Mass Spectrom 11:440–442. doi:10.1002/oms.1210110418
65. Gross JH, Veith HJ (1993) Unimolecular Fragmentations of Long-Chain Aliphatic Iminium Ions. Org Mass Spectrom 28:867–872. doi:10.1002/oms.1210280808
66. Bowen RD, Wright AD, Derrick PJ (1992) Unimolecular Reactions of Ionized Methyl Allyl Ether. Org Mass Spectrom 27:905–915. doi:10.1002/oms.1210270812
67. Cao JR, George M, Holmes JL (1992) Fragmentation of 1- and 3-Methoxypropene Ions. Another Part of the $[C_4H_8O]^{+\cdot}$ Cation Radical Potential Energy Surface. J Am Soc Mass Spectrom 3:99–107. doi:10.1016/1044-0305(92)87042-W
68. Millington DS, Smith JA (1977) Fragmentation Patterns by Fast Linked Electric and Magnetic Field Scanning. Org Mass Spectrom 12:264–265. doi:10.1002/oms.1210120418
69. Morgan RP, Porter CJ, Beynon JH (1977) On the Formation of Artefact Peaks in Linked Scans of the Magnet and Electric Sector Fields in a Mass Spectrometer. Org Mass Spectrom 12:735–738. doi:10.1002/oms.1210121206
70. Lacey MJ, Macdonald CG (1980) The Use of Two Linked Scanning Modes in Alternation to Analyze Metastable Peaks. Org Mass Spectrom 15:134–137. doi:10.1002/oms.1210150306
71. Lacey MJ, Macdonald CG (1980) Interpreting Metastable Peaks from Double Focusing Mass Spectrometers. Org Mass Spectrom 15:484–485. doi:10.1002/oms.1210150306
72. Mouget Y, Bertrand MJ (1995) Graphical Method for Artefact Peak Interpretation, and Methods for Their Rejection, Using Double and Triple Sector Magnetic Mass Spectrometers. Rapid Commun Mass Spectrom 9:387–396. doi:10.1002/rcm.1290090506
73. Evers EAIM, Noest AJ, Akkerman OS (1977) Deconvolution of Composite Metastable Peaks: A New Method for the Determination of Metastable Transitions Occurring in the First Field Free Region. Org Mass Spectrom 12:419–420. doi:10.1002/oms.1210120702
74. Boyd RK, Porter CJ, Beynon JH (1981) A New Linked Scan for Reversed Geometry Mass Spectrometers. Org Mass Spectrom 16:490–494. doi:10.1002/oms.1210161104
75. Lacey MJ, Macdonald CG (1979) Constant Neutral Spectrum in Mass Spectrometry. Anal Chem 51:691–695. doi:10.1021/ac50042a027
76. Boyd RK, Beynon JH (1977) Scanning of Sector Mass Spectrometers to Observe the Fragmentations of Metastable Ions. Org Mass Spectrom 12:163–165. doi:10.1002/oms.1210120311
77. Jennings KR (1984) Scanning methods for double-focusing mass spectrometers. In: Almoster Ferreira MA (ed) Ion Processes in the Gas Phase. D. Reidel Publishing, Dordrecht, pp 7–21

78. Fraefel A, Seibl J (1984) Selective Analysis of Metastable Ions. Mass Spectrom Rev 4:151–221. doi:10.1002/mas.1280040202
79. Boyd RK (1994) Linked-Scan Techniques for MS/MS Using Tandem-in-Space Instruments. Mass Spectrom Rev 13:359–410. doi:10.1002/mas.1280130502
80. Walther H, Schlunegger UP, Friedli F (1983) Quantitative Determination of Compounds in Mixtures by $B^2E = const$. Linked Scans. Org Mass Spectrom 18:572–575. doi:10.1002/oms.1210181215
81. Futrell JH (2000) Development of Tandem Mass Spectrometry. One Perspective. Int J Mass Spectrom 200:495–508. doi:10.1016/S1387-3806(00)00353-5
82. Fenselau C (1992) Tandem Mass Spectrometry: The Competitive Edge for Pharmacology. Annu Rev Pharmacol Toxicol 32:555–578. doi:10.1146/annurev.pa.32.040192.003011
83. Srinivas R, Sülzle D, Weiske T, Schwarz H (1991) Generation and Characterization of Neutral and Cationic 3-Silacyclopropenylidene in the Gas Phase. Description of a New BEBE Tandem Mass Spectrometer. Int J Mass Spectrom Ion Proc 107:369–376. doi:10.1016/0168-1176(91)80071-T
84. Bordaz-Nagy J, Despeyroux D, Jennings KR, Gaskell SJ (1992) Experimental Aspects of the Collision-Induced Decomposition of Ions in a Four-Sector Tandem Mass Spectrometer. Org Mass Spectrom 27:406–415. doi:10.1002/oms.1210270410
85. Stults JT, Lai J, McCune S, Wetzel R (1993) Simplification of High-Energy Collision Spectra of Peptides by Amino-Terminal Derivatization. Anal Chem 65:1703–1708. doi:10.1021/ac00061a012
86. Biemann K, Papyannopoulos IA (1994) Amino Acid Sequencing of Proteins. Acc Chem Res 27:370–378. doi:10.1021/ar00047a008
87. Papyannopoulos IA (1995) The Interpretation of Collision-Induced Dissociation Tandem Mass Spectra of Peptides. Mass Spectrom Rev 14:49–73. doi:10.1002/mas.1280140104
88. Lehmann WD (1996) Massenspektrometrie in der Biochemie. Spektrum Akademischer Verlag, Heidelberg
89. Chapman JR (ed) (2000) Mass Spectrometry of Proteins and Peptides. Humana Press, Totowa
90. Snyder AP (2000) Interpreting Protein Mass Spectra. Oxford University Press, New York
91. Kinter M, Sherman NE (2000) Protein Sequencing and Identification Using Tandem Mass Spectrometry. John Wiley & Sons, Chichester
92. Yost RA, Enke CG (1978) Selected Ion Fragmentation with a Tandem Quadrupole Mass Spectrometer. J Am Chem Soc 100:2274–2275. doi:10.1021/ja00475a072
93. Yost RA, Enke CG, McGilvery DC, Smith D, Morrison JD (1979) High Efficiency Collision-Induced Dissociation in an Rf-Only Quadrupole. Int J Mass Spectrom Ion Phys 30:127–136. doi:10.1016/0020-7381(79)80090-X
94. Yost RA, Enke CG (1979) Triple Quadrupole Mass Spectrometry for Direct Mixture Analysis and Structure Elucidation. Anal Chem 51:1251A–1262A. doi:10.1021/ac50048a002
95. Hunt DF, Shabanowitz J, Giordani AB (1980) Collision Activated Decompositions in Mixture Analysis with a Triple Quadrupole Mass Spectrometer. Anal Chem 52:386–390. doi:10.1021/ac50053a004
96. Dawson PH, French JB, Buckley JA, Douglas DJ, Simmons D (1982) The Use of Triple Quadrupoles for Sequential Mass Spectrometry: The Instrument Parameters. Org Mass Spectrom 17:205–211. doi:10.1002/oms.1210170503
97. Dawson PH, French JB, Buckley JA, Douglas DJ, Simmons D (1982) The Use of Triple Quadrupoles for Sequential Mass Spectrometry: A Detailed Case Study. Org Mass Spectrom 17:212–219. doi:10.1002/oms.1210170504
98. Inglebert RL, Hennequin JF (1980) Overall Transmission of Quadrupole Mass Spectrometers. Adv Mass Spectrom 8B:1764–1770
99. Cerezo A, Miller MK (1991) Einzel Lenses in Atom Probe Designs. Surf Sci 246:450–456. doi:10.1016/0039-6028(91)90450-7
100. Thomson BA, Douglas DJ, Corr JJ, Hager JW, Jolliffe CL (1995) Improved Collisionally Activated Dissociation Efficiency and Mass Resolution on a Triple Quadrupole Mass Spectrometer System. Anal Chem 67:1696–1704. doi:10.1021/ac00106a008

101. Zeller M, Koenig S (2004) The Impact of Chromatography and Mass Spectrometry on the Analysis of Protein Phosphorylation Sites. Mass Spectrometric Phosphorylation Analysis. Anal Bioanal Chem 378:889–909. doi:10.1007/s00216-003-2391-2
102. Schwartz JC, Schey KL, Cooks RG (1990) A Penta-Quadrupole Instrument for Reaction Intermediate Scans and Other MS-MS-MS Experiments. Int J Mass Spectrom Ion Proc 101:1–20. doi:10.1016/0168-1176(90)80017-W
103. Gozzo FC, Sorrilha AEPM, Eberlin MN (1996) The Generation, Stability, Dissociation and Ion/Molecule Chemistry of Sulfinyl Cations in the Gas Phase. J Chem Soc Perkin Trans 2:587–596. doi:10.1039/P29960000587
104. Juliano VF, Gozzo FC, Eberlin MN, Kascheres C, do Lago CL (1996) Fast Multidimensional (3D and 4D) MS^2 and MS^3 Scans in a High-Transmission Pentaquadrupole Mass Spectrometer. Anal Chem 68:1328–1334. doi:10.1021/ac9508659
105. Eberlin MN (1997) Triple-Stage Pentaquadrupole (QqQqQ) Mass Spectrometry and Ion/Molecule Reactions. Mass Spectrom Rev 16:113–144. doi:10.1002/(SICI)1098-2787(1997)16:3<113::AID-MAS1>3.0.CO;2-K
106. March RE (1998) Quadrupole Ion Trap Mass Spectrometry: Theory, Simulation, Recent Developments and Applications. Rapid Commun Mass Spectrom 12:1543–1554. doi:10.1002/(SICI)1097-0231(19981030)12:20<1543::AID-RCM343>3.0.CO;2-T
107. Griffiths IW (1990) Recent Advances in Ion-Trap Technology. Rapid Commun Mass Spectrom 4:69–73. doi:10.1002/rcm.1290040302
108. Siethoff C, Wagner-Redeker W, Schäfer M, Linscheid M (1999) HPLC-MS with an Ion Trap Mass Spectrometer. Chimia 53:484–491
109. Schwartz JC, Jardine I (1992) High-Resolution Parent-Ion Selection/Isolation Using a Quadrupole Ion-Trap Mass Spectrometer. Rapid Commun Mass Spectrom 6:313–317. doi:10.1002/rcm.1290060419
110. Remes PM, Glish GL (2009) On The Time Scale of Internal Energy Relaxation of AP-MALDI and Nano-ESI Ions in a Quadrupole Ion Trap. J Am Soc Mass Spectrom 20:1801–1812. doi:10.1016/j.jasms.2009.05.018
111. Louris JN, Cooks RG, Syka JEP, Kelley PE, Stafford GC Jr, Todd JFJ (1987) Instrumentation, Applications, and Energy Deposition in Quadrupole Ion-Trap Tandem Mass Spectrometry. Anal Chem 59:1677–1685. doi:10.1021/ac00140a021
112. McLuckey SA, Glish GL, Kelley PE (1987) Collision-Activated Dissociation of Negative Ions in an Ion Trap Mass Spectrometer. Anal Chem 59:1670–1674. doi:10.1021/ac00140a019
113. Cooks RG, Amy JW, Bier M, Schwartz JC, Schey K (1989) New mass spectrometers. Adv Mass Spectrom 11A:33–52
114. Murrell J, Konn DO, Underwood NJ, Despeyroux D (2003) Studies into the Selective Accumulation of Multiply Charged Protein Ions in a Quadrupole Ion Trap Mass Spectrometer. Int J Mass Spectrom 227:223–234. doi:10.1016/S1387-3806(03)00109-X
115. Hashimoto Y, Hasegawa H, Yoshinari K (2003) Collision-Activated Infrared Multiphoton Dissociation in a Quadrupole Ion Trap Mass Spectrometer. Anal Chem 75:420–425. doi:10.1021/ac025866x
116. March RE, Todd JFJ (2005) Quadrupole Ion Trap Mass Spectrometry. John Wiley & Sons, Hoboken
117. Kuzma M, Jegorov A, Kacer P, Havlícek V (2001) Sequencing of New Beauverolides by High-Performance Liquid Chromatography and Mass Spectrometry. J Mass Spectrom 36:1108–1115. doi:10.1002/jms.213
118. Hopfgartner G, Husser C, Zell M (2003) Rapid Screening and Characterization of Drug Metabolites Using a New Quadrupole-Linear Ion Trap Mass Spectrometer. J Mass Spectrom 38:138–150. doi:10.1002/jms.420
119. Pekar Second T, Blethrow JD, Schwartz JC, Merrihew GE, MacCoss MJ, Swaney DL, Russell JD, Coon JJ, Zabrouskov V (2009) Dual-Pressure Linear Ion Trap Mass Spectrometer Improving the Analysis of Complex Protein Mixtures. Anal Chem 81:7757–7765. doi:10.1021/ac901278y

120. Magparangalan DP, Garrett TJ, Drexler DM, Yost RA (2010) Analysis of Large Peptides by MALDI Using a Linear Quadrupole Ion Trap with Mass Range Extension. Anal Chem 82:930–934. doi:10.1021/ac9021488
121. Londry FA, Hager JW (2003) Mass Selective Axial Ion Ejection from a Linear Quadrupole Ion Trap. J Am Soc Mass Spectrom 14:1130–1147. doi:10.1016/S1044-0305(03)00446-X
122. Hopfgartner G, Varesio E, Tschaeppaet V, Grivet C, Bourgogne E, Leuthold LA (2004) Triple Quadrupole Linear Ion Trap Mass Spectrometer for the Analysis of Small Molecules and Macromolecules. J Mass Spectrom 39:845–855. doi:10.1002/jms.659
123. Moberg M, Markides KE, Bylund D (2005) Multi-Parameter Investigation of Tandem Mass Spectrometry in a Linear Ion Trap Using Response Surface Modelling. J Mass Spectrom 40:317–324. doi:10.1002/jms.787
124. Olsen JV, Schwartz JC, Griep-Raming J, Nielsen ML, Damoc E, Denisov E, Lange O, Remes P, Taylor D, Splendore M, Wouters ER, Senko M, Makarov A, Mann M, Horning S (2009) A Dual Pressure Linear Ion Trap Orbitrap Instrument with Very High Sequencing Speed. Mol Cell Proteomics 8:2759–2769. doi:10.1074/mcp.M900375-MCP200
125. Olsen JV, Macek B, Lange O, Makarov A, Horning S, Mann M (2007) Higher-Energy C-Trap Dissociation for Peptide Modification Analysis. Nat Methods 4:709–712. doi:10.1038/nmeth1060
126. Olsen JV, de Godoy LMF, Li G, Macek B, Mortensen P, Pesch R, Makarov A, Lange O, Horning S, Mann M (2005) Parts Per Million Mass Accuracy on an Orbitrap Mass Spectrometer via Lock Mass Injection into a C-Trap. Mol Cell Proteomics 4:2010–2021. doi:10.1074/mcp.T500030-MCP200
127. Senko MW, Remes PM, Canterbury JD, Mathur R, Song Q, Eliuk SM, Mullen C, Earley L, Hardman M, Blethrow JD, Bui H, Specht A, Lange O, Denisov E, Makarov A, Horning S, Zabrouskov V (2013) Novel Parallelized Quadrupole/Linear Ion Trap/Orbitrap Tribrid Mass Spectrometer Improving Proteome Coverage and Peptide Identification Rates. Anal Chem 85:11710–11714. doi:10.1021/ac403115c
128. Lebedev AT, Damoc E, Makarov AA, Samgina TY (2014) Discrimination of Leucine and Isoleucine in Peptides Sequencing with Orbitrap Fusion Mass Spectrometer. Anal Chem 86:7017–7022. doi:10.1021/ac501200h
129. Guan S, Marshall AG (1996) Stored Waveform Inverse Fourier Transform (SWIFT) Ion Excitation in Trapped-Ion Mass Spectrometry: Theory and Applications. Int J Mass Spectrom Ion Proc 157(158):5–37. doi:10.1016/S0168-1176(96)04461-8
130. Heck AJR, Derrick PJ (1997) Ultrahigh Mass Accuracy in Isotope-Selective Collision-Induced Dissociation Using Correlated Sweep Excitation and Sustained Off-Resonance Irradiation: A Fourier Transform Ion Cyclotron Resonance Mass Spectrometry Case Study on the $[M+2H]^{2+}$ Ion of Bradykinin. Anal Chem 69:3603–3607. doi:10.1021/ac970254b
131. Heck AJR, Derrick PJ (1998) Selective Fragmentation of Single Isotopic Ions of Proteins Up to 17 KDa Using 9.4 Tesla Fourier Transform Ion Cyclotron Resonance. Eur Mass Spectrom 4:181–188. doi:10.1255/ejms.207
132. Cody RB, Freiser BS (1982) Collision-Induced Dissociation in a Fourier-Transform Mass Spectrometer. Int J Mass Spectrom Ion Phys 41:199–204. doi:10.1016/0020-7381(82)85035-3
133. Cody RB, Burnier RC, Freiser BS (1982) Collision-Induced Dissociation with Fourier Transform Mass Spectrometry. Anal Chem 54:96–101. doi:10.1021/ac00238a029
134. Gauthier JW, Trautman TR, Jacobson DB (1991) Sustained Off-Resonance Irradiation for Collision-Activated Dissociation Involving FT-ICR-MS. CID Technique that Emulates Infrared Multiphoton Dissociation. Anal Chim Acta 246:211–225. doi:10.1016/0003-2670(91)80053-V
135. Senko MW, Speir JP, McLafferty FW (1994) Collisional Activation of Large Multiply Charged Ions Using Fourier Transform Mass Spectrometry. Anal Chem 66:2801–2808. doi:10.1021/ac00090a003

136. Boering KA, Rolfe J, Brauman JI (1992) Control of Ion Kinetic Energy in Ion Cyclotron Resonance Spectrometry: Very-Low-Energy Collision-Induced Dissociation. Rapid Commun Mass Spectrom 6:303–305. doi:10.1002/rcm.1290060416
137. Lee SA, Jiao CQ, Huang Y, Freiser BS (1993) Multiple Excitation Collisional Activation in Fourier-Transform Mass Spectrometry. Rapid Commun Mass Spectrom 7:819–821. doi:10.1002/rcm.1290070908
138. Mihalca R, van der Burgt YEM, Heck AJR, Heeren RMA (2007) Disulfide Bond Cleavages Observed in SORI-CID of Three Nonapeptides Complexed with Divalent Transition-Metal Cations. J Mass Spectrom 42:450–458. doi:10.1002/jms.1175
139. Mirgorodskaya E, O'Connor PB, Costello CE (2002) A General Method for Precalculation of Parameters for Sustained Off Resonance Irradiation/Collision-Induced Dissociation. J Am Soc Mass Spectrom 13:318–324. doi:10.1016/S1044-0305(02)00340-9
140. Woodin RL, Bomse DS, Beauchamp JL (1978) Multiphoton Dissociation of Molecules with Low Power Continuous Wave Infrared Laser Radiation. J Am Chem Soc 100:3248–3250. doi:10.1021/ja00478a065
141. Håkansson K, Cooper HJ, Emmet MR, Costello CE, Marshall AG, Nilsson CL (2001) Electron Capture Dissociation and Infrared Multiphoton Dissociation MS/MS of an *N*-Glycosylated Tryptic Peptic to Yield Complementary Sequence Information. Anal Chem 73:4530–4536. doi:10.1021/ac0103470
142. Little DP, Senko MW, O'Conner PB, McLafferty FW (1994) Infrared Multiphoton Dissociation of Large Multiply-Charged Ions for Biomolecule Sequencing. Anal Chem 66:2809–2815. doi:10.1021/ac00090a004
143. Watson CH, Baykut G, Eyler JR (1987) Laser Photodissociation of Gaseous Ions Formed by Laser Desorption. Anal Chem 59:1133–1138. doi:10.1021/ac00135a015
144. Eyler JR (2009) Infrared Multiple Photon Dissociation Spectroscopy of Ions in Penning Traps. Mass Spectrom Rev 28:448–467. doi:10.1002/mas.20217
145. Brodbelt JS, Wilson JJ (2009) Infrared Multiphoton Dissociation in Quadrupole Ion Traps. Mass Spectrom Rev 28:390–424. doi:10.1002/mas.20216
146. Hashimoto Y, Hasegawa H, Waki I (2004) High Sensitivity and Broad Dynamic Range Infrared Multiphoton Dissociation for a Quadrupole Ion Trap. Rapid Commun Mass Spectrom 18:2255–2259. doi:10.1002/rcm.1619
147. Newsome GA, Glish GL (2009) Improving IRMPD in a Quadrupole Ion Trap. J Am Soc Mass Spectrom 20:1127–1131. doi:10.1016/j.jasms.2009.02.003
148. Newsome GA, Glish GL (2011) A New Approach to IRMPD Using Selective Ion Dissociation in a Quadrupole Ion Trap. J Am Soc Mass Spectrom 22:207–213. doi:10.1007/s13361-010-0039-y
149. Madsen JA, Gardner MW, Smith SI, Ledvina AR, Coon JJ, Schwartz JC, Stafford GC, Brodbelt JS (2009) Top-Down Protein Fragmentation by Infrared Multiphoton Dissociation in a Dual Pressure Linear Ion Trap. Anal Chem 81:8677–8686. doi:10.1021/ac901554z
150. Gardner MW, Smith SI, Ledvina AR, Madsen JA, Coon JJ, Schwartz JC, Stafford GC, Brodbelt JS (2009) Infrared Multiphoton Dissociation of Peptide Cations in a Dual Pressure Linear Ion Trap Mass Spectrometer. Anal Chem 81:8109–8118. doi:10.1021/ac901313m
151. Campbell JL, Hager JW, Le Blanc JCY (2009) On Performing Simultaneous Electron Transfer Dissociation and Collision-Induced Dissociation on Multiply Protonated Peptides in a Linear Ion Trap. J Am Soc Mass Spectrom 20:1672–1683. doi:10.1016/j.jasms.2009.05.009
152. Ledvina AR, Lee MV, McAlister GC, Westphall MS, Coon JJ (2012) Infrared Multiphoton Dissociation for Quantitative Shotgun Proteomics. Anal Chem 84:4513–4519. doi:10.1021/ac300367p
153. Zubarev RA, Kelleher NL, McLafferty FW (1998) Electron Capture Dissociation of Multiply Charged Protein Cations. A Nonergodic Process. J Am Chem Soc 120:3265–3266. doi:10.1021/ja973478k

154. Axelsson J, Palmblad M, Håkansson K, Håkansson P (1999) Electron Capture Dissociation of Substance P Using a Commercially Available Fourier Transform Ion Cyclotron Resonance Mass Spectrometer. Rapid Commun Mass Spectrom 13:474–477. doi:10.1002/(SICI)1097-0231(19990330)13:6<474::AID-RCM505>3.0.CO;2-1
155. Cerda BA, Horn DM, Breuker K, Carpenter BK, McLafferty FW (1999) Electron Capture Dissociation of Multiply-Charged Oxygenated Cations. A Nonergodic Process. Eur Mass Spectrom 5:335–338. doi:10.1255/ejms.293
156. Håkansson K, Emmet MR, Hendrickson CL, Marshall AG (2001) High-Sensitivity Electron Capture Dissociation Tandem FTICR Mass Spectrometry of Microelectrosprayed Peptides. Anal Chem 73:3605–3610. doi:10.1021/ac010141z
157. Leymarie N, Berg EA, McComb ME, O'Conner PB, Grogan J, Oppenheim FG, Costello CE (2002) Tandem Mass Spectrometry for Structural Characterization of Proline-Rich Proteins: Application to Salivary PRP-3. Anal Chem 74:4124–4132. doi:10.1021/ac0255835
158. Tsybin YO, Ramstroem M, Witt M, Baykut G, Hakansson P (2004) Peptide and Protein Characterization by High-Rate Electron Capture Dissociation Fourier Transform Ion Cyclotron Resonance Mass Spectrometry. J Mass Spectrom 39:719–729. doi:10.1002/jms.658
159. Zubarev RA, Horn DM, Fridriksson EK, Kelleher NL, Kruger NA, Lewis MA, Carpenter BK, McLafferty FW (2000) Electron Capture Dissociation for Structural Characterization of Multiply Charged Protein Cations. Anal Chem 72:563–573. doi:10.1021/ac990811p
160. Zubarev RA (2003) Reactions of Polypeptide Ions with Electrons in the Gas Phase. Mass Spectrom Rev 22:57–77. doi:10.1002/mas.10042
161. Leymarie N, Costello CE, O'Connor PB (2003) Electron Capture Dissociation Initiates a Free Radical Reaction Cascade. J Am Chem Soc 125:8949–8958. doi:10.1021/ja028831n
162. Turecek F (2003) N-C_α Bond Dissociation Energies and Kinetics in Amide and Peptide Radicals. Is the Dissociation a Non-Ergodic Process? J Am Chem Soc 125:5954–5963. doi:10.1021/ja021323t
163. McFarland MA, Marshall AG, Hendrickson CL, Nilsson CL, Fredman P, Mansson JE (2005) Structural Characterization of the GM1 Ganglioside by Infrared Multiphoton Dissociation, Electron Capture Dissociation, and Electron Detachment Dissociation Electrospray Ionization FT-ICR MS/MS. J Am Soc Mass Spectrom 16:752–762. doi:10.1016/j.jasms.2005.02.001
164. Oh HB, Lin C, Hwang HY, Zhai H, Breuker K, Zabrouskov V, Carpenter BK, McLafferty FW (2005) Infrared Photodissociation Spectroscopy of Electrosprayed Ions in a Fourier Transform Mass Spectrometer. J Am Chem Soc 127:4076–4083. doi:10.1021/ja040136n
165. Dunbar RC (2004) BIRD (Blackbody Infrared Radiative Dissociation): Evolution, Principles, and Applications. Mass Spectrom Rev 23:127–158. doi:10.1002/mas.10074
166. Tsybin YO, Hakansson P, Budnik BA, Haselmann KF, Kjeldsen F, Gorshkov M, Zubarev RA (2001) Improved Low-Energy Electron Injection Systems for High Rate Electron Capture Dissociation in Fourier Transform Ion Cyclotron Resonance Mass Spectrometry. Rapid Commun Mass Spectrom 15:1849–1854. doi:10.1002/rcm.448
167. Tsybin YO, Witt M, Baykut G, Kjeldsen F, Hakansson P (2003) Combined Infrared Multiphoton Dissociation and Electron Capture Dissociation with a Hollow Electron Beam in Fourier Transform Ion Cyclotron Resonance Mass Spectrometry. Rapid Commun Mass Spectrom 17:1759–1768. doi:10.1002/rcm.1118
168. Syka JEP, Coon JJ, Schroeder MJ, Shabanowitz J, Hunt DF (2004) Peptide and Protein Sequence Analysis by Electron Transfer Dissociation Mass Spectrometry. Proc Natl Acad Sci U S A 101:9528–9533. doi:10.1073/pnas.0402700101
169. Cooper HJ, Hakansson K, Marshall AG (2005) The Role of Electron Capture Dissociation in Biomolecular Analysis. Mass Spectrom Rev 24:201–222. doi:10.1002/mas.20014
170. Swaney DL, McAlister GC, Wirtala M, Schwartz JC, Syka JEP, Coon JJ (2007) Supplemental Activation Method for High-Efficiency Electron-Transfer Dissociation of Doubly Protonated Peptide Precursors. Anal Chem 79:477–485. doi:10.1021/ac061457f
171. Coon JJ, Syka JEP, Schwartz JC, Shabanowitz J, Hunt DF (2004) Anion Dependence in the Partitioning Between Proton and Electron Transfer in Ion/Ion Reactions. Int J Mass Spectrom 236:33–42. doi:10.1016/j.ijms.2004.05.005

172. Good DM, Wirtala M, McAlister GC, Coon JJ (2007) Performance Characteristics of Electron Transfer Dissociation Mass Spectrometry. Mol Cell Proteomics 6:1942–1951. doi:10.1074/mcp.M700073-MCP200
173. Chi A, Huttenhower C, Geer LY, Coon JJ, Syka JEP, Bai DL, Shabanowitz J, Burke DJ, Troyanskaya OG, Hunt DF (2007) Analysis of Phosphorylation Sites on Proteins from Saccharomyces Cerevisiae by Electron Transfer Dissociation (ETD) Mass Spectrometry. Proc Natl Acad Sci U S A 104:2193–2198. doi:10.1073/pnas.0607084104
174. Liang X, Hager JW, McLuckey SA (2007) Transmission Mode Ion/Ion Electron-Transfer Dissociation in a Linear Ion Trap. Anal Chem 79:3363–3370. doi:10.1021/ac062295q
175. McAlister GC, Berggren WT, Griep-Raming J, Horning S, Makarov A, Phanstiel D, Stafford G, Swaney DL, Syka JEP, Zabrouskov V, Coon JJ (2008) A Proteomics Grade Electron Transfer Dissociation-Enabled Hybrid Linear Ion Trap-Orbitrap Mass Spectrometer. J Proteome Res 7:3127–3136. doi:10.1021/pr800264t
176. Williams DK Jr, McAlister GC, Good DM, Coon JJ, Muddiman DC (2007) Dual Electrospray Ion Source for Electron-Transfer Dissociation on a Hybrid Linear Ion Trap-Orbitrap Mass Spectrometer. Anal Chem 79:7916–7919. doi:10.1021/ac071444h
177. McAlister GC, Phanstiel D, Good DM, Berggren WT, Coon JJ (2007) Implementation of Electron-Transfer Dissociation on a Hybrid Linear Ion Trap-Orbitrap Mass Spectrometer. Anal Chem 79:3525–3534. doi:10.1021/ac070020k
178. Haselmann KF, Budnik BA, Kjeldsen F, Nielsen ML, Olsen JV, Zubarev RA (2002) Electronic Excitation Gives Informative Fragmentation of Polypeptide Cations and Anions. Eur J Mass Spectrom 8:117–121. doi:10.1255/ejms.479
179. Budnik BA, Haselmann KF, Zubarev RA (2001) Electron Detachment Dissociation of Peptide Di-Anions: An Electron-Hole Recombination Phenomenon. Chem Phys Lett 342:299–302. doi:10.1016/S0009-2614(01)00501-2
180. Kjeldsen F, Silivra OA, Ivonin IA, Haselmann KF, Gorshkov M, Zubarev RA (2005) C_{α}-C Backbone Fragmentation Dominates in Electron Detachment Dissociation of Gas-Phase Polypeptide Polyanions. Chem Eur J 11:1803–1812. doi:10.1002/chem.200400806
181. Anusiewicz I, Jasionowski M, Skurski P, Simons J (2005) Backbone and Side-Chain Cleavages in Electron Detachment Dissociation (EDD). J Chem Phys A 109:11332–11337. doi:10.1021/jp055018g
182. Yang J, Mo J, Adamson JT, Haakansson K (2005) Characterization of Oligodeoxynucleotides by Electron Detachment Dissociation Fourier Transform Ion Cyclotron Resonance Mass Spectrometry. Anal Chem 77:1876–1882. doi:10.1021/ac048415g
183. Huzarska M, Ugalde I, Kaplan DA, Hartmer R, Easterling ML, Polfer NC (2010) Negative Electron Transfer Dissociation of Deprotonated Phosphopeptide Anions: Choice of Radical Cation Reagent and Competition Between Electron and Proton Transfer. Anal Chem 82:2873–2878. doi:10.1021/ac9028592
184. Adlhart C, Hinderling C, Baumann H, Chen P (2000) Mechanistic Studies of Olefin Metathesis by Ruthenium Carbene Complexes Using Electrospray Ionization Tandem Mass Spectrometry. J Am Chem Soc 122:8204–8214. doi:10.1021/ja9938231
185. Hinderling C, Adlhart C, Chen P (2000) Mechanism-Based High-Throughput Screening of Catalysts. Chimia 54:232–235
186. Volland MAO, Adlhart C, Kiener CA, Chen P, Hofmann P (2001) Catalyst Screening by Electrospray Ionization Tandem Mass Spectrometry: Hofmann Carbenes for Olefin Metathesis. Chem Eur J 7:4621–4632. doi:10.1002/1521-3765(20011105)7:21<4621::AID-CHEM4621>3.0.CO;2-C
187. Schwarz H (2003) Relativistic Effects in Gas-Phase Ion Chemistry: An Experimentalist's View. Angew Chem Int Ed 42:4442–4454. doi:10.1002/anie.200300572
188. Schwarz H (2004) On the Spin-Forbiddeness of Gas-Phase Ion-Molecule Reactions: A Fruitful Intersection of Experimental and Computational Studies. Int J Mass Spectrom 237:75–105. doi:10.1016/j.ijms.2004.06.006

189. Boehme DK, Schwarz H (2005) Gas-Phase Catalysis by Atomic and Cluster Metal Ions: The Ultimate Single-Site Catalysts. Angew Chem Int Ed 44:2336–2354. doi:10.1002/chin.200525226
190. Schlangen M, Schroeder D, Schwarz H (2007) Pronounced Ligand Effects and the Role of Formal Oxidation States in the Nickel-Mediated Thermal Activation of Methane. Angew Chem Int Ed 46:1641–1644. doi:10.1002/anie.200603266
191. Kaltashov IA, Eyles SJ (2005) Mass Spectrometry in Biophysics: Conformation and Dynamics of Biomolecules. John Wiley & Sons, Hoboken
192. Somogyi A (2008) Probing Peptide Fragment Ion Structures by Combining Sustained Off-Resonance Collision-Induced Dissociation and Gas-Phase H/D Exchange (SORI-HDX) in Fourier Transform Ion-Cyclotron Resonance (FT-ICR) Instruments. J Am Soc Mass Spectrom 19:1771–1775. doi:10.1016/j.jasms.2008.08.012
193. Bythell BJ, Somogyi A, Paizs B (2009) What Is the Structure of B_2 Ions Generated from Doubly Protonated Tryptic Peptides? J Am Soc Mass Spectrom 20:618–624. doi:10.1016/j.jasms.2008.11.021
194. Harrison AG (1997) The Gas-Phase Basicities and Proton Affinities of Amino Acids and Peptides. Mass Spectrom Rev 16:201–217. doi:10.1002/(SICI)1098-2787(1997)16:4<201::AID-MAS3>3.0.CO;2-L
195. McMahon TB (2000) Thermochemical Ladders: Scaling the Ramparts of Gaseous Ion Energetics. Int J Mass Spectrom 200:187–199. doi:10.1016/S1387-3806(00)00308-0
196. Cooks RG, Kruger TL (1977) Intrinsic Basicity Determination Using Metastable Ions. J Am Chem Soc 99:1279–1281. doi:10.1021/ja00446a059
197. Cooks RG, Wong PSH (1998) Kinetic Method of Making Thermochemical Determinations: Advances and Applications. Acc Chem Res 31:379–386. doi:10.1021/ar960242x
198. Cooks RG, Patrick JS, Kotiaho T, McLuckey SA (1994) Thermochemical Determinations by the Kinetic Method. Mass Spectrom Rev 13:287–339. doi:10.1002/mas.1280130402
199. Kukol A, Strehle F, Thielking G, Grützmacher HF (1993) Methyl Group Effect on the Proton Affinity of Methylated Acetophenones Studied by Two Mass Spectrometric Techniques. Org Mass Spectrom 28:1107–1110. doi:10.1002/oms.1210281021
200. Bouchoux G, Salpin JY (1996) Gas-Phase Basicity and Heat of Formation of Sulfine CH_2=S=O. J Am Chem Soc 118:6516–6517. doi:10.1021/ja9610601
201. Bouchoux G, Salpin JY, Leblanc D (1996) A Relationship Between the Kinetics and Thermochemistry of Proton Transfer Reactions in the Gas Phase. Int J Mass Spectrom Ion Proc 153:37–48. doi:10.1016/0168-1176(95)04353-5
202. Witt M, Kreft D, Grützmacher HF (2003) Effects of Internal Hydrogen Bonds Between Amide Groups: Protonation of Alicyclic Diamides. Eur J Mass Spectrom 9:81–95. doi:10.1255/ejms.535
203. Danis PO, Wesdemiotis C, McLafferty FW (1983) Neutralization-Reionization Mass Spectrometry (NRMS). J Am Chem Soc 105:7454–7456. doi:10.1021/ja00363a048
204. Gellene GI, Porter RF (1983) Neutralized Ion-Beam Spectroscopy. Acc Chem Res 16:200–207. doi:10.1021/ar00090a003
205. Terlouw JK, Kieskamp WM, Holmes JL, Mommers AA, Burgers PC (1985) The Neutralization and Reionization of Mass-Selected Positive Ions by Inert Gas Atoms. Int J Mass Spectrom Ion Proc 64:245–250. doi:10.1016/0168-1176(85)85013-8
206. Holmes JL, Mommers AA, Terlouw JK, Hop CECA (1986) The Mass Spectrometry of Neutral Species Produced from Mass-Selected Ions by Collision and by Charge Exchange. Experiments with Tandem Collision Gas Cells. Int J Mass Spectrom Ion Proc 68:249–264. doi:10.1016/0168-1176(86)87051-3
207. Blanchette MC, Holmes JL, Hop CECA, Mommers AA (1988) The Ionization of Fast Neutrals by Electron Impact in the Second Field-Free Region of a Mass Spectrometer of Reversed Geometry. Org Mass Spectrom 23:495–498. doi:10.1002/oms.1210230611
208. McLafferty FW (1992) Neutralization-Reionization Mass Spectrometry. Int J Mass Spectrom Ion Proc 118(119):221–235. doi:10.1016/0168-1176(92)85063-6

209. Goldberg N, Schwarz H (1994) Neutralization-Reionization Mass Spectrometry: a Powerful "Laboratory" to Generate and Probe Elusive Neutral Molecules. Acc Chem Res 27:347–352. doi:10.1021/ar00047a005
210. Schalley CA, Hornung G, Schroder D, Schwarz H (1998) Mass Spectrometry As a Tool to Probe the Gas-Phase Reactivity of Neutral Molecules. Int J Mass Spectrom Ion Proc 172:181–208. doi:10.1016/S0168-1176(97)00115-8
211. Schalley CA, Hornung G, Schroder D, Schwarz H (1998) Mass Spectrometric Approaches to the Reactivity of Transient Neutrals. Chem Soc Rev 27:91–104. doi:10.1039/A827091Z
212. Blanchette MC, Bordas-Nagy J, Holmes JL, Hop CECA, Mommers AA, Terlouw JK (1988) Neutralization-Reionization Experiments: A Simple Metal Vapor Cell for VG Analytical ZAB-2F Mass Spectrometers. Org Mass Spectrom 23:804–807. doi:10.1002/oms.1210231114
213. Zhang MY, McLafferty FW (1992) Organic Neutralization Agents for Neutralization-Reionization Mass Spectrometry. J Am Soc Mass Spectrom 3:108–112. doi:10.1016/1044-0305(92)87043-X
214. Zagorevskii DV, Holmes JL (1994) Neutralization-Reionization Mass Spectrometry Applied to Organometallic and Coordination Chemistry. Mass Spectrom Rev 13:133–154. doi:10.1002/mas.1280130203
215. Zagorevskii DV, Holmes JL (1999) Neutralization-Reionization Mass Spectrometry Applied to Organometallic and Coordination Chemistry (Update: 1994–1998). Mass Spectrom Rev 18:87–118. doi:10.1002/(SICI)1098-2787(1999)18:2<87::AID-MAS1>3.0.CO;2-J
216. Weiske T, Wong T, Krätschmer W, Terlouw JK, Schwarz H (1992) Proof of the Existence of an Endohedral Helium-Fullerene ($He@C_{60}$) Structure via Gas-Phase Neutralization of $[HeC_{60}]^+$. Angew Chem Int Ed 31:183–185. doi:10.1002/anie.199201831
217. Keck H, Kuchen W, Tommes P, Terlouw JK, Wong T (1992) The Phosphonium Ylide CH_2PH_3 Is Stable in Gas Phase. Angew Chem Int Ed 31:86–87. doi:10.1002/anie.199200861
218. Schröder D, Schwarz H, Wulf M, Sievers H, Jutzi P, Reiher M (1999) Experimental Evidence for the Existence of Neutral P_6: A New Allotrope of Phosphorus. Angew Chem Int Ed 38:313–315. doi:10.1002/(SICI)1521-3773(19991203)38:23<3513::AID-ANIE3513>3.0.CO;2-I
219. Sleno L, Volmer DA (2004) Ion Activation Methods for Tandem Mass Spectrometry. J Mass Spectrom 39:1091–1112. doi:10.1002/jms.703